6-19-2014

Measuring Scaling Effects in Small Two-Stroke Internal Combustion Engines

Alex K. Rowton

MEASURING SCALING EFFECTS IN SMALL TWO-STROKE INTERNAL COMBUSTION ENGINES

THESIS
JUNE 2014

Alex K. Rowton, Captain, USAF

AFIT-ENY-T-14-J-36

DEPARTMENT OF THE AIR FORCE
AIR UNIVERSITY

AIR FORCE INSTITUTE OF TECHNOLOGY

Wright-Patterson Air Force Base, Ohio

AFIT-ENY-T-14-J-36

MEASURING SCALING EFFECTS IN SMALL TWO-STROKE INTERNAL COMBUSTION ENGINES

THESIS

Presented to the Faculty

Department of Aeronautics and Astronautics

Graduate School of Engineering and Management

Air Force Institute of Technology

Air University

Air Education and Training Command

In Partial Fulfillment of the Requirements for the

Degree of Master of Science in Aeronautical Engineering

Alex K. Rowton, BS

Captain, USAF

June 2014

AFIT-ENY-T-14-J-36

MEASURING SCALING EFFECTS IN SMALL TWO-STROKE INTERNAL COMBUSTION ENGINES

Alex K. Rowton, BS

Captain, USAF

Approved:

//signed//	30 May 2014
Marc D. Polanka, PhD (Chairman)	Date
//signed//	30 May 2014
Timothy C. Radsick, LtCol, USAF (Member)	Date
//signed//	30 May 2014
Paul I. King, PhD (Member)	Date

Abstract

As internal combustion (IC) engine displacement decreases, cylinder surface area to swept volume ratio increases. Examining power output of IC engines with respect to cylinder surface area to swept volume ratio shows that there is a dramatic change in power scaling trends at approximately 1.5 cm^{-1}. At this size, thermal quenching and friction losses are expected to dominate engine performance. As a result, power production and efficiency characteristics suffer. Furthermore, small IC engines (< 100 cc displacement) have limited technical performance data, so quantifying efficiency trends is difficult. Therefore, establishing accurate performance figures for a family of geometrically similar engines in the size class of approximately 1.5 cm^{-1} is beneficial in understanding the thermal losses as well as other phenomena that contribute to lower efficiencies in small IC engines.

Three small two-stroke engines were considered in this scaling study. They spanned the transition size regime of 1.5 cm^{-1}. The engines shared a similar design to reduce performance variability due to factors other than size. A performance baseline was established for each engine. Measured performance values were used to determine scaling relationships for engines of this size. The results of this study show that brake fuel conversion efficiency diminished with decreasing engine size. Furthermore, friction losses increased as engine size was reduced as a result of increasing cylinder surface area to swept volume ratio. Equivalence ratio was not held constant during testing due to the limitations of each engine's carburetor. Therefore, definitive relationships concerning engine heat rejection were not realized.

Acknowledgments

I would like to thank all those who were involved with the support of this study. I am grateful for the advice and assistance of the following people who helped me to accomplish this research: Dr. Marc Polanka, Lt. Joseph Ausserer, Capt. Josh Rittenhouse, Mr. Paul Litke, Mr. Keith Grinstead, Mr. Adam Brown, Mr. JR Groenewegen, Lt. Col. Timothy Radsick, Dr. Paul King, Lt. Kevin Horn, and Lt. Anthony Trombley. I would like to specifically acknowledge the immense help of Mr. Rich Ryman for his patience and advice regarding test bench integration and hardware. I would like to thank Mr. Dave Burris for his help in developing and improving the LabVIEW control software without which this project would have been nearly impossible.

Alex K. Rowton

Table of Contents

Page

List of Figures

Page

List of Tables

Page

Nomenclature

Symbol	Definition
A	cross-sectional area
A/F	air to fuel ratio
B	bore
L	stroke
$\dot{m}_a$	air mass flow
$\dot{m}_{cool}$	cooling air mass flow
$\dot{m}_f$	fuel mass flow
mep	mean effective pressure
N	engine rotational speed
n_R	crank revolutions per power stroke
p	pressure
P_b	brake power
P_f	friction power
P_i	indicated power
P_{meas}	measured power
P_{mfr}	manufacturer rated power
Q_{cool}	heat transfer to engine cooling medium
Q_{HV}	calorific heating value of fuel
R	universal gas constant
r_c	compression ratio
SA	cylinder surface area
$\bar{S}_p$	mean piston speed
sfc	specific fuel consumption
T	temperature
T	torque
V	volume
V_c	clearance volume

Symbol	Definition
V_d	swept volume
$W_{c,i}$	indicated work per cycle
β	cutoff ratio
γ	ratio of specific heats
η_c	combustion efficiency
η_f	fuel conversion efficiency
η_m	mechanical efficiency
η_t	thermal efficiency
ϕ	equivalence ratio

List of Abbreviations

Abbreviation	Definition
AKI	anti-knock index
AFIT	Air Force Institute of Technology
AFRL	Air Force Research Laboratory
BMEP	brake mean effective pressure
BSFC	brake specific fuel consumption
BTDC	before top dead center
CAD	crank angle degrees
CI	compression ignition
COTS	commercial off the shelf
CoV	coefficient of variance
DAQ	data acquisition system
DI	direct injection
DoD	Department of Defense
ECU	engine control unit
EGT	exhaust gas temperature
FI	forced induction
FMEP	friction mean effective pressure
GUI	graphical user interface
IC	internal combustion
IMEP	indicated mean effective pressure
ISR	intelligence, surveillance, reconnaissance
MAP	manifold absolute pressure
MON	motor octane number
MSL	mean sea level
NA	naturally aspirated
PFI	port fuel injection
PRF	primary reference fuel
RON	research octane number

Abbreviation	Definition
RPA	remotely piloted aircraft
SI	spark ignition
TBI	throttle body injection
UMD	University of Maryland

MEASURING SCALING EFFECTS IN SMALL TWO-STROKE INTERNAL COMBUSTION ENGINES

I. Introduction

The purpose of this research is to provide insight into the scaling effects of cylinder surface area to swept volume ratio on small internal combustion (IC) engines in the 25 cc to 100 cc regime. The primary motivation behind this research is to better define the performance of small IC engine propulsion systems typically used on remotely piloted aircraft (RPA) platforms. Historically, engines of this size have been adapted from hobby aircraft or handheld equipment to act as propulsion sources for small RPA. Unfortunately, little to no accurate technical performance data is available for these engines. This research aims to reduce this knowledge gap by characterizing a series of small two-stroke IC engines that are representative of the propulsion systems used in small RPA.

1.1 Motivation

In recent years the demand for small RPA has increased dramatically for the purpose of intelligence, surveillance, and reconnaissance (ISR) among other US Department of Defense (DoD) needs [1]. There are many different airframe designs to satisfy various mission requirements, so power requirements can change depending on size, weight, and payload configuration. Typically though, small RPA power requirements fall within a range of 1-10 kW for propulsion systems. This corresponds to Group 2 RPA according to the US Air Force's *RPA Vector* [1]. Group 2 RPA are

typically 21-55 lbs in weight and fly at altitudes < 3,500 ft above ground level. Flight speeds for this classification of RPA are < 250 kts.

As the US DoD relies more heavily on unmanned flying ISR platforms, the demand for longer range, endurance, and loiter times is ever increasing. These goals can be achieved with increased on-board energy stores or by reducing airframe weight, thereby reducing lift requirements for lower aerodynamic drag. RPAs typically use state of the art materials already, so performance gains by way of weight reduction are very small or non-existent. As a result, on-board energy storage remains an area of particular interest for small RPA performance improvement. Two of the most common propulsion system configurations for this type of aircraft are an electric motor in conjunction with a battery for energy storage and an IC engine burning hydrocarbon fuels. Although technological advancements have allowed great improvements in the capability of the motor and battery configuration in recent years, the energy density of today's state of the art battery is still much lower than a typical hydrocarbon fuel used in IC engine operation according to research on the design of hybrid-electric RPA by Ausserer [2]. Therefore, a RPA incorporating a hydrocarbon fueled IC engine into its design can typically achieve better range, endurance, and loiter time compared to its battery-powered, electric motor equipped counterpart. As IC engine size is reduced, however, efficiency tends to fall off. The scope of this research will focus on an investigation of the capability of appropriately sized IC engines for the advancement of small RPA technology and performance. Ultimately, this research aims to accurately measure power production and efficiency levels as a baseline for future improvement in engine design and RPA performance capability.

Manufacturers of RPAs are encouraged to keep costs low, so commercial off the shelf (COTS) components are used wherever possible, most notably the IC engine used for propulsion. Unfortunately, RPA manufacturers adapt appropriately sized IC engines from the radio-controlled hobbyist aircraft industry or the hand-held equipment industry. Historically, the need for thorough technical performance data in these applications was unnecessary, so the research support required to generate these data was simply non-existent. In the realm of ISR RPAs, rigorous technical performance data is an absolute must for reliable and predictable mission performance. Engines in the automotive or passenger aircraft industry all the way up to massive shipboard marine diesel IC engines correspond to medium to large IC engine size classes (approximately 1000 cc and up). The widespread use of engines in these size classes has led to thorough technical investigations of many aspects of performance and loss characterization; there is a plethora of accurate technical performance data in the literature. Scaling down IC engines to smaller displacements (< 100 cc); however, tend to introduce less well-defined performance trends. When considering the power output of IC engines with respect to their cylinder surface area to swept volume ratio, there is a dramatic change in power scaling trends at approximately 1.5 cm^{-1}. At this size, loss mechanisms like thermal quenching and friction are expected to dominate causing performance and efficiency characteristics suffer [3]. Thermal quenching is a phenomenon in which a combustion flame front is extinguished because the energy necessary to propagate a reaction is extracted from the burning mixture. In IC engines, this typically caused by the interaction of the flame front with the relatively cool cylinder walls. Furthermore, small IC engines (> 1 cm^{-1}) have limited technical performance data available compared to IC

engines in larger size classes. Therefore, it is important to establish accurate performance figures for a family of geometrically similar engines in the size class of approximately 1.5 cm^{-1} in order to better predict and model the loss mechanisms as well as other phenomena that contribute to lower efficiencies in small IC engines. This research focuses primarily on losses associated with friction and heat transfer to engine cooling. Because the cylinder surface area to swept volume ratio of engines increases with reduction in engine size, it is expected that surface area based losses like friction and heat transfer will dominate more in smaller engines. Engine size in this case can be correlated to cylinder bore since IC engines do not usually stray greatly from a bore/stroke ratio of unity. Heywood cites that typical IC engine bore/stroke ratios range from 0.8 to 1.2 for small to medium sized IC engines [4].

1.2 Research Objectives

The overarching goal of this endeavor is to improve the efficiency and performance of the typical small IC engine. Before improvements can be made; however, a series of small IC engines must be tested to establish a baseline of performance. This research aims to identify the loss mechanisms that cause poor performance in small IC engines by accomplishing the following research objectives:

1. Develop a test facility capable of testing small IC engines in the 1-10 kW power range and gathering relevant data to characterize performance and efficiency.
2. Test a series of engines spanning the power scaling transition regime of approximately 1.5 cm^{-1} (in terms of cylinder surface area to swept volume ratio) to establish accurate performance baselines.

3. Analyze and create scaling relationships for performance and efficiency among the scaling study engines.

Obtaining baseline performance data for a series of engines in this size regime is the first step in identifying the accurate capabilities of small IC engines. With accurate performance data, scaling relationships can be generated for improved engine selection based on RPA power requirements. Identifying the significant loss mechanisms will guide future research endeavors in an effort to improve small IC engine performance. Ultimately, the results of this study will emphasize characteristics of the engines in need of improvement so modifications and further testing can be completed in the future.

1.3 Methodology

To begin this process, I performed an investigative survey of the scientific literature related work in small IC engine performance characterization to determine the existence and availability of published data on IC engines of this size. I determined that the literature lacked sufficient data to accurately estimate the baseline performance of engines in the 25 cc to 100 cc size regime, so a series of engines was chosen to perform a baseline scaling study. More information on engine selection is discussed in Chapter III of this document. A team of researchers constructed a test bench capable of testing these engines. I tested and recorded the baseline performance of each engine. I evaluated instrumentation uncertainty and performed multiple independent test runs of each engine to ensure correct data was obtained. I analyzed the performance results to generate scaling relationships among the engines in terms performance changes with respect to engine size.

1.4 Thesis Overview

This chapter serves as introduction to the research of this work. It discusses the motivation behind this endeavor, research objectives, and how the work was performed. Chapter II includes a review of pertinent aspects of IC engine operation and performance as well as discussion of related work. The description of the scaling study engines, test facility, and test methodologies is contained in Chapter III. The experimental results are shown and discussed in Chapter IV. Chapter V reviews the conclusions that were drawn from the experimental results. It also provides recommendations pertaining to future work associated with this project.

II. Literature Review

The United States Department of Defense (DoD) has an ever-increasing interest in the use of small remotely piloted aircraft (RPA) as intelligence, surveillance, and reconnaissance (ISR) mission assets. Consequently, the demand for small, long range, high loiter time RPA has increased in recent years. Current technology encourages the design of propulsion systems for these classes of aircraft to utilize hydrocarbon fueled, reciprocating internal combustion (IC) engines based on a combination of high energy density and relative energy conversion efficiency. This leads to a problem. Customer requirements including low cost and high availability encourage RPA manufacturers to use IC engines that are typically found in hobbyist aircraft or even hand held power equipment. For these applications manufacturers do not often provide thorough performance data and in some cases the data is non-existent. In the case of RPA propulsion, however, performance data is critical to mission effectiveness. This knowledge gap presents an opportunity to research the performance characteristics of typical engines. This particular investigation is focused on smaller engines in the 1-10 kW size class. Specifically, this research aims to discover scaling trends in order to enable more effective RPA design and mission profiling. This thesis will take advantage of that opportunity by investigating the performance of a series of small IC engines designed for small aircraft propulsion. Each is a single cylinder, spark ignited, two-stroke, air-cooled, carbureted engine. With identical compression ratios and similar gas exchange port configurations, this scaling study seeks to understand performance variations due to fundamental design differences and focus on the losses inherent in down-sized ICengines. This chapter will outline the fundamental concepts of how an

internal combustion engine operates and the parameters necessary to characterize its performance. Discussion will then lead to measurement techniques used to quantify engine performance and how performance scales with engine size.

2.1 Background on IC Engines

Internal combustion engines operate on the governing principles of work exchange between a piston and a working fluid within a cylinder. In an internal combustion engine, a mixture of air and fuel (the working fluid) flows into a cylinder. A piston will impart work on the fluid via compression. The high pressure, high density fluid is ignited starting a combustion event. As the combusting gas increases in temperature and pressure it expands, thus imparting a greater amount of work on the piston resulting in a net positive work output. At the end of the expansion process, products of combustion are exhausted from the cylinder so that the cylinder volume can be replaced with a fresh charge of fuel and air in order to repeat the process [5]. This entire process is known as one engine cycle. Although all internal combustion engines operate on these same principles, there are variations on cycles, ignition sources, fuel delivery, and air delivery. A discussion of these engine characteristics follows.

2.1.1 Terminology

A discussion of accepted IC engine performance terms is included here for reference. The primary dimensions of an engine cylinder are bore, B and stroke, L. Cylinder swept volume, V_d is the volume of a cylinder bounded by the plane of the piston at TDC, the plane of the piston and BDC, and the cylinder walls. Clearance volume, V_c is

the volume above the piston in the combustion chamber when the piston is at TDC. These parameters are shown graphically in Figure 1.

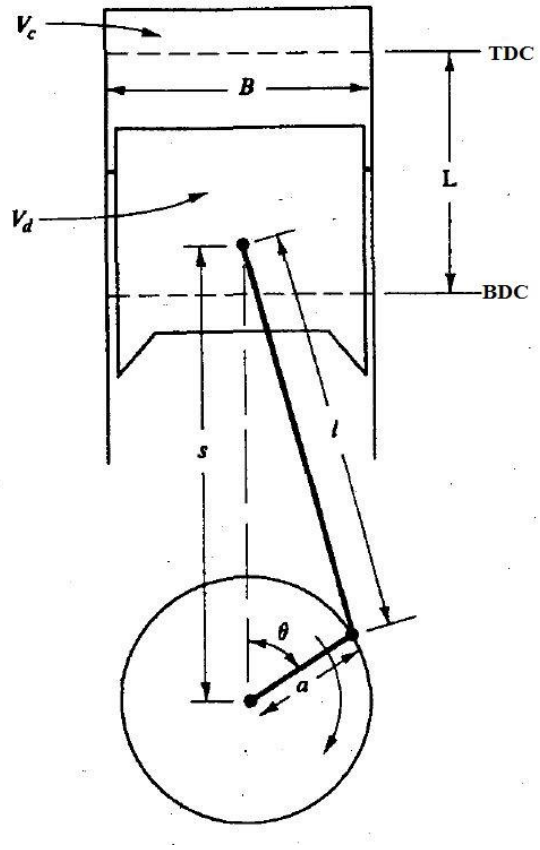

Figure 1: Generic IC engine cylinder geometric parameters [4]

The compression ratio, r_c is the ratio of maximum cylinder volume to minimum cylinder volume over an entire engine cycle. IC engine compression ratio is calculated by the following in Equation 1 where V_d is swept volume (the displacement due to piston movement) and V_c is clearance volume (remaining volume when piston is at top dead center).

$$r_c = \frac{V_d + V_c}{V_c} \quad (1)$$

Torque exerted by an engine is denoted as T. Engine Power output, P is a function of engine speed, N and engine torque, T [4].

$$\boldsymbol{P(kW) = 2\pi N(\frac{rev}{s})T(N \cdot m) \times 10^3} \quad \textbf{(2)}$$

Performance values can vary based on the reference or where a particular parameter is measured. For example, if power is measured at a dynamometer it is referred to as brake power, P_b, but if it is inferred from in-cylinder pressure measurements it is referred to as indicated power, P_i. This subscripting convention is common among all engine performance parameters. Mean effective pressure, mep, is a performance measure that indicates an engine's ability to do work normalized by its displacement volume. Mean effective pressure is a function of engine power, swept volume, engine speed, and a term that references number of crank revolutions per power stroke, n_R (1 for two-stroke, 2 for four-stroke) [4].

$$\boldsymbol{mep(kPa) = \frac{P(kW)n_R}{V_d(dm^3)N(\frac{rev}{s})}} \quad \textbf{(3)}$$

Mean effective pressure can have subscripts of i, b, or f corresponding to indicated, brake, or friction measurements, respectively. Mean effective pressure can also be denoted as IMEP, BMEP, and FMEP for indicated, brake, and friction references, respectively. Specific fuel consumption, sfc, is a measure of an engine's fuel flow rate (mass basis), $\dot{m}_f$ normalized by power output, P [4].

$$\boldsymbol{sfc(\frac{g}{kW \cdot h}) = \frac{\dot{m}_f(\frac{g}{h})}{P(kW)}} \quad \textbf{(4)}$$

Specific fuel consumption is typically normalized by P_b or P_i and is denoted as $bsfc$ or $isfc$, respectively [4].

2.1.2 IC Engine Cycles

There are two fundamental IC engine cycle types: two-stroke and four-stroke. Four-stroke cycle engines are so named because of the number of strokes of the piston required to complete one engine cycle. Given one cylinder of a four-stroke cycle engine, the cycle is described as follows. Starting at top dead center position, a charge of fuel-air mixture is drawn into the cylinder during the piston's first downward stroke called the intake stroke (Figure 2a). As the piston returns to top dead center, the mixture is compressed. This is known as the compression stroke (Figure 2b). At a certain point while the piston is approaching top dead center, the mixture is ignited to begin combustion (Figure 2c). The expansion process of the combusting mixture imparts work on the piston in its second downward stroke, known as the power stroke (Figure 2d). Finally, the burned gases of combustion are then exhausted from the cylinder during the piston's second upward stroke or exhaust stroke (Figure 2e) [4]. A pressure trace of the fluid within the cylinder as a function of cylinder volume for a typical four-stroke cycle is shown in Figure 3.

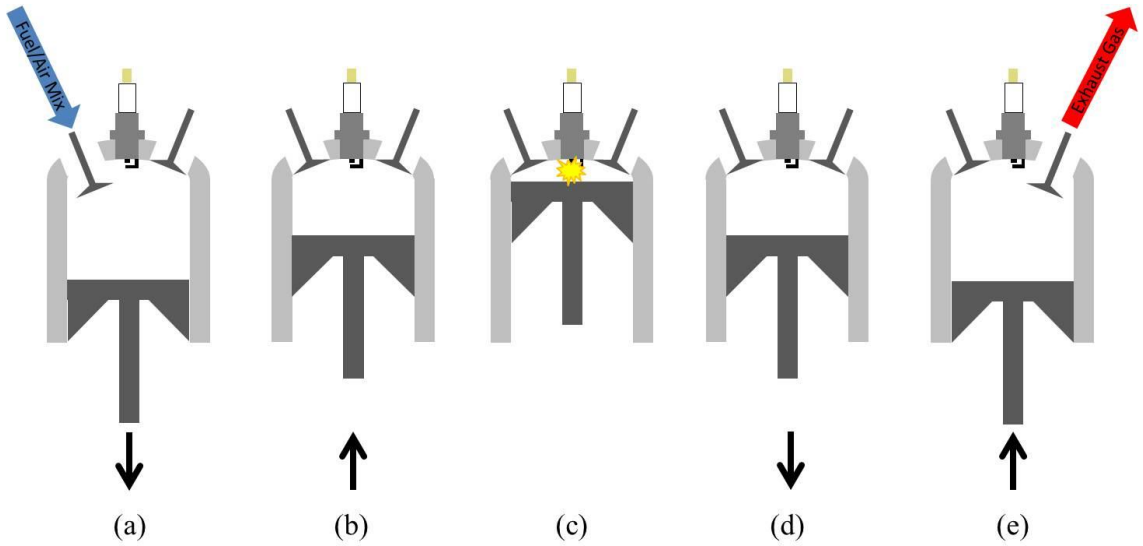

Figure 2: Four-stroke IC engine cycle. (a) Intake stroke (b) Compression stroke (c) Ignition (d) Power stroke (e) Exhaust stroke

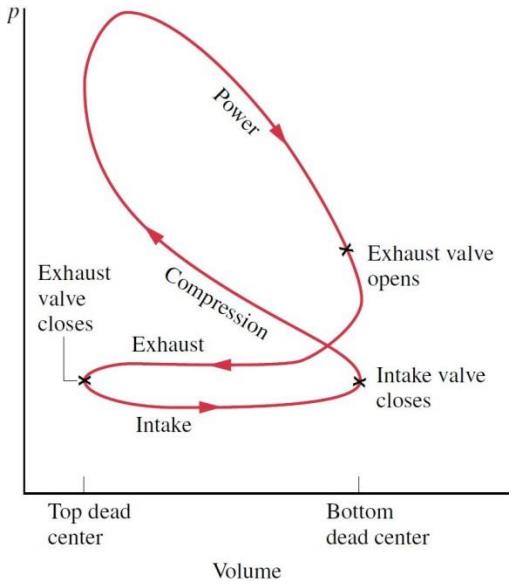

Figure 3: Four-stroke cycle IC engine p-V diagram [6]

An important characteristic of the four-stroke cycle is that there is one power stroke for every two revolutions of the crankshaft. There is an entire crankshaft revolution devoted to pumping out spent exhaust gases and drawing in a fresh charge of

air and fuel. This is known as the pumping loop and contributes negatively to the net work output of a four-stroke cycle engine if the engine is naturally aspirated. The pumping loop can contribute positively to the net work output if the intake air is pressurized above atmospheric conditions. This is called supercharging and is discussed further in Section 2.1.5.

The primary difference between two-stroke cycle engines and four-stroke cycle engines is the gas exchange process. According to a text on two-stroke cycle engines by Heywood and Sher [7], gas exchange is the process of an engine exchanging spent exhaust gases within a cylinder for a fresh charge of fuel/air mixture. Instead of devoting an entire crankshaft revolution to gas exchange like the four-stroke cycle, a two-stroke cycle gas exchange occurs during the transition from the piston's downward stroke to its upward stroke [7]. Given one cylinder of a two-stroke cycle engine, the cycle is described as follows. Starting at the top dead center position, a combusting fuel-air mixture expands and drives the piston downward in the cylinder's power stroke (Figure 4a). At a point in crank angle space determined by position on the cylinder wall, the exhaust port will open causing exhaust blowdown (Figure 4b). At a point later in the cycle, transfer ports will open allowing a fresh charge of fuel-air mixture to enter the cylinder. At this point both exhaust and transfer ports are open, thus facilitating the gas exchange, or scavenging process. Gas exchange continues through the piston's bottom dead center position until the piston moves upward again (Figure 4c). This process is completed when all ports (transfer and exhaust) are once again closed. The piston continues to travel upward in its compression stroke, thus completing the two-stroke engine cycle (Figure 4d) [7]. A pressure trace of the fluid within the cylinder as a

function of cylinder volume for a typical two-stroke cycle is shown in Figure 5. The terminology in Figure 5 refers to the piston's position corresponding to important events in the cycle. In this particular case, EO refers to the point at which the exhaust port opens. SO refers to the transfer port opening. Likewise, SC and EC refer to the transfer and exhaust ports closing. TC and BC in this case indicate the piston at top dead center and bottom dead center respectively.

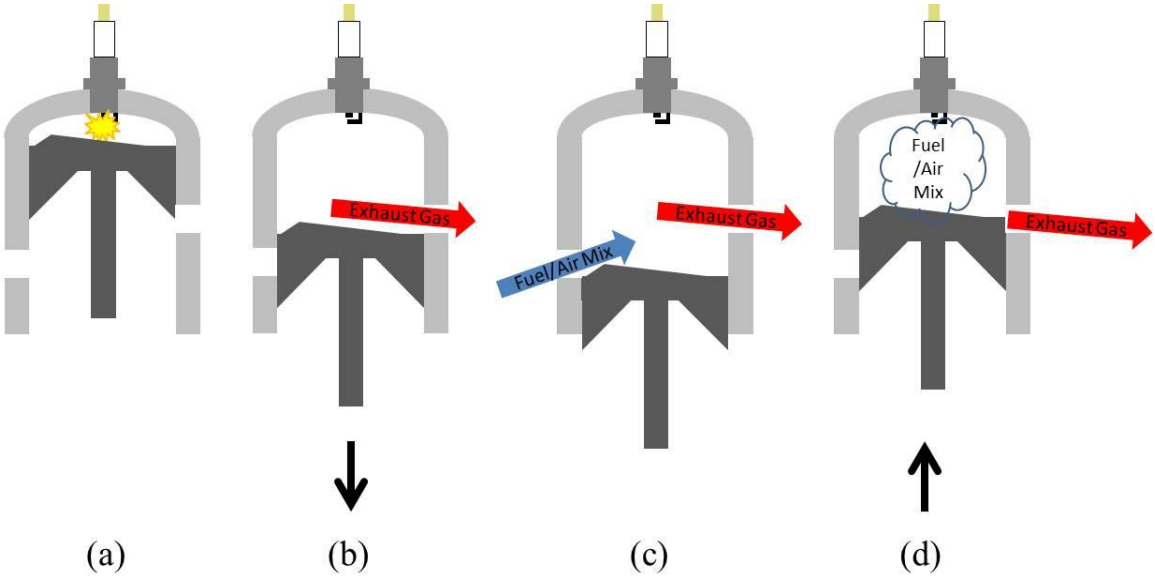

Figure 4: Two-stroke IC engine cycle. (a) Power stroke (b) Exhaust blowdown (c) Gas exchange (d) Compression stroke

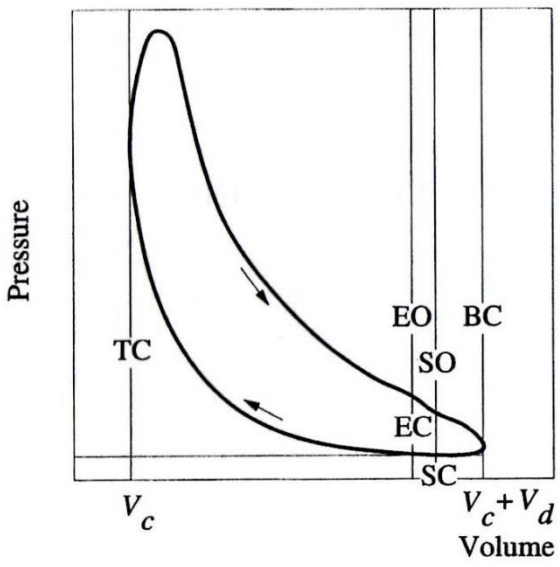

Figure 5: Two-stroke cycle IC engine p-V diagram [7]

The two-stroke cycle allows for one power stroke for every revolution of the crankshaft. It also typically employs a much less complex valve train design, thus allowing for smaller, lighter designs as compared to a four-stroke cycle engine. Two-stroke cycle engines are commonly less efficient than their four-stroke counterparts due in large part to the fact that during the gas exchange process, fresh fuel-air mixture passes through the cylinder directly into the exhaust in a process known as short-circuiting. According to Heywood and Sher, a typical two-stroke engine short-circuits approximately 20% of the delivered fuel/air mixture, thus reducing the ability of two-stroke engines in general to convert available fuel energy to useful work as compared to a four-stroke cycle engine [7]. Steps can be taken to mitigate this process, but short of implementing a direct-injection system, short-circuiting cannot be eliminated. The benefit of direct injection is that only air is scavenged during the gas exchange process. Fuel is then injected into the combustion chamber after all cylinder ports have closed thus eliminating any loss of fuel to the exhaust stream. Engine efficiencies will be discussed

further in Section 2.1.6. Fuel injection methods including direct injection will be expanded upon in Section 2.1.4.

2.1.3 Types of Ignition

Internal combustion engines rely on the combustion of fuel-air mixtures to produce a positive net work output. In order to combust a given fuel-air mixture there are two primary types of ignition source. These are spark ignition (SI) and compression ignition. SI engines discharge a supplied voltage across an open gap within the combustion chamber in order to create a stable flame kernel that will propagate throughout the combustion chamber consuming the fuel-air mixture in the process of combustion. This is done with a spark plug protruding into the combustion chamber that includes a positive and negative electrode electrically isolated from each other apart from a small air gap. SI engines typically use gasoline as a fuel due to its higher relative anti-knock index (AKI). AKI is a rating for fuel based on its chemical resistance to autoignition. AKI is an average of two octane rating numbers, the research octane number (RON) and the motor octane number (MON). Both octane rating methods are based on the results of laboratory testing on a single cylinder engine. The RON method is run at moderate mixture temperatures and 600 ± 6 rpm. The MON method is run at higher mixture temperatures and 900 ± 9 rpm. The octane rating index is based on the corresponding characteristics of a mixture of isooctane and *n*-heptane (typically referred to as a primary reference fuel, PRF). Since the octane rating of isooctane is 100 while that of *n*-heptane is 0, a fuel with a given octane rating will have the same resistance to autoignition as its corresponding blend of primary reference fuel [8]. SI engines require a fuel with resistance to autoignition due in large part to the fact that air and fuel are pre-

mixed before entering the combustion chamber. Therefore, the fuel must be able to resist ignition during compression so that it can be ignited at precisely the right time to maximize power output. The remaining reason SI engines utilize autoignition resistant fuels is that once ignition has occurred from spark discharge, the expanding flame kernel can cause increases in temperature and pressure ahead of the flame front which would otherwise cause fuel autoignition were it not for the fuel's chemical resistance.

In a study performed by Arcoumanis and Bae [9] on correlations between spark characteristics and combustion, they found that gap between a spark plug's electrodes had an effect on energy release and flame propagation speed. They studied spark plugs with gaps ranging from 0.6 mm to 1.9 mm. In a given test they reported an increase in released energy from 15 mJ to 30 mJ from the 0.6 mm spark plug gap to the 1.9 mm spark plug gap which led to faster flame propagation after the onset of spark. Furthermore, they discovered that the lean combustion limit was extended to an equivalence ratio of 0.55 for spark plug gaps larger than 1.6 mm when a spark duration of 5 ms was used [9].

Compression ignition (CI) engines rely on auto-ignition to initiate combustion during an engine cycle. During intake, only air flows into the cylinder. Near the end of the compression stroke, fuel is injected directly into the combustion chamber. Conditions in the cylinder are above the ignition point for the fuel, so autoignition occurs shortly after fuel has been injected. CI engines typically utilize heavier fuels, or fuels with larger hydrocarbon chains due to their lower anti-knock thresholds. Since CI engines do not mix air and fuel until late in the engine cycle, chemical ignition resistance is not a

required characteristic of the fuel. This means CI engines can operate at compression ratios (r_c) ranging from 12 to 24 depending on design [4].

By comparison, SI engines typically are limited to compression ratios ranging from 8 to 12 due to the fact that air and fuel are mixed early in the engine cycle. An engine's compression ratio is the ratio of cylinder volume when the piston is at bottom dead center (BDC) to the cylinder volume when the piston is at top dead center (TDC). Diesel fuels are compared based on their cetane number. Cetane number is a measure of the delay before ignition occurs after fuel is injected into a combustion chamber. A higher cetane number corresponds to a fuel that will ignite more readily. Like MON and RON methods, the cetane number measurement method requires particular conditions. They are as follows: inlet temperature is 339K, jacket temperature is 373K, engine speed is 900 rpm. The engine used for cetane number measurements has a variable compression ratio. Under the stated operating conditions, compression ratio is adjusted so that the ignition delay is 13° of crank angle. Therefore, injection timing occurs at 13° before TDC for optimum ignition timing [10]. The calculation of cetane number is shown in Equation 5.

$$\boldsymbol{Cetane\ No.} = \%\ \boldsymbol{hexadecane} + \mathbf{0.15} \cdot \%\ \boldsymbol{heptamethylnonane} \qquad \mathbf{(5)}$$

A relationship between cetane number and MON is shown in Figure 6 below. It can be seen that typical diesel fuels have a relatively low MON meaning their tendency to autoignite is high. This makes CI fuels poor candidates for operation in a SI engine without taking proper precautions [10]. In their work characterizing the performance of a SI two-stroke direct injection IC engine operating on a kerosene based aviation fuel,

Falkowski, Abata, and Cho [11] found that SI engine operation was possible with a low octane fuel at moderate speeds and loads. High engine loads and speeds were never achieved without the presence of knock. Falkowski, Abata, and Cho found that retarding spark timing was the most effective method for reducing or eliminating knock. Knock was eliminated at up to 60% of maximum fuel delivery by retarding spark timing to 5° before TDC at 2000 rpm [11].

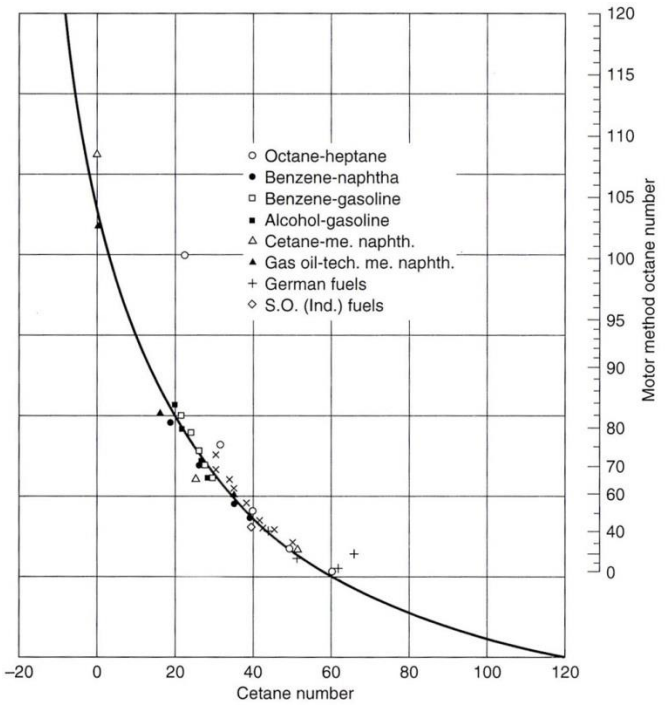

Figure 6: Cetane number versus MON for common ICE hydrocarbon fuels [10]

2.1.4 Fuel Delivery

Fuel metering and delivery is an important factor in the performance and efficiency of an internal combustion engine. The air to fuel (A/F) ratio that makes up the fresh charge must be maintained within the limits of combustibility in order for the engine to operate. Typically there are two different mechanisms for metering and delivering fuel, the carburetor or fuel injector. A/F ratio is the ratio of air to fuel on a

mass basis or mass flow basis in the case of a moving fluid which is common in IC engines.

Carburetors rely on low pressure within a venturi to draw fuel into the intake air stream. The pressure difference is caused by the acceleration of air through the venturi. Fuel is discharged through a tube directly into the air stream. As the fuel and air mix, the fuel disperses into small droplets that eventually evaporate to create a combustible air and fuel vapor mixture before entering the cylinder's combustion chamber. Key carburetor components such as the venture, fuel discharge tube, and throttle plate among others are depicted in Figure 7 which shows a basic carburetor design. The typical ideal behavior of air and fuel flow and the mixture process is identified by red and blue dots corresponding to fuel and air particles respectively. Since fuel flow depends on intake air stream velocity, more fuel is drawn in as an engine's throttle plate is opened [4]. Carburetors rely completely on mechanical systems to meter fuel; therefore, they do not require electrical power or various sensors and instrumentation for proper operation. On the other hand, they must be adjusted precisely and cannot adapt easily to changing conditions during engine operation. This introduces the largest drawback to carbureted engines which is the lack of precise control over A/F ratio over a broad range engine speeds and loads [12].

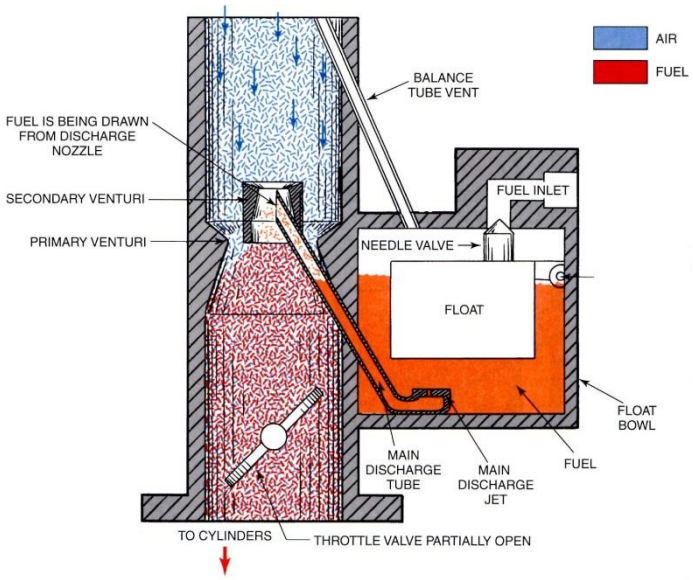

Figure 7: Basic carburetor schematic [13]

In order to overcome this problem, fuel injection has been used heavily in various IC engine applications due to its ability to precisely meter fuel flow and hence A/F ratio. Fuel injection is used in a variety of configurations including throttle body injection (TBI), port fuel injection (PFI), and direct injection (DI) and can be controlled electronically or mechanically. Mechanical fuel injection does not realize the full benefits of fuel flow control that electronic fuel injection does due primarily to the same reasons as in carburetors. Most modern IC engines employing fuel injection are electronically controlled, so it will be the control method discussed further.

The difference among TBI, PFI, and DI is the location of the fuel injector. In a TBI configuration, fuel is injected at a single point upstream of the throttle plate. A PFI system injects fuel into the intake port of an engine's cylinder, so there is usually one injector per cylinder in a multi-cylinder engine application. A DI system injects fuel directly into the combustion chamber [4]. Regardless of configuration, the fuel injector operates on the same principle. Fuel is supplied to the injector via an electric fuel pump

at a relatively high fixed pressure. A passage inside the injector is held closed by a spring-loaded plunger. The fuel passage is highlighted in orange in Figure 8. The plunger is actuated electromagnetically by applying an electric current pulse to the injector solenoid as shown by the solenoid winding. Fuel metering is performed by varying the duration of the current pulse. A cross-sectional view of an electronic fuel injector is shown in Figure 8. Key components such as the solenoid, spring, and fuel passages are indicated.

Fuel injection systems require feedback from an assortment of sensors to operate correctly. A lambda sensor in the exhaust stream is used to detect the partial pressure of oxygen in the exhaust relative to the partial pressure of oxygen in atmospheric air. This assessment of exhaust gas composition is used to determine the A/F ratio and adjust the amount of fuel injected accordingly to maintain conditions at or close to stoichiometric. Intake manifold pressure, temperature, and air flow rate are typically measured so the engine's control system can account for changes in ambient conditions or rapid changes in throttle or engine load. An additional advantage of fuel injectors is their ability to atomize fuel. Large pressure drop across a very small orifice as fuel exits an injector causes fuel droplets to atomize and evaporate much faster compared to a carbureted engine, thus promoting more efficient and faster burn characteristics during the combustion process. Taking all of these characteristics into account, electronically controlled fuel injection allows for more control over A/F ratio which leads to higher IC engine operating efficiencies. Unfortunately, these benefits require a more complex array of sensors and control systems as well as electrical power to maintain functionality [4].

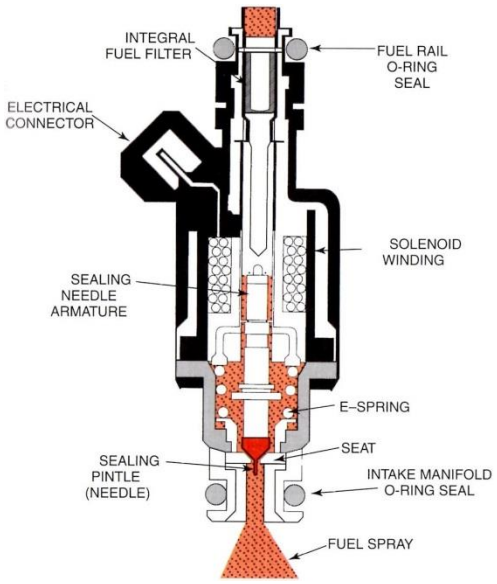

Figure 8: Cutaway view of an electronic fuel injector [13]

2.1.5 Induction Methods

Just as fuel delivery is an important aspect of internal combustion engine performance, air induction is equally as important. Air induction can be categorized into two main classes, natural aspiration (NA) and forced induction (FI). Engine performance is dependent on the temperature and pressure of air delivered to the combustion chamber. These factors ultimately dictate air density. As air density increases, more air can be delivered to the combustion chamber during a given engine cycle. Assuming stoichiometric conditions, more fuel must then be delivered. During the combustion event, higher pressures will be attained, increasing work output. Conversely, as air density decreases work output will also decrease [4].

NA engines rely on vacuum pressure to draw air through the throttle body, intake manifold, and into the combustion chamber. The vacuum pressure (also known as engine load) necessary for this method occurs naturally as a result of engine operation. Vacuum pressure scales with engine speed and is largely affected by throttle plate position. An

engine at high speed with a closed throttle will have a very high vacuum pressure while an engine at idle with an open throttle will have little to no vacuum pressure. This induction method has the least complexity but suffers considerable performance losses due to pressure drops or temperature increases [4].

To overcome performance losses due to lack of air density, intake air can be pressurized above atmospheric conditions by a variety of different methods. Typical FI methods for pressurizing intake air are supercharging and turbocharging. The primary difference between the two stems from how they are driven. Superchargers use the engine crankshaft to spin a compressor while turbochargers utilize the expansion of hot, high pressure exhaust gases to spin a compressor [13]. In an attempt to increase air density, these devices compress air as it enters the engine. This process also increases air temperature which has adverse effect on air density, so FI engines are typically fitted with a heat exchanger downstream of the compression device to reduce intake air temperatures. Supercharging or turbocharging adds a significant level of complexity to an engine's induction system, but performance becomes much less sensitive to decreases in ambient air density.

Another advantage of FI engines is that pumping work (work required to draw in and compress a fresh intake charge), which contributes negatively to net work output in a typical NA four-stroke application for example, becomes positive and increases the net work output of an engine over a given cycle. For example, the pumping loop (lower loop) indicated in the four-stroke pressure-volume diagram of Figure 3 would be situated above the ambient pressure reference line, and therefore would contribute positive work to the overall work output of the engine's cycle. Typically superchargers, being

crankshaft driven, exhibit a fast response time in terms of intake compression versus engine speed change via throttle input. The drawback to this configuration is that the supercharger compressor is constantly drawing power from the crankshaft in order to perform work on the intake air. Alternatively, turbochargers are driven by exhaust gases, so they do not draw power from the engine's crankshaft. This configuration's drawback is the time delay that exists as exhaust gas imparting work on a turbine must overcome rotational inertia and spool the turbocharger to a sufficient speed in order to compress intake air. This time delay is commonly referred to as turbo lag.

An alternative to supercharging or turbocharging is the use of a pressure wave supercharger. A pressure wave supercharger is a device in which a rotor is driven off the engine's crankshaft. Hot, high pressure exhaust gas is directed through an end wall down the rotor's longitudinal axis. Simultaneously, low temperature, low pressure intake air is inducted through the opposing end wall in the opposite direction of exhaust gas flow. As the gases meet in the rotor, the high pressure exhaust wave compresses the intake air. Upon gas interaction, the flows reflect off each other and exit through the same end walls they entered. The time in which this process occurs is sufficiently fast that the temperature of the intake air does not rise so much as to be detrimental to engine performance. Mataczynski has successfully modeled and built a pressure wave supercharger for a 95 cc IC engine in order to recover performance losses when operating at high pressure altitudes [14]. The pressure wave supercharger is shown to have a smaller lag time compared to a similarly sized turbocharger. The device is capable of higher efficiencies with smaller spatial requirements as compared to conventional turbochargers or superchargers [14].

2.1.6 Efficiency

IC engine efficiencies are an important metric to consider in performance characterization. An IC engine cycle is a thermodynamic process, and therefore must follow the first law of thermodynamics. In its simplest form, an IC engine can be reduced to a single piston-cylinder combustion system. Energy enters the system as chemical potential energy in the form of fuel enthalpy. This energy is dispersed among several different paths including to the engine's cooling medium, surface friction (piston-cylinder, bearings, etc.), exhaust enthalpy, incomplete combustion, as well as other miscellaneous pathways like radiation and oil cooling. The energy flow paths in an IC engine are shown in Figure 9. See Table 1 for a list of relevant terms. This work will focus on the measurement and characterization of brake and indicated power which yields frictional losses as well as energy loss to the engine cooling medium. Estimations of exhaust chemical and sensible enthalpies can be made based on assumptions from literature.

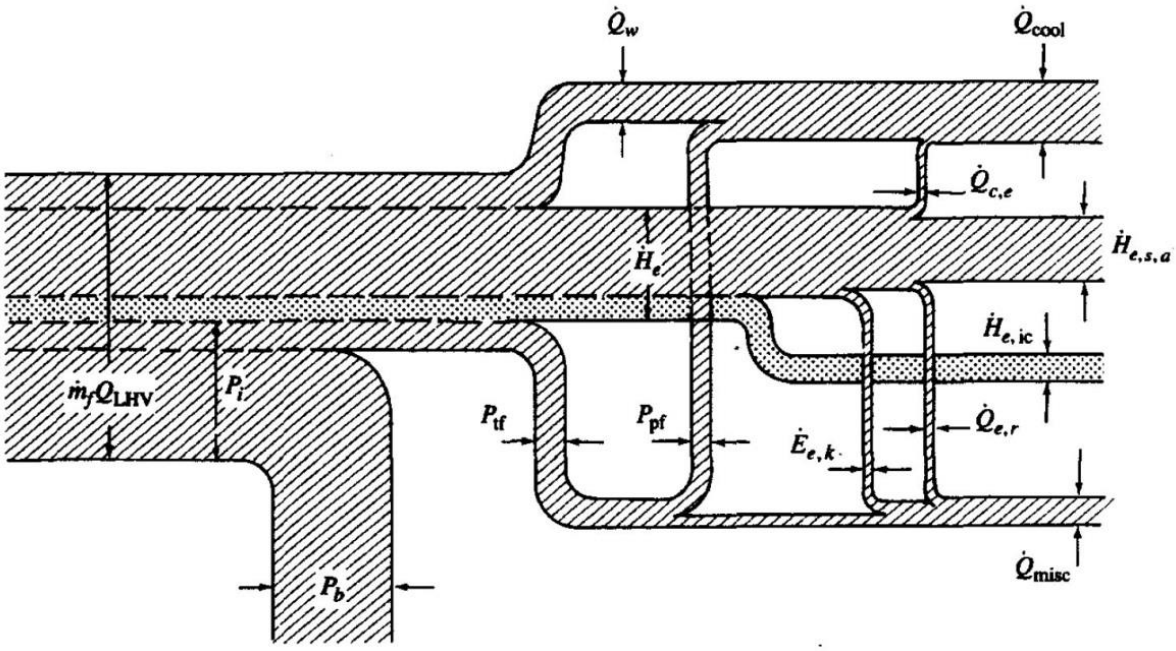

Figure 9: ICE energy flow diagram [4]

Table 1: ICE energy flow diagram terms [4]

$\dot{m}_f$	fuel mass flow	$\dot{Q}_{cool}$	heat rejection rate to coolant
Q_{LHV}	fuel lower heating value	$\dot{Q}_{c,e}$	heat transfer rate to coolant from exhaust ports
P_i	indicated power	$\dot{H}_{e,s,a}$	exhaust sensible enthalpy flux entering atmosphere
P_b	brake power	$\dot{H}_{e,ic}$	exhaust enthalpy flux due to incomplete combustion
$\dot{Q}_w$	heat transfer rate to combustion chamber wall	$\dot{E}_{e,k}$	exhaust kinetic energy flux
$\dot{H}_e$	exhaust enthalpy flux	$\dot{Q}_{e,r}$	heat flux radiated from exhaust
P_{tf}	total friction power	$\dot{Q}_{misc}$	remaining energy fluxes and transfers
P_{pf}	piston friction power		

Depending on the design of an IC engine, it follow the principles of either the Otto cycle or the Diesel cycle pictured in Figure 10a and Figure 10b respectively. The

Otto cycle consists of four internally reversible processes. Concerning Figure 10a, 1 to 2 is an isentropic compression, 2 to 3 is a constant volume heat addition, 3 to 4 is an isentropic expansion, and 4 to 1 is a constant volume heat rejection. The constant volume heat addition assumes a virtually instantaneous burn rate for fuel and air such that volume does not change. The area under 3-4 represents work out of the cycle while the area under 1-2 represents work into the cycle. Therefore, the area enclosed by 1-2-3-4 indicates the net work out of the system. The Otto cycle usually corresponds to gasoline-fueled spark ignition engines. Performing a cycle analysis yields the thermal efficiency, η_t of each cycle as a function of compression ratio, r_c and ratio of specific heats, γ. Compression ratio in Figure 10a is depicted as the volume at 1 divided by the volume at 2 [6].

$$\boldsymbol{\eta_{t_{Otto}} = 1 - r_c^{1-\gamma}} \qquad \textbf{(6)}$$

The Diesel cycle assumes a constant pressure heat addition from 2 to 3; otherwise it operates similarly to the Otto cycle. Like the Otto cycle, net work out is represented by the area enclosed by 1-2-3-4. This cycle usually corresponds to diesel-fueled compression ignition engines. A cycle analysis yields the thermal efficiency as a function of compression ratio, ratio of specific heats, and cutoff ratio, β. Cutoff ratio is depicted as the volume at 3 divided by the volume at 2 in Figure 10b [6].

$$\boldsymbol{\eta_{t_{Diesel}} = 1 - \frac{1}{r_c^{\gamma-1}} \frac{\beta^{\gamma}-1}{\gamma(\beta-1)}} \qquad \textbf{(7)}$$

Engine thermal efficiencies are a theoretical maximum attainable efficiency. In reality, an IC engine cannot achieve efficiencies this high due to many other losses.

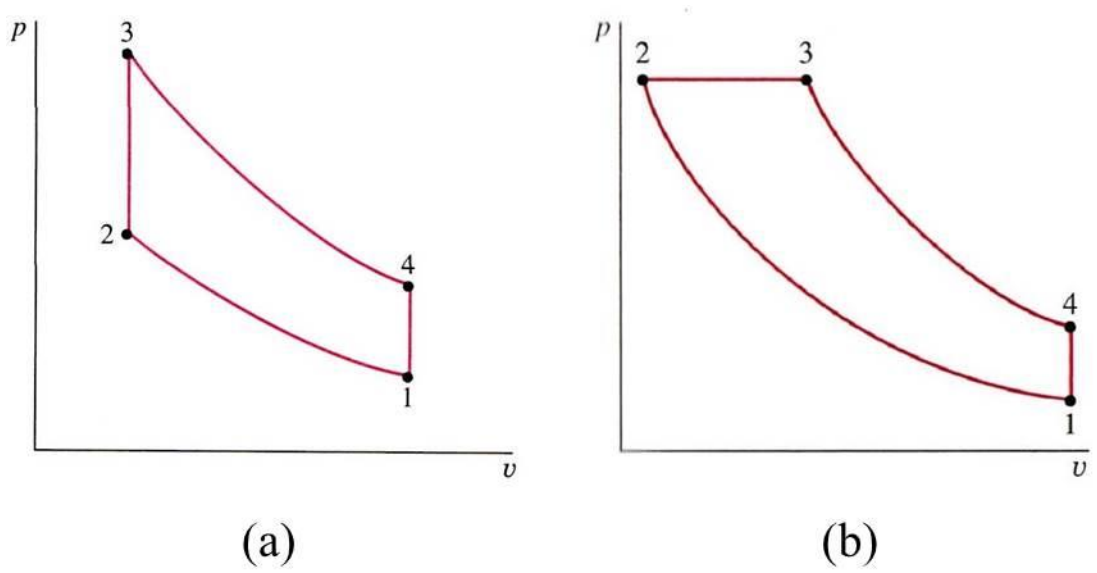

Figure 10: Ideal thermal engine cycles, (a) Otto cycle, (b) Diesel cycle [6]

In an ideal case, fuel and air would enter at stoichiometric conditions and react completely during a combustion event; however, this is never the case. Approximately 95% of fuel delivered in a cycle reacts during a combustion event in a typical best case scenario. The ratio of fuel burned versus fuel delivered in a single engine cycle is known as an engine's combustion efficiency, η_c. Many factors tend to lower this percentage further including fuel-rich mixture ratios and thermal quenching losses. Mixture ratio and its effects on performance are discussed further in Section 2.2.1. Thermal quenching losses and their dependence on engine size are covered in more detail in Section 2.4.

In a practical application, an IC engine must transmit work to some sort of load via a drivetrain. Regardless of design, said drivetrain will exhibit some amount of power dissipative loss (friction) that must be taken into account. The ratio of power delivered to the load versus indicated power in considered mechanical efficiency, η_m.

2.2 Engine Performance

There are multiple factors that must be optimized in order to attain the highest performance and efficiency from an IC engine. The principles that govern engine performance consist of combustion physics and fluid flow. These topics will be discussed in the following sections in terms of equivalence ratios, ignition timings, abnormal combustion, short-circuiting, and blow-by.

2.2.1 Equivalence Ratio

The ratio of fuel to air in an induction charge has a significant effect on engine performance. In an ideal case, a prescribed mass of fuel will react with a mass of oxidizer (usually air) dictated by the fuel's corresponding global combustion reaction equation. The ratio of these amounts of fuel and air is known as the stoichiometric air-to-fuel ratio, $(A/F)_S$. In a realistic situation, the proportions of air and fuel can diverge from stoichiometric conditions yielding a different A/F ratio. An equivalence ratio, ϕ, is defined as the ratio of $(A/F)_S$ to actual A/F.

$$\boldsymbol{\phi = \frac{(A/F)_S}{(A/F)}} \qquad \textbf{(8)}$$

An equivalence ratio of unity indicates operating conditions are at stoichiometric. Equivalence ratios less than unity correspond to fuel-lean conditions while equivalence ratios greater than unity correspond to fuel-rich conditions.

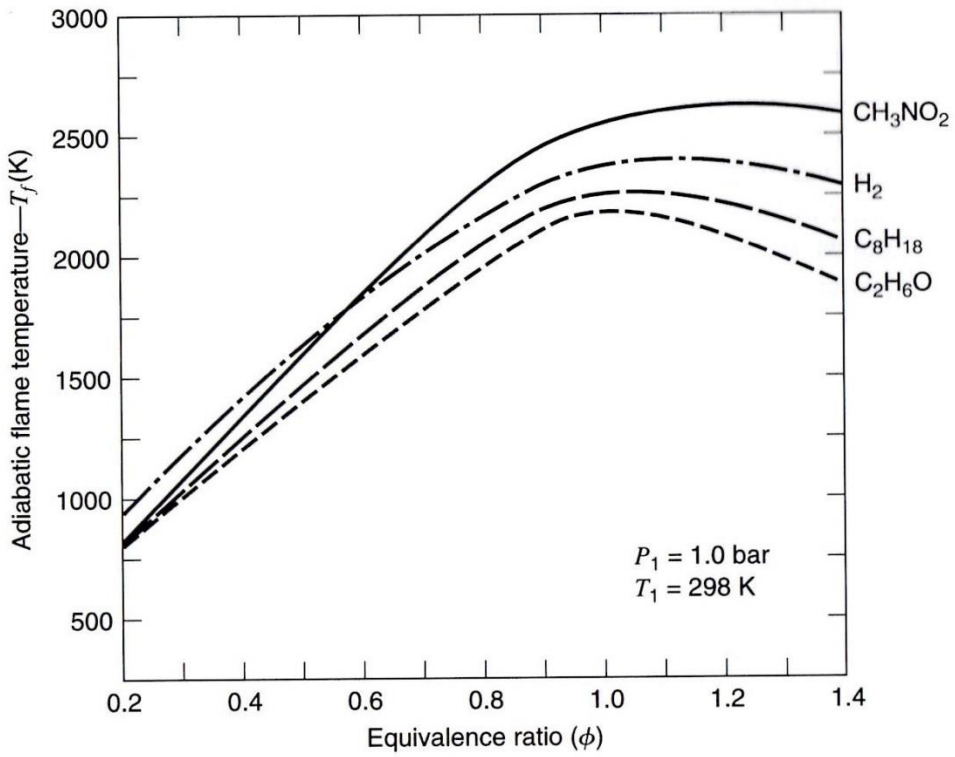

Figure 11: Adiabatic flame temperature as a function of equivalence ratio, ϕ [10]

Engine work output on a per cycle basis directly corresponds to the amount of pressure acting on the piston inside the cylinder. According to the ideal gas law, maximum pressures can be realized when the combustion reaction temperature is maximized. Figure 11 shows adiabatic flame temperatures for a variety of fuels in air as a function of equivalence ratio. If the enthalpy of products is the same as the enthalpy of reactants in a combustion reaction, the resultant temperature change would yield the adiabatic flame temperature. Octane (C_8H_{18}) is a large constituent of typical gasoline blends; therefore its behavior closely reflects that of gasoline. For octane, flame temperature peaks at an equivalence ratio of unity or slightly higher [10]. Therefore it is beneficial to maintain stoichiometric conditions as much as possible in order to extract the maximum amount of energy from a combustion reaction.

Combustion efficiency is an ever-present factor though, so even at stoichiometric conditions there will be a residual fraction of unburned fuel. Heywood cites that typical SI engines have a maximum combustion efficiency of 95% at equivalence ratios of 1 or lower [4]. As equivalence ratio increases, a lack of sufficient oxygen limits the amount of fuel that can be burned, so combustion efficiency decreases at an approximately linear rate [4]. This phenomenon can be seen in the plot of combustion efficiency as a function of equivalence ratio for a collection of SI and CI engines in Figure 12.

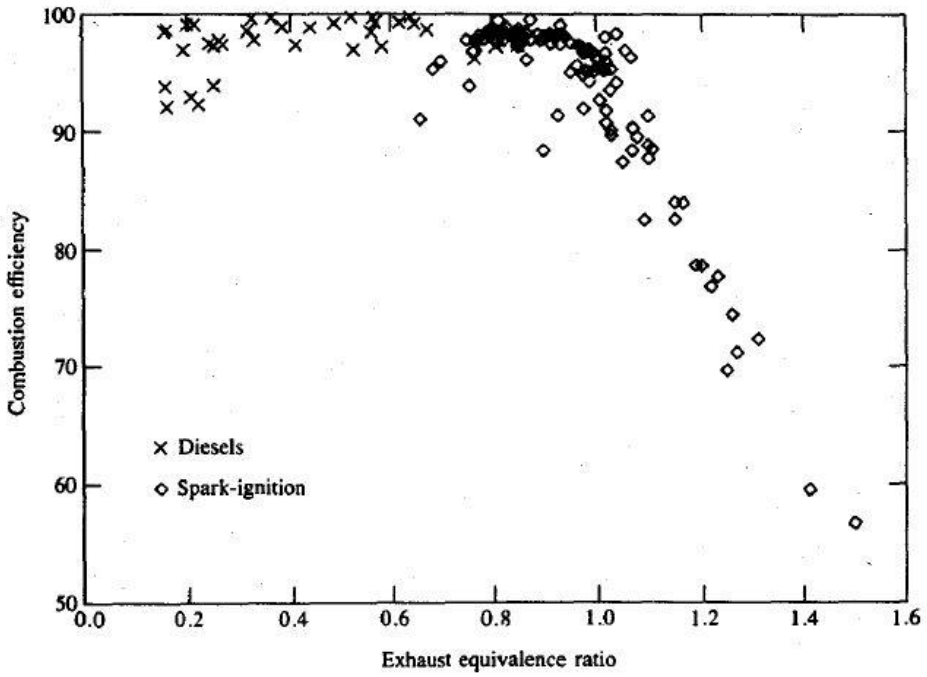

Figure 12: Combustion efficiency vs. equivalence ratio for SI and CI engines [4]

A higher ratio of air to fuel increases the probability of a fuel molecule colliding and reacting with an oxygen molecule. Running lean can increase combustion efficiency. On the other hand, operating at rich conditions will leave a large fraction of fuel left over due to the fact that most oxygen molecules will be reacted towards the end of the reaction. It follows that fuel efficiency is lower in this case; however, a benefit is that

residual fuel can have a cooling effect on the reaction products that will bring the overall temperature of the spent mixture down [8]. Typically, IC engines are tuned to operate at slightly rich conditions for higher loads and speeds as the cooler relative temperatures will limit the propensity of knock or pre-ignition. It is possible to reduce combustion temperatures by running excessively lean as well, but the amount of power loss realized by reducing fuel flow for lean conditions has a more detrimental effect on engine mean effective pressures. In other words, fuel energy converted to shaft power (the desired outcome) falls off at a faster rate than fuel energy converted to waste heat. Knock and pre-ignition are forms of abnormal combustion that can cause severe engine damage. These concepts are discussed in more detail in Section 2.2.3.

2.2.2 Ignition Timing

When a combustion event initiates, a flame front propagates from the ignition point(s) until all reactants are consumed. There is a characteristic time delay involved in this process that corresponds to the flame speed of the particular fuel-oxidizer mixture and the distance over which the flame must travel. In a compression ignition engine, ignition timing is governed by the geometry of the combustion chamber and is not typically an externally controlled variable. In a SI engine, ignition timing is largely a function of engine speed. When ignition occurs too early in the engine cycle, combusting gases in the cylinder pressurize rapidly while the piston is still rising in its compression stroke. This rapid increase in pressure works against the motion of the piston and can damage internal engine components if left unchecked for prolonged operating periods. Conversely, when ignition occurs too late in the cycle, the piston is already moving downward in its expansion stroke. This results in the combusting gas having to fill the

void left by the expanding cylinder volume before actually imparting work on the piston, thus decreasing net work output.

2.2.3 Abnormal Combustion

Thermal efficiency in IC engines has a positive correlation to compression ratio for both the Otto cycle and the Diesel cycle as described by the functions in Equations 6 and 7. These efficiencies are the theoretical maximum efficiencies that can be obtained from an IC engine operating on the Otto or Diesel cycle, respectively. Realistically, however, an IC engine will experience a variety of losses that will reduce the overall thermal efficiency to a value lower than what was dictated by the corresponding compression ratio. Even though an engine cannot reach these levels of theoretical efficiency, the actual efficiency of an IC engine also scales with compression ratio as can be seen in Figure 13 which compares fuel conversion efficiencies at varying compression ratios for three ratios of specific heat [4].

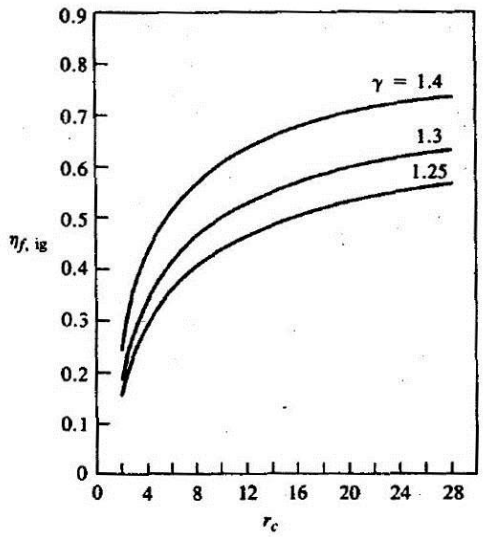

Figure 13: Fuel conversion efficiency as a function of compression ratio [4]

As a SI engine's compression ratio increases, the fuel in the combustion chamber experiences larger increases temperature and pressure during the compression process. At a certain point, conditions can be sufficient to cause the fuel/air mixture to autoignite before the spark discharge. This is known as preignition. Ignition timing is critical to maximizing the amount of work out of the working fluid, so preignition must be avoided. Preignition is a phenomenon unique to IC engines that ingest fuel and air into the combustion chamber already premixed. It can be avoided by keeping fuel and air separate until the end of the compression process. This feature is typical of a direct injection engine. Direct injection is a relatively new and developing technology for SI engines, but it is ubiquitous with CI engines. Another drawback to high compression ratios in SI engines is knock. Knock is the autoignition of fuel/air mixture after the spark discharge, in areas ahead of the expanding flame front due to the additional increase in temperature and pressure from initial combustion. This phenomenon leads to an effective limit on practical compression ratio for engines that operate on typical fuels like gasoline. This concept is known as 'knock limited.' Modern gasoline fueled SI IC engines have compression ratios ranging from 8 to 12 [4]. Partial burn or misfire is another common abnormal combustion characteristic that can occur in SI IC engines. This is usually the result of the spark failing to discharge or not supplying enough energy to create a stable flame kernel that is capable of expanding throughout the combustion chamber. In an investigation of abnormal combustion of a highly turbocharged PFI spark ignition engine, Attard et al. discovered that increasing ignition energy delivered to the combustion chamber from 50 mJ to 100 mJ eliminated the occurrence of partial burns and misfires up to 25 bar BMEP [15].

In compression ignition engines, autoignition is essential to IC engine operation. A critical factor in the effectiveness of the Diesel cycle is injection timing. The start of fuel injection must correspond to the ignition lag time of the fuel. Ignition lag time is based on cylinder temperature and pressure as well as the combustibility of the fuel. Ignition lag time has a negative correlation to temperature and a positive correlation to pressure. In other words, as temperature decreases lag time increases. Therefore adjustments must be made for a CI engine to operate effectively during periods of engine warm-up. Ignition lag time increases with increasing cylinder pressure. This places a limit on the practical compression ratio of a CI engine because excess pressures can cause fuel to ignite before sufficient mixing occurs. In this case, smoke formation occurs as a result of poor mixing leading to suboptimal performance [5].

2.2.4 Short-Circuiting

Heywood and Sher note that short-circuiting is a phenomenon in which a portion of fresh fuel-air mixture passes directly through an engine's combustion chamber into the exhaust stream without combusting [7]. Short circuiting is more common in two-stroke engines given that the fresh charge induction process occurs simultaneously to the exhaust blow down process. Two-stroke engines employ design features to mitigate short-circuiting. Some examples are loop scavenging in which the fresh charge is inducted into the cylinder on the same side as the exhaust port, but in the opposite direction so that it must loop around the entire combustion chamber before being able to exit the exhaust [7]. Another example found in a cross-flow scavenge design is a deflector in between the intake and exhaust ports [7]. This deflector is typically part of the combustion face of the piston and is meant to re-direct the flow of fresh charge away

from the exhaust port. Inevitably, the gas exchange process is highly variable and never perfect.

In any given cycle, a portion of exhaust gas will remain in the cylinder and short-circuiting will occur. Heywood and Sher state that a typical two-stroke engine short-circuits approximately 20% of the mass of delivered fuel at any given operating condition [7]. The actual amount of short-circuiting in an engine is dependent on many factors including exchange port design, cylinder geometry, engine speed, and engine load among others. In their investigation into performance improvement of a small two-stroke engine, Mavinahally et al. employed a unique transfer port design that allowed the intake charge to enter the cylinder in a stratified manner. The first portion was primarily air or very fuel-lean while the remaining portion was the typical stoichiometric (or close to) mixture of fuel and air [16]. By measuring exhaust gas composition, Mavinahally et al. were able to verify the reduction in short-circuiting with their design and coincidentally observe reductions in fuel consumption and emissions. They documented an emissions reduction of 28% compared to the baseline engine [16].

2.2.5 Blow-by

In order to operate effectively, an IC engine must be able to keep high pressure combustion gases from leaking around the piston through the gap along the cylinder wall. This leakage is known as blow-by and is usually reduced by the use of piston rings. A piston ring is a circular ring that wraps around the outside of the piston. The ring seats in a ring groove and its diameter is slightly larger than the cylinder bore. The ring has a gap in one end in order to flex down to the size of the bore. The spring force of the ring to return to its original shape effectively creates a seal between the piston and cylinder wall.

Ring gaps are measured precisely in order to account for material expansion at operating temperatures. Multiple piston rings with their gaps indexed away from each other are used commonly to reduce blow-by further. Over the course of an engine cycle, approximately 5-10% of the cylinder charge becomes trapped in voids between the piston rings. Heywood mentions that typically about 1% of the cylinder charge makes it into the crankcase while the remainder returns to the combustion chamber to be exhausted as unburnt hydrocarbons [4]. This small contribution to the amount of unburned fuel passing into the exhaust is an issue for all IC engines that contain combustion sealing piston rings, including the scaling study engines that are considered in this research.

One drawback of piston rings is the amount of friction created as the moving piston ring slides against the stationary cylinder wall. In a study on the theoretical limits of scaled-down IC engines, Sher and Sher cite that in very small IC engines piston ring friction loss can be on the order of engine power output due to the high cylinder surface area to swept volume ratio; therefore, combustion sealing with piston rings becomes an infeasible solution [3]. According to Attard et al., piston rings also provide an additional path for heat conduction that can adversely affect combustion [15].

2.3 Performance Measurement

The following section covers topics dealing with instrumentation and methods of measuring IC engine performance. Although this is not an all-inclusive list, it includes some of the more prevalent measurement techniques. Every engine must transmit its output power to some sort of load in a real world application. In a test environment, this load can be replicated by a dynamometer. The dynamometer has an inherent drawback in that it must be coupled to the engine by some sort of drivetrain which introduces losses

that, along with internal engine pumping losses, cannot be quantified by a dynamometer. This is where the application of in cylinder pressure measurements is valuable as will be discussed. Finally, an examination of an IC engine's exhaust emissions can give indications of performance in terms of combustion and gas exchange.

2.3.1 Dynamometers

A dynamometer is used to provide a braking force to reciprocating engine crankshaft. This braking force causes a reactionary moment that is usually measured by a load cell at the end of a torque arm. Coupled with a rotational speed sensor a dynamometer can measure power delivered to the brake, also known as brake power (P_b). Dynamometers can apply the braking force by different means including hydraulically, electromagnetically, or by friction. Dynamometers are usually attached to an IC engine by means of some sort of drivetrain that adds to frictional losses. Unfortunately, a dynamometer alone will not quantify the drivetrain frictional losses. Menon, Moulton, and Cadou from the University of Maryland have developed a novel approach to measuring small IC engine power output [17]. Their design consists of a test bench that can load a running engine with a hysteresis brake for continuous load adjustability like many conventional dynamometer test stands; however, the reaction forces created from the load are measured at the engine mounts instead of a torque arm attached to the brake. This is done by mounting the engine inside of a cradle that rotates along the engine's crank axis. With a load attached, the cradle acts as a torque arm. The advantage in this case is that any amount of drivetrain componentry downstream of the engine cradle becomes negligible in the calculation of power based on torque and speed measurements during operation [17].

2.3.2 In Cylinder Pressure

In cylinder pressure measurement is a valuable performance indicator for IC engines. Power output is a direct result of combustion pressures acting on the piston. Indicated work per cycle ($W_{c,i}$) is the amount of work delivered to the piston from the working fluid over a given engine cycle [4]. By plotting pressure as a function of cylinder volume during an engine cycle, a p-V diagram is produced. Integrating around the curve will yield an engine's indicated work per cycle.

$$\boldsymbol{W_{c,i} = \oint p\, dV} \qquad \textbf{(9)}$$

Indicated work per cycle can then be converted to indicated power (P_i) at a given engine speed. Indicated power differs from brake power in that brake power is the amount of power delivered to the load after frictional losses from within the engine as well as any drivetrain components between the engine and the brake. Indicated power is therefore always higher in magnitude than brake power by an amount equal to what is known as friction power (P_f). As a result, knowledge of an engine's indicated and corresponding brake power enables one to begin quantifying the frictional losses between an engine and it load. In cylinder pressure measurements also allow for monitor of abnormal combustion events such as knock or pre-ignition. This behavior is characterized by large spikes and oscillatory behavior in pressure. This type of detection is valuable alternative fuels research among other fields.

2.3.3 Exhaust Emissions

Exhaust gas composition measurements provide good insight into the operating conditions of an IC engine. With a given fuel, concentrations of species in an exhaust

stream can enable the calculation of combustion efficiency as well as equivalence ratio. In his research on the performance of a 34 cc Fuji four-stroke IC engine operating on alternative fuels, Groenewegen was able to measure the partial fraction of unburned hydrocarbons in the exhaust stream as well as various combustion products to determine engine operating conditions like equivalence ratio and combustion efficiency [18].

Another important aspect of analyzing exhaust gas composition is the ability to accurately determine the amount of energy leaving an IC engine in terms of enthalpy. In consideration of overall efficiency, energy exiting the engine via the exhaust stream can account for the largest percentage of available fuel energy in terms of energy flows out of the engine, often on the order of 35% or more [4]. The following data in Table 2 are representative values for energy pathway fractions as percentages of total available fuel energy for typical automotive sized IC engines as cited by Heywood [4].

Table 2: Nominal automotive engine energy balance [4]

	Brake power	Engine cooling	Misc. heat transfer	Incomplete combustion	Exh. sens. enthalpy
SI Engine*	25-28	17-26	3-10	2-5	34-45
Diesel*	34-38	16-35	2-6	1-2	22-35

*Values reported are percentages of total available fuel energy

The data in Table 2 suggest that the largest portion of outgoing energy for a SI IC engine is exhaust sensible enthalpy. However, these data refer to a four-stroke engine that is considerably larger than the engines tested in this study. It is expected that the higher cylinder surface area to volume ratio of the smaller engines along with the fact that they are two-stroke cycle engines will yield a much greater percentage of incomplete combustion products (primarily unburned hydrocarbons) due to thermal quenching and short-circuiting.

2.4 Scaling Behavior

When investigating the effects of engine scaling on performance, it is important to recognize that performance phenomena are dependent on two geometrical parameters: cylinder surface area and cylinder volume. Considering one cylinder of an IC engine, its geometric properties (surface area and swept volume) stem from two dimensional measurements: bore, B and stroke, L. Small to medium sized IC engines have a bore to stroke ratio ranging from 0.8 to 1.2. In comparison, large, slow-speed IC engines can have a bore to stroke ratio as low as 0.5 [4]. This scaling study is concerned with small IC engines, so only they will be considered further. One can hold a cylinder dimension fixed (bore or stroke) and change the other by varying the bore to stroke ratio to examine the change in cylinder surface area and swept volume with respect to the changing dimension. Figure 14 shows that a cylinder's swept volume is more sensitive to dimensional change than surface area. Therefore volume based performance parameters like power output scale faster in either direction than surface area based performance parameters like thermal quenching and surface friction. In other words, when IC engines are scaled down, power output falls off at a faster rate than loss mechanisms such as thermal quenching and cylinder surface friction. Thus small IC engines generally have lower efficiencies than their larger counterparts.

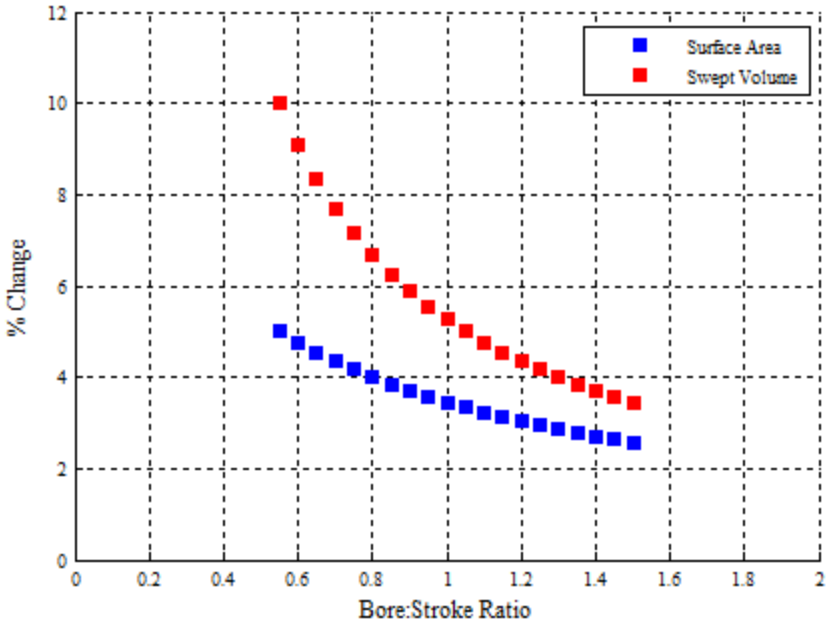

Figure 14: Cylinder geometry sensitivity to spatial dimension change

Figure 15 shows a collection of IC engine power ratings as a function of cylinder surface area to swept volume ratio. Engines considered include two-strokes and four-strokes, SI and CI, carbureted and fuel-injected engine designs. The three engines used in this scaling study are indicated as the yellow, green, and magenta data points. The inset in the upper-right of Figure 15 shows a close-up of the transition region in which power scaling trends appear to change. It should be emphasized at this point that all power values displayed are manufacturer rated numbers and have not been measured or verified by any secondary, independent sources. I performed a curve fit of the data to yield the expression in Equation 10. This function is a potential model for describing the power scaling trends of IC engines across a wide range of sizes and is depicted as the black line in Figure 15.

$$P_{mfr} = 22\left(\frac{SA}{V_d}\right)^{-3} \quad (10)$$

The model closely approximates the power scaling trends of this particular collection of IC engines. Cylinder surface area to swept volume ratio can be converted to an approximate displacement if a square engine is assumed (bore/stroke ratio equal to 1). Using this information, rates of power increase per unit increase in displacement can be determined for large and small engines in Figure 15. The model indicates a power increase with respect to decreasing surface area to volume ratio of approximately 390 kW/cm^{-1} for large engines. For comparison, small engines only realize power increases of approximately 1 kW/cm^{-1} of surface area to volume decrease.

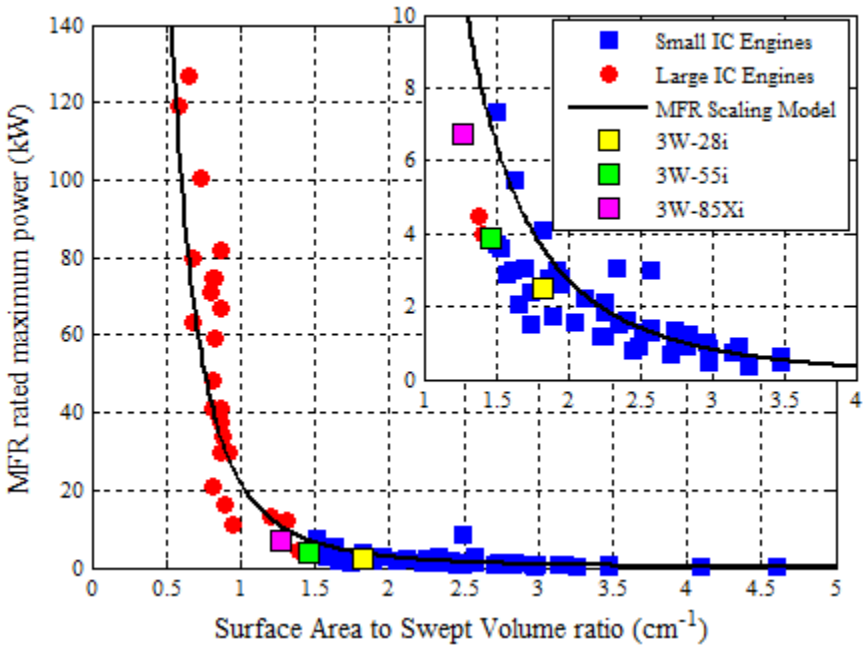

Figure 15: Manufacturer rated max. power vs. cylinder surface area to swept volume ratio for a collection of IC engines [19-29]

The delineation between large and small IC engines for the concern of this study is 1.5 cm^{-1}. Assuming a square engine (bore/stroke ratio equal to 1), this equates to an

engine swept volume of roughly 50 cc. Medium to large IC engine size classes (approximately 1000 cc and up) correspond to IC engines used commonly in the automotive or passenger aircraft industry all the way up to massive shipboard marine diesel IC engines. The widespread use of engines in these size classes has led to thorough technical investigations of many aspects of performance and loss characterization; there is a plethora of accurate technical performance data in the literature. Historically, as engines get smaller, their applications are reduced to hobbyist vehicles or handheld power equipment among other things. Generally engines in this size class (approximately 100 cc and lower) are designed to low complexity and low cost customer requirements, so thorough technical investigations are deemed not worthy from a cost-benefit perspective. This results in a large variety of small IC engines with little to no accurate technical performance data.

2.4.1 Related Work in Small IC Engine Scaling

Menon [30] has performed a scaling study on miniature IC engines at the University of Maryland. His work involved developing a test facility for acquiring quality measurements of engine performance parameters such as torque, engine speed, and fuel flow among other things for very small engines (0.16 cc - 7.54 cc). His efforts were the first to gain technical performance data for engines with masses less than 500 grams [30]. Menon's findings are shown in Figure 16 as data points corresponding to the 'UMD Scaling Study.' To the best of this author's knowledge, this is the only technical investigation of performance on IC engines of this size.

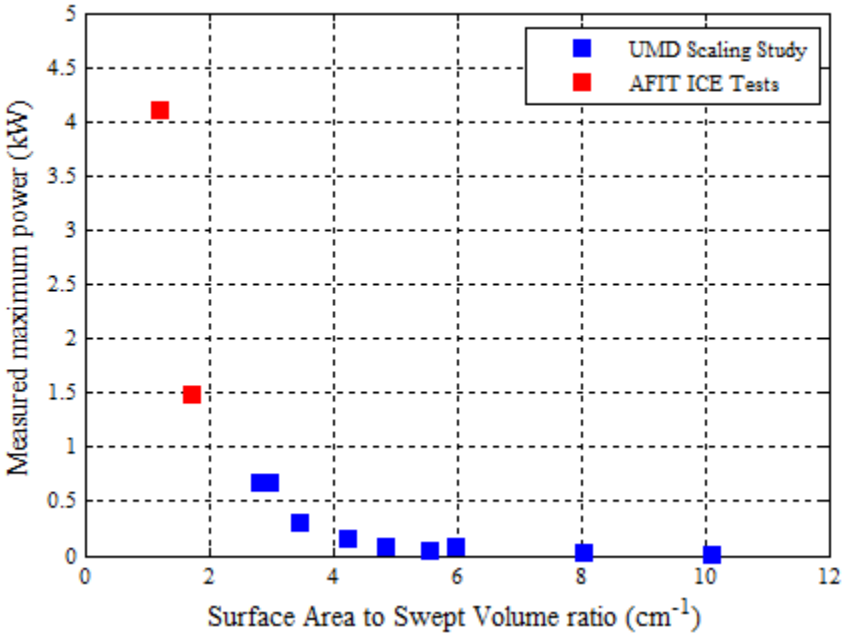

Figure 16: Measured power vs. cylinder surface area to swept volume ratio for small ICEs [30] [31] [32]

Previous work at the Air Force Institute of Technology (AFIT) has been done by Crosbie [31] and Wilson [32] to characterize the performance of larger IC engines. In Crosbie's work, baseline testing of a 95 cc Brison two-stroke SI engine was performed.

Subsequently the engine was tested at pressure altitudes ranging from sea level to 15,000 feet above mean sea level (MSL). These tests were done by placing the engine in a custom vacuum chamber capable of simulating lower atmospheric pressures up to 15,000 feet MSL. Improvements to engine performance were made by converting the engine's fuel metering system from a carburetor to TBI. Performance losses of up to 91% were realized with the carburetor at altitude. These performance losses were regained by converting to TBI. Peak power was matched with TBI versus carburetion, but moderate engine speeds and loads yielded much improved fuel consumption values with TBI [31]. To maintain consistency with other data, only Crosbie's baseline sea level test results are included in Figure 16 as the 'AFIT ICE Test' datum point with a higher power output.

Wilson's work consisted of performance mapping for a 34 cc Fuji four-stroke SI engine. Performance parameters were investigated for the engine running on isooctane (octane rating of 100) and *n*-heptane (octane rating of 0). Wilson found that the engine was capable of operating at a series of propeller load points with zero octane fuel sufficiently enough to propel a small RPA. Furthermore, fuel consumption was decreased by an average of 4.1% across all load points when using zero octane fuel [32]. Since the Fuji engine was designed to operate on high octane fuel the isooctane tests are considered as baseline performance testing and performance results are reflected in Figure 16 as the lower output datum point of the two 'AFIT ICE Test' points. The results of the UMD scaling study and previous AFIT work are published data in the scientific literature and will be used in combination with the results of this scaling study to re-evaluate the suggested scaling model of equation (10) with measured results as opposed

to manufacturer claimed performance values. The modified scaling model is discussed in further detail in Chapter IV.

Well documented and supported heat transfer models exist for larger IC engines, but concerning small engine cylinder heat transfer phenomena, the literature is very limited. Rittenhouse et al. [33] has investigated three techniques to evaluate the thermal energy pathways of a small IC engine. His work was performed on a 3W-55i two-stroke SI engine with a displacement of 55 cc. The three techniques included an energy balance, enclosing the engine to determine heat rejection via air-cooling, and utilizing a cylinder instrumented with heat flux gauges. Rittenhouse's findings showed that the engine would reject energy via heat equal to 40% of the total fuel energy via the energy balance method. The enclosure method and the heat flux gauge method yielded a heat rejection fraction of 10% of total fuel energy. The engine exhibited a peak fuel conversion efficiency of 15.4% and a peak power of 3.0 kW [33]. The engine enclosure measurement technique provided results that align with the scientific literature, so this method was used to characterize the energy loss to engine cooling air for each test engine in this research.

III. Methodology

The research team constructed a test bench for the purpose of testing small IC engines in the 1-10 kW power range. This range of power production correlates to engines in the size regime of 25 cc to 100 cc in terms of displacement volume. An examination of rated power outputs for engines in this size regime indicates that power scaling trends change significantly as a result of loss mechanisms associated with cylinder surface area like friction and thermal quenching. The purpose of this study is to test a series of engines that span this transitional size regime to obtain accurate performance information and establish scaling relationships among engines of this size. This chapter provides a description of the scaling study experiment. Included are discussions on the sizes and types of engines, how the test bench was configured, the design approach used to maintain consistency among the engines, and how test data was acquired. An uncertainty analysis follows with discussion of methods involved and relevant performance parameter accuracies.

3.1 Engine Selection

In order to establish scaling trends in the transition regime of Figure 15, the research team chose a series of engines with cylinder surface area to swept volume ratios spanning the transition point vicinity of approximately 1.5 cm^{-1}. These engines were the 3W-28i, 3W-55i, and the 3W-85Xi. Each was manufactured by 3W Modellmotoren GmbH. They are particularly designed for use in hobbyist remote control aircraft. Each engine is single cylinder, two-stroke cycle, Schnurle loop scavenged, spark-ignited, air-cooled, and carbureted. The engines utilize crankcase compression for gas transfer. Compression ratio remains constant among the engines at 10:1. Although port timing

values vary by as much as 11° of crank angle among the engines, general layout and design of the gas exchange ports is similar among all engines. Pertinent geometric parameters and manufacturer rated performance values are shown in Table 3.

Figure 17: 3W Modellmotoren engines used in scaling study [19]

Qualitatively, the engines have the same design as shown in Figure 17. The engines ingest air/fuel mixture through a dual mixing screw carburetor to the crankcase. Crankcase compression drives the scavenging process. Each engine has transfer ports on three sides of the cylinder head while the fourth side is used for the exhaust port. The combustion chamber volume for each engine is hemispherical with the spark plug located centrally and aligned with the direction of piston motion. Ignition timing signals are detected by a Hall Effect sensor and embedded magnets in the propeller drive flange. The same ECU is supplied with each engine from the manufacturer. Being two-stroke engines, the crankcases are void of an oil sump, so needle roller bearings are used on both ends of the connecting rods. Important geometric properties and manufacturer claimed performance values for each engine are shown in Table 3. One key difference in the 85 cc engine versus the remaining two scaling study engines is the presence of a second

combustion sealing piston ring (the others only have one). A piston ring can contribute a significant amount of friction loss to an IC engine system, sometimes on the order of the engine's power output according to Sher and Sher [3]. It is possible that the additional friction losses of the second piston ring outweigh the performance benefits of the added combustion sealing, thus causing a reduction in brake performance for the 85 cc engine.

Table 3: Scaling study engine geometric parameters and manufacturer rated performance values

Engine	3W-28i	3W-55i	3W-85Xi
Displacement (cc)	28	55	85
Manufacturer Rated Power (kW)	2.5	3.9	6.8
Mass (kg)	1.21	1.94	2.40
Power density (kW/kg)	2.07	2.01	2.83
Bore (cm)	3.6	4.5	5.1
Stroke (cm)	2.8	3.5	4.1
Compression ratio	10:1	10:1	10:1
Exhaust Port timing (CAD)	106°	103°	97°
Surface area to swept volume ratio (cm^{-1})	1.83	1.46	1.27

3.2 Test Bench

A primary objective of this research was to obtain quality technical performance data by employing measurement and detection methods usually not performed on engines this small. To that end, important external variables were maintained such as intake air temperature and drivetrain configuration. Care was taken to ensure measurement techniques did not significantly alter the performance of each engine. Further discussion of the various instrumentation and measurement techniques follow. A diagram of the test bench is shown in Figure 18. This depicts primary components and their general layout for clarity. In Figure 19, the fully constructed test bench is shown for descriptive purposes.

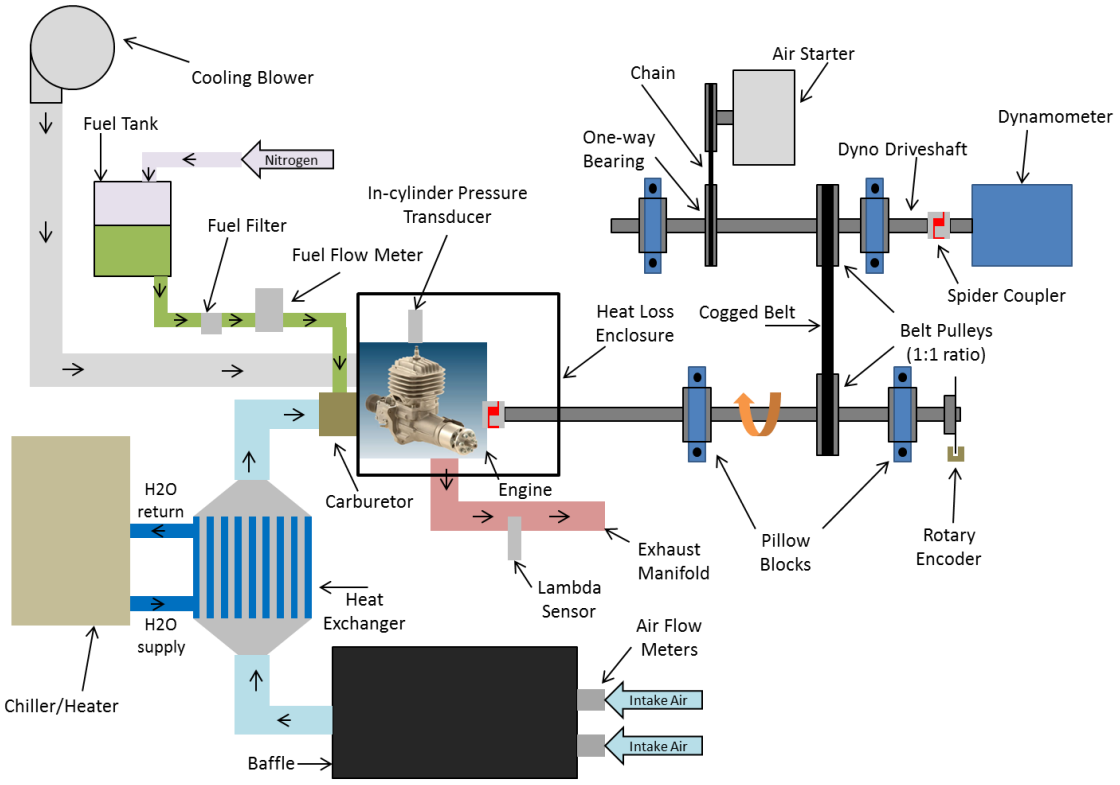

Figure 18: Small engine test bench diagram

The small engine test bench used an eddy current dynamometer to load the engines. Intake air was supplied through a heat exchanger coupled to a heater/chiller unit to maintain consistent intake manifold temperatures. A large baffle was installed to damp flow oscillations for steadier air flow measurements. Cooling air was forced over the engine through an insulated enclosure for the purpose of measuring heat rejection to the cooling medium during operation. The aforementioned components can be seen in Figure 18 and Figure 19. These components and associated measurement techniques will be discussed further in the remainder of this chapter.

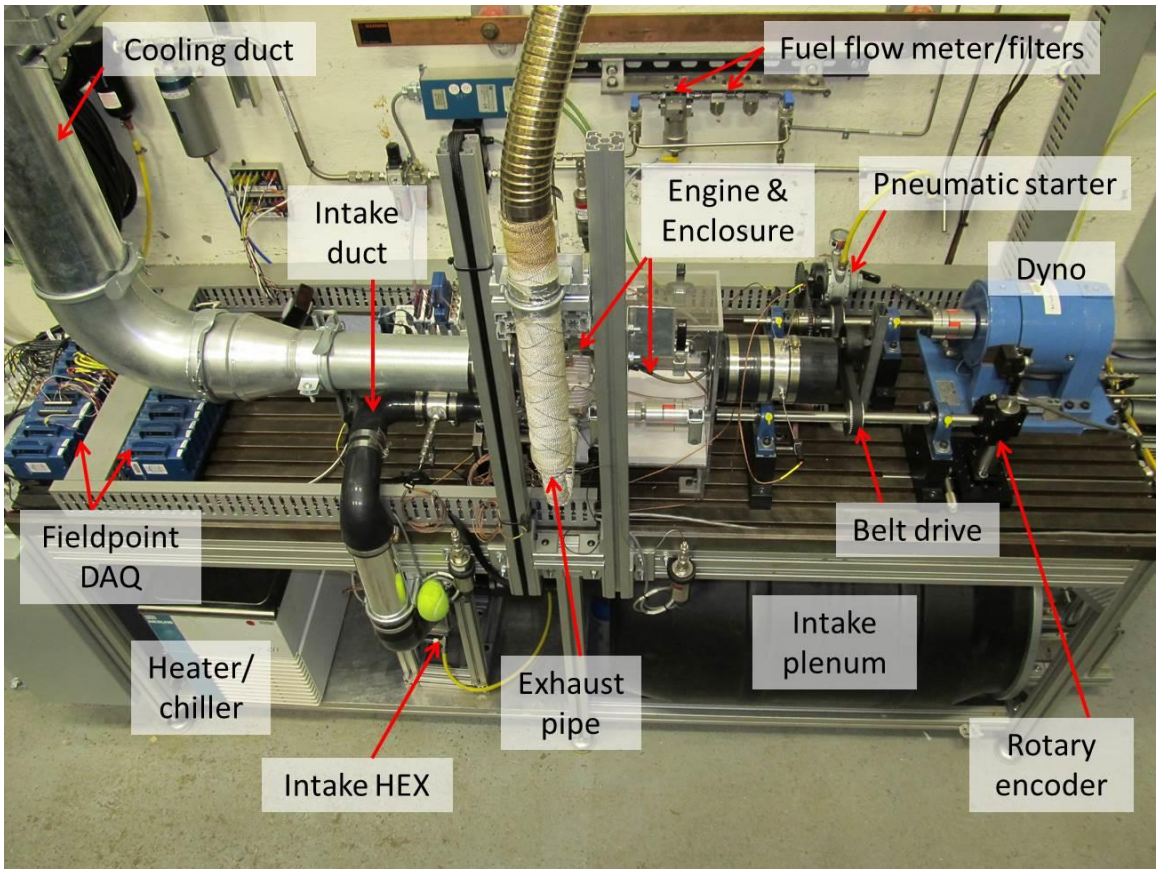

Figure 19: Small engine test bench with major components labeled

The test bench was designed and constructed with a modular approach to engine testing. Therefore, each engine was able to be integrated onto the bench using the same drivetrain components in the same locations. Not only did this simplify transition between engines, but it provided for consistency performance data measurement. Each engine had a different mounting bolt pattern, so adapter plates were manufactured to account for the different mounting points. The adapter plates were mounted to an engine riser. The engine risers for each engine were the same for ease of mounting. The engine risers were machined from billet steel with the intended purpose of having excess mass for strength, rigidity, and vibration reduction. The engine riser and adapter plate for the 55 cc engine are shown in Figure 20. Each engine was mounted in such a way that the

respective shaft centerlines were the same height for shaft alignment purposes. The engines had to be adapted to an ANSI ¾" shaft, so shaft adapters were fabricated for each engine based on the propeller bolt pattern. The shaft adapters were aligned using a dial indicator accurate to ±0.001". The engines had their own servo motors for operating choke and throttle plates that were attached to the engine riser. Due to the difference in exhaust port dimensions an exhaust pipe was fabricated for each of the engines; however, the exhaust pipes were designed to be mounted in the same orientation. Exhaust pipe design is discussed in more detail in Section 3.2.7.

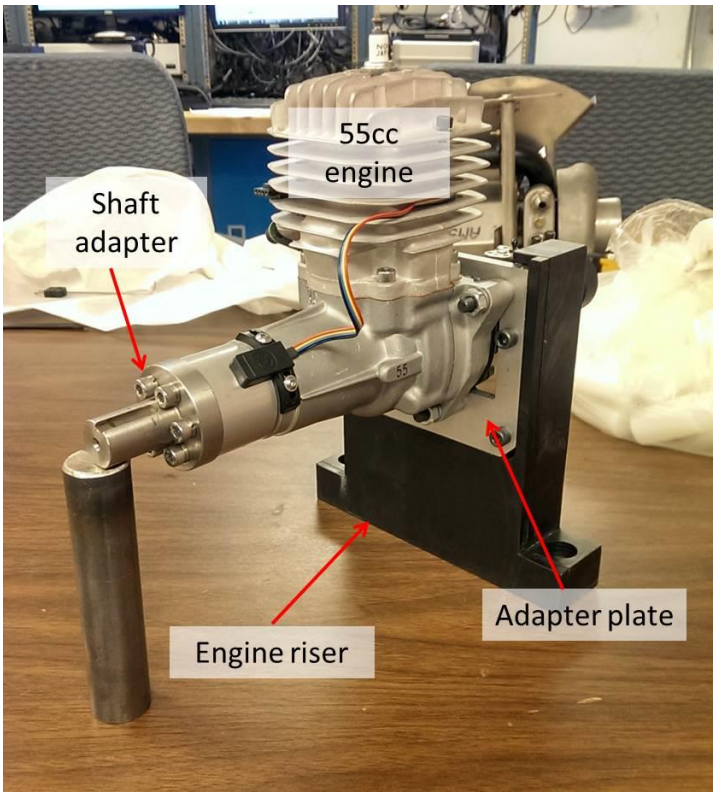

Figure 20: 3W-55i mounted with adapter plate to engine riser

3.2.1 Air Flow

In the case of the 28 cc and 55 cc engines, intake air was drawn through two airflow meters in parallel to measure air flow rate. TSI model 40211 high performance

linear mass flow meters capable of 0-300 SLPM with an accuracy of ±3% of reading were used for measurement. A common characteristic in small two-stroke engines that utilize crankcase compression to drive gas transfer is the possibility of momentary flow reversal through the carburetor. Although the engines considered in this study were equipped with a reed valve at the crankcase induction port to reduce this phenomenon, there was still a possibility of backwards flow. The flow meters are essentially hot-wire anemometers, hence they are unable to detect flow reversal thus introducing a large amount of error in the measurement. To avoid erroneous measurements a large plenum was installed between the flow meters and the engine. The purposes of the plenum were to damp flow oscillations and eliminate the occurrence of flow reversal at the point of measurement. The plenum (a 55 gallon drum) was on the order of 2400 times larger in volume than the displacement of the largest engine to ensure steady airflow for all engines at the highest speeds and loads. The intake plenum and the temperature modulation system are shown in Figure 21.

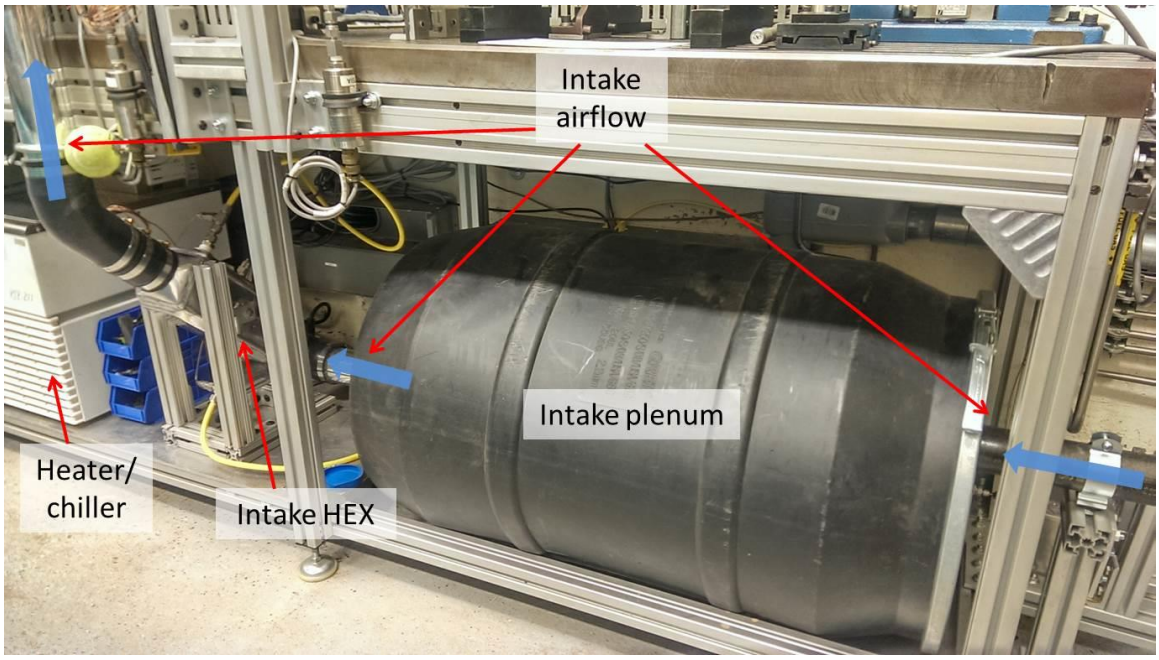

Figure 21: Test bench intake setup including baffled intake plenum

In the case of the 85 cc engine, restricted airflow from the aforementioned intake configuration was found to be detrimental to engine performance. Performance measurements were taken with various configurations of the intake components connected. Resulting data showed that the parallel TSI flow meters were the cause of flow restriction. The TSI flow meters were replaced by an Omega Engineering air velocity transmitter. It is capable of measuring velocities from 0 m/s to 5.08 m/s with an accuracy of 2% of full scale. The air velocity transmitter (another hot-wire anemometer) was placed in a #2 standard pipe attached to the intake plenum. The sensor was positioned 15 diameters downstream of the inlet and 5 diameters upstream of the entrance to the intake plenum for adequate measurement of fully-developed flow. The intake setup can be seen in Figure 22. The air velocity measurement was converted to a mass flow rate, $\dot{m}_a$ based on cross sectional area of the flow channel, A and concurrent ambient temperature, T and pressure, P readings based on the ideal gas behavior of air in

Equation 11. A value of 287 J/kg-K was used for the universal gas constant, R in this case.

$$\dot{m}_a = \left(\frac{P}{RT}\right) AV \qquad (11)$$

Temperature measurements were performed with Omega Engineering J-type 1/16" probe style thermocouples. The thermocouples are capable of temperature measurements from 0°C to 750°C with an accuracy of the greater of ±1.1°C or 0.4% of reading. Ambient pressure was measured with a Honeywell Model TJE pressure transducer capable of 0-15 psia pressure measurements with an accuracy of ±0.10% of full scale.

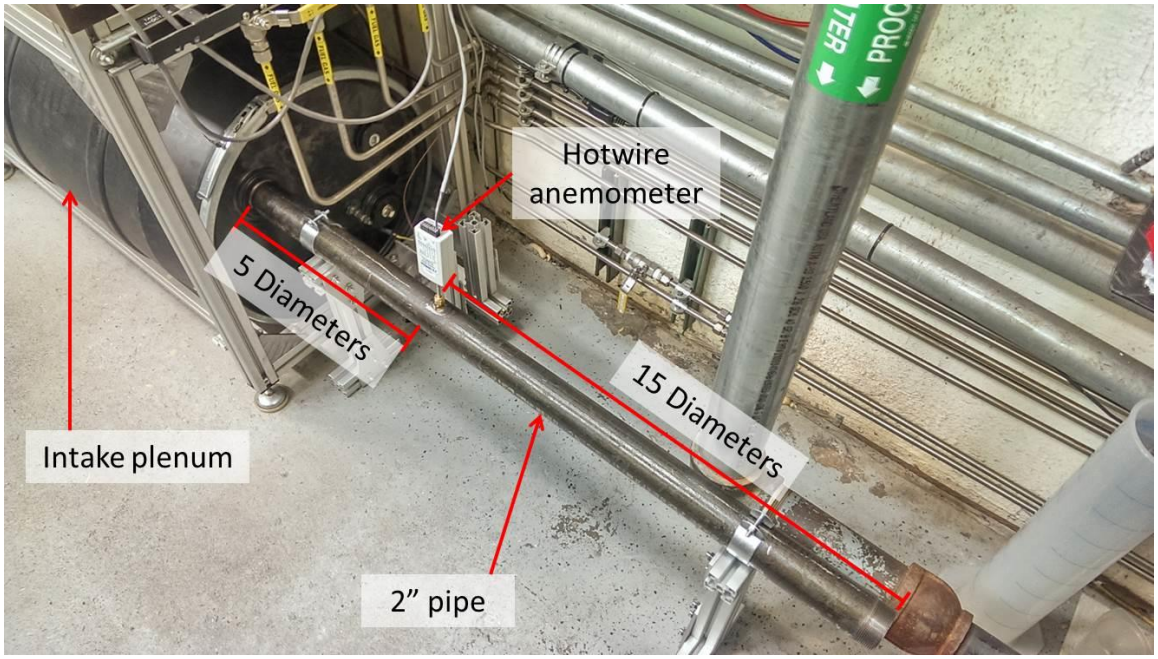

Figure 22: 85cc engine intake airflow measurement apparatus

In order to maintain consistency over several runs, intake air flowed through a shell and tube heat exchanger downstream of the plenum. The intake air flowed through the heat exchanger as the tube-side fluid. Water flowed through the heat exchanger as the

shell-side fluid. The water temperature was held at a constant value using a NESLAB RTE 211 heater/chiller unit. The heater/chiller unit can operate over a temperature range of -25°C to +100°C. Intake air temperature was measured downstream of the heat exchanger to assure consistent operating conditions despite changes in ambient temperature.

Before entering the engine, air flowed through the carburetor past choke and throttle plates. For the three engines, choke and throttle were actuated remotely by Hitec HS-85MG+ analog metal gear servos. Linkages and positioning of the servo motors was adjusted in each case to ensure full movement from closed to fully open. The setup of the throttle actuating servo during an experiment is shown in Figure 23.

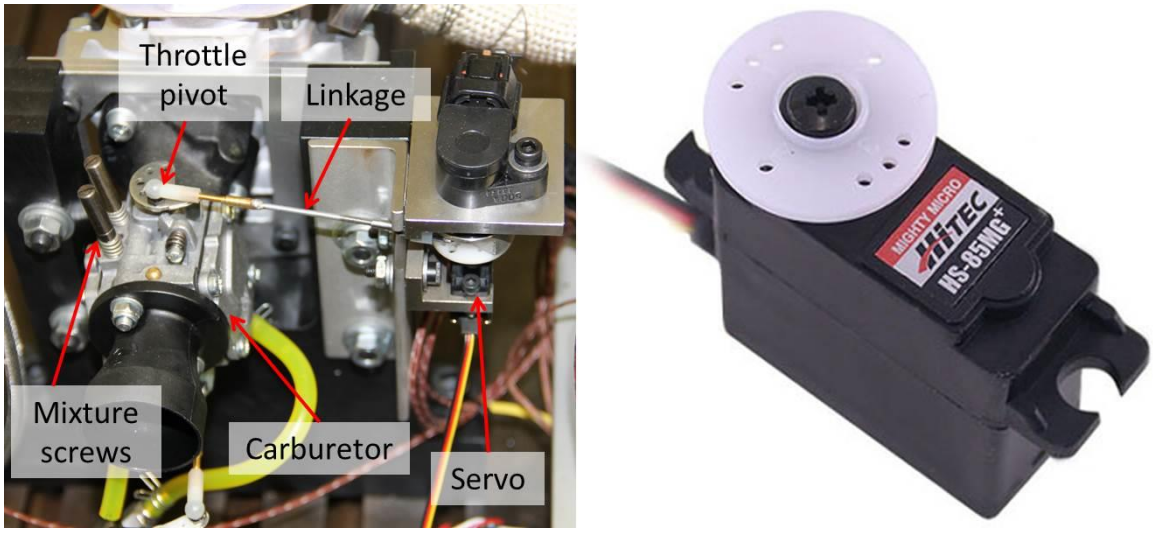

Figure 23: Servo motor, linkage, and carburetor [34]

3.2.2 Fuel Flow

The fuel used to run the engines was a primary reference fuel consisting of iso-octane and *n*-heptane in a ratio of 98:2 respectively. Synthetic two-stroke oil was added per manufacturer recommendation for proper lubrication. Oil used in this experiment was AMSoil Saber Professional synthetic, smokeless two-stroke oil mixed at a fuel/oil

ratio of 100:1. The fuel system was pressurized to approximately 2 psig with an external nitrogen supply to maintain sufficient pressure as fuel flowed through a 40 micron filter, a 7 micron filter and a piston flow meter before proceeding to the carburetor. The piston flow meter was a Max Machinery 213 piston flow meter capable of measuring flow rates between 1 and 1800 cc/min at an accuracy of ±0.2% of reading. The primary components of the test bench fuel system are shown in Figure 24.

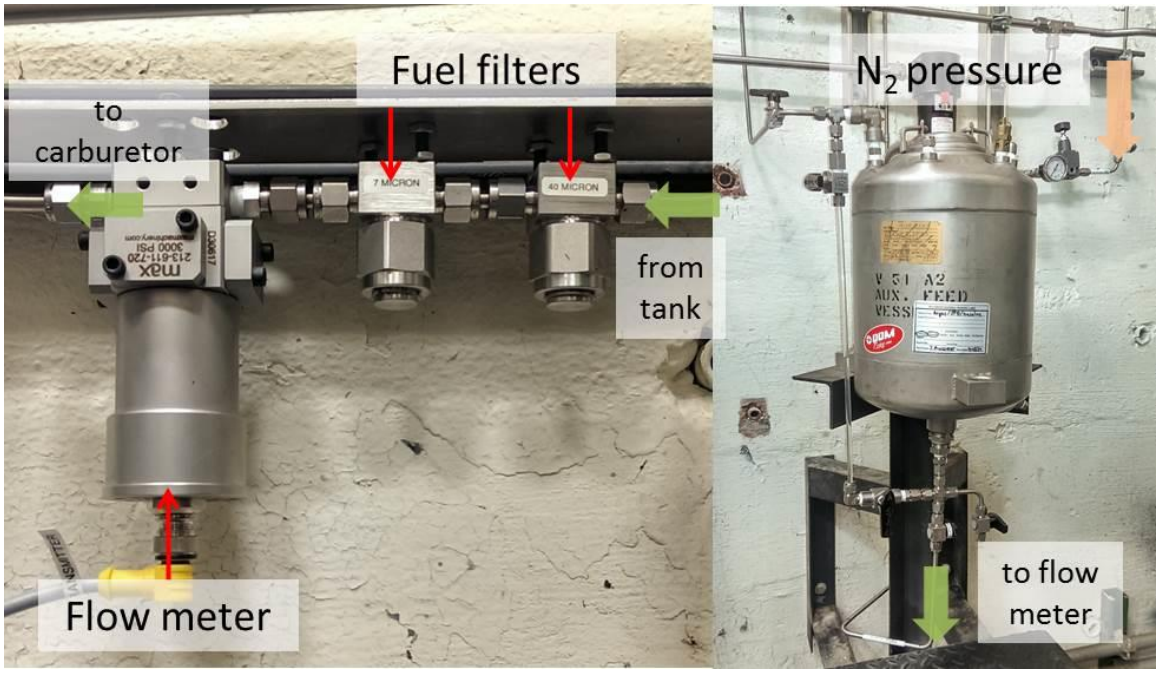

Figure 24: Test bench fuel supply and flow rate measurement system

3.2.3 Ignition

The manufacturer supplied the same engine control unit (ECU) with each of the test engines, so a single ECU was employed in all engine tests for this study. The ECU had a built-in speed limiter that activated at 8000 rpm. The ECU limited engine speed by withholding the spark discharge to force the engine speed down. Once engine speed was reduced enough, normal operation would resume. During testing, engine speeds were kept at or below 7900 rpm to avoid the influence of non-firing cycles on high-speed

performance data. As a result, the maximum mean piston speed achievable by the test engines scaled with engine stroke only. This phenomenon led to narrower performance envelopes as the engines decrease in size. Given a constant rotational speed, each engine's piston passes through top dead center (TDC) position at a constant frequency. However, as the engines get larger, stroke increases, so the piston must travel over longer distances in the same amount of time between TDC positions. As a result, a given rotational speed does not have the same effect across engines of varying sizes. Therefore, comparison data in this study will be presented in terms of mean piston speed in which rotational speed is normalized by stroke to arrive at a parameter that has appropriate meaning across a range of engine sizes. Mean piston speed, $\bar{S}_p$ in meters/second can be calculated from engine rotational speed, N in revolutions/second by Equation 12 where L is engine stroke length in meters [4].

$$\bar{S}_p = 2LN \quad (12)$$

Spark timing was measured using a Fluke Instruments induction current clamp. Induced voltage signals were processed with AVL Indicom combustion analysis software to obtain spark timing as a function of CAD. The 3W ECU timing map was a linear function of speed changing from 12.5° BTDC at 4000 rpm to 32.2° BTDC at 7900 rpm as can be seen in Figure 25.

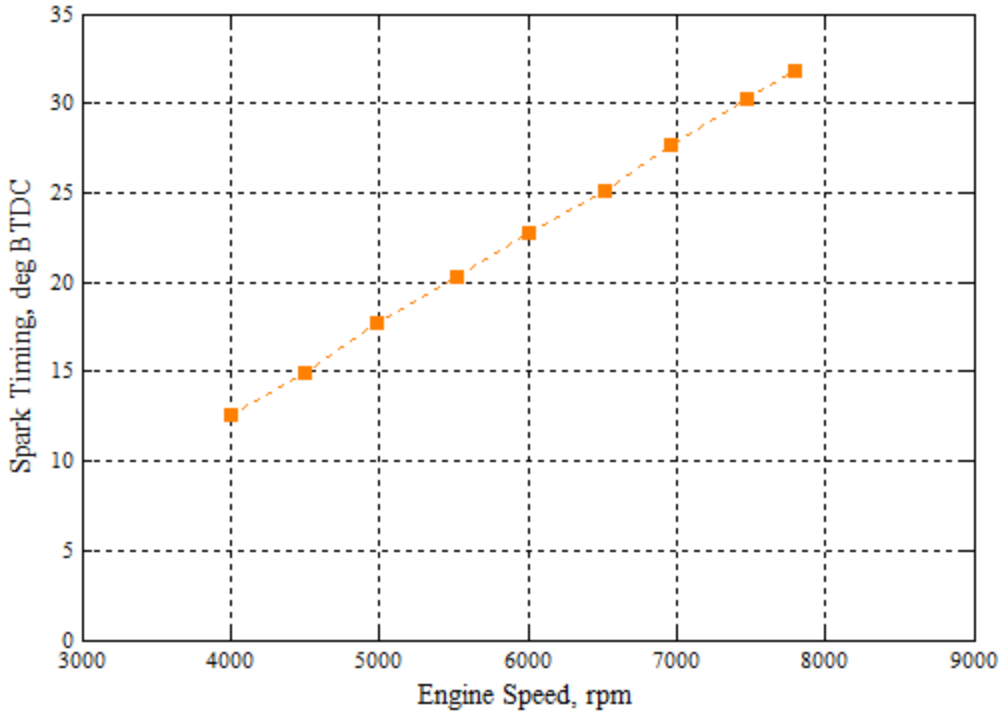

Figure 25: 3W ECU spark timing map

3.2.4 Indicated Pressure Measurements

In cylinder or indicated pressure measurements were taken using a Kistler type 6113B pressure measuring spark plug capable of detecting pressure from 0-200 bar with an accuracy of ±1%. Voltage signals from the pressure transducer were amplified with a Kistler 2852 Signal Conditioning Platform.

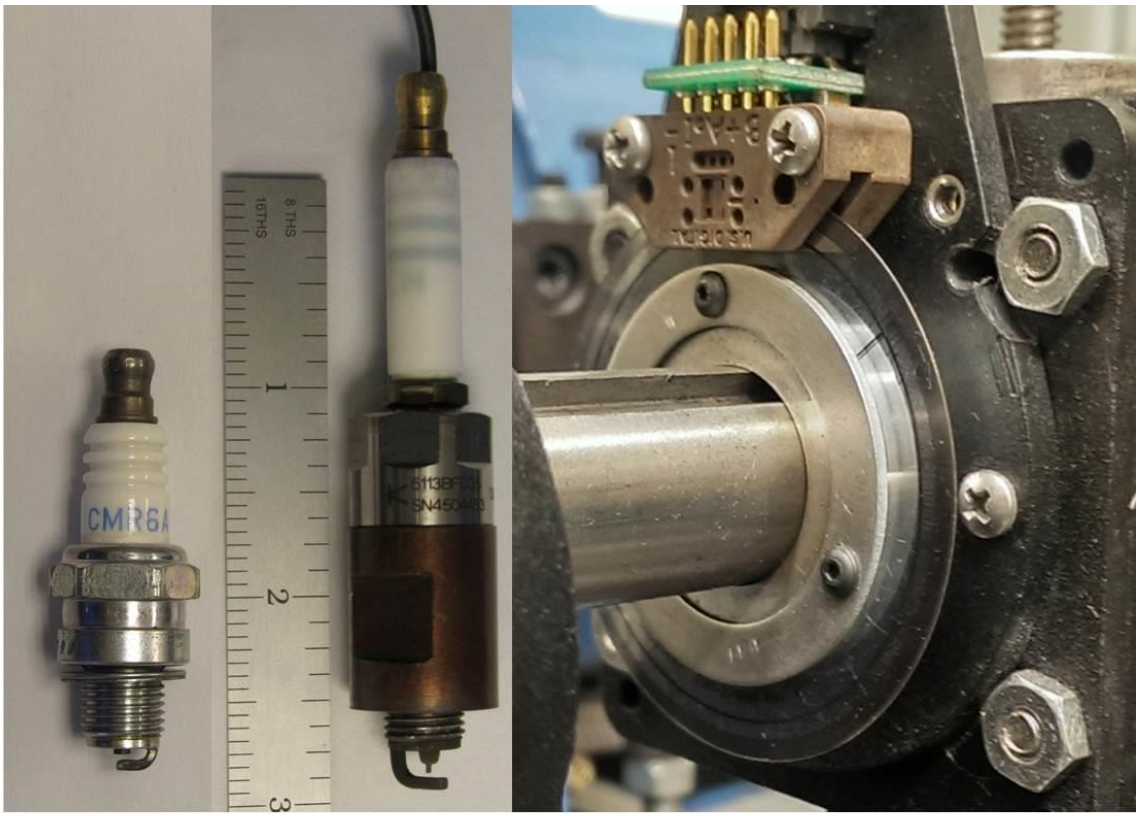

Figure 26: Stock spark plug, measuring spark plug, optical encoder

Crank angle position was measured using a US Digital E6 optical encoder with 1800 counts/revolution. The measuring spark plug and optical encoder are shown in Figure 26. The stock spark plug from the test engines is included for comparison. Pressure data and crank angle position were collected using an AVL Indismart combustion analyzer to produce indicated performance measurements. Location of piston top dead center (TDC) in terms of crank angle degrees (CAD) was a critical piece of information for calculating indicated performance. In this study, TDC was determined based on a pressure trace of a motored (non-firing) engine cycle as shown in Figure 27. A thermodynamic loss angle of 0.7° CAD was implemented based on a correlation of

larger IC engine pressure data. TDC is then assumed to correspond to the zero CAD mark where peak pressure occurs as shown in less the 0.7 CAD correction factor as shown in Figure 27. The pressure trace data of Figure 27 is for the 55 cc engine at approximately 1500 rpm, corresponding to the speed at which the pneumatic starter motor was capable of spinning the drivetrain and engine.

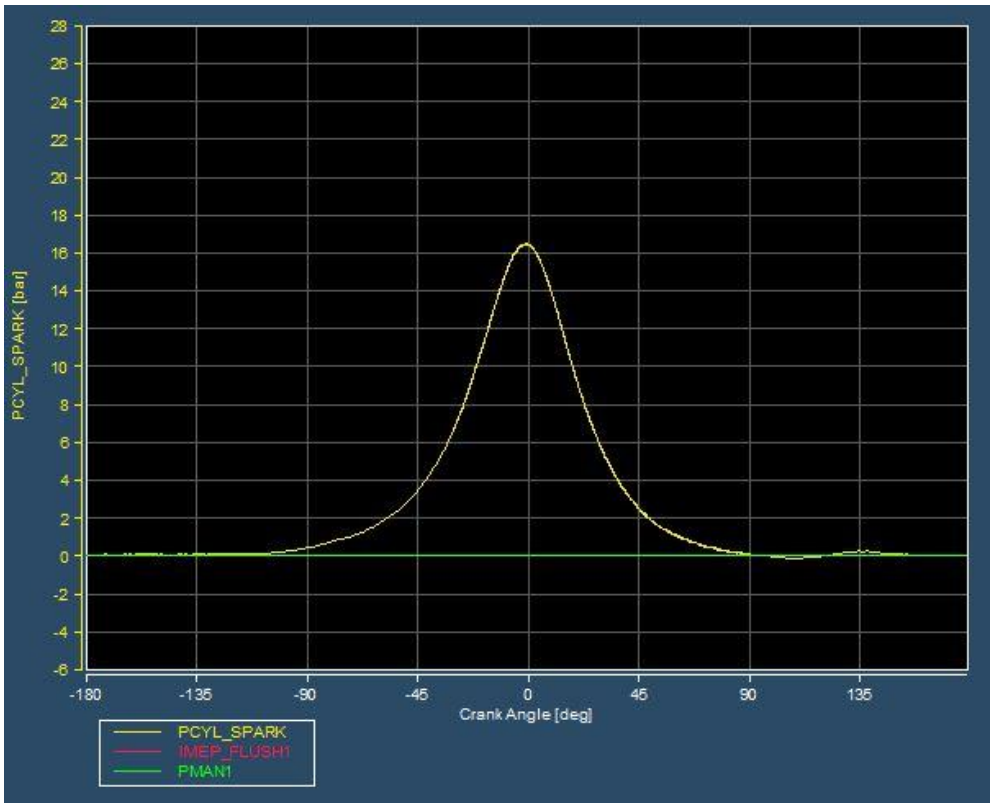

Figure 27: Motored pressure trace of a test engine from AVL software

3.2.5 Drivetrain & Dynamometer

The drivetrain was configured so that the engine and dynamometer drive shafts were linked together by a cogged belt and rotated on parallel axes. Initially, a 0.5" wide belt was used with a spring-loaded idler pulley tensioner supporting the non-loaded side of the belt. Belt de-lamination occurred at too high of a rate in this configuration possibly due to overloading, alignment tolerances, or lack of belt tension. The belt was

replaced with a larger 1” wide version and an idler pulley was added to the upper, loaded side of the belt to shorten the unsupported path length and eliminate belt vibration. No belt failures were experienced in subsequent testing with this configuration. The improved belt drive setup can be seen in the lower left of Figure 28. Initially, the engine and dynamometer were coupled to their respective drive shafts by Ruland keyed shaft steel bellows couplers (upper right of Figure 28). The bellows couplers proved to have a high failure rate, most likely due to excessive vibrations and cyclic loading causing metal fatigue. The bellows couplers were replaced with Ruland jaw couplers with 98 Shore A hardness spiders (right center and lower right of Figure 28). It should be noted that the engine side driveshaft coupler was obscured from view in the photograph in the lower left of Figure 28 because of the engine enclosure and cooling air outlet. No shaft coupler failures were experienced during subsequent testing. Although the drivetrain went through multiple iterations that likely changed the friction characteristics that dissipated power between the engine and dynamometer, all three engines were tested using the same drivetrain configuration for consistency. This included the shaft couplers, belt drive, and pillow block arrangement.

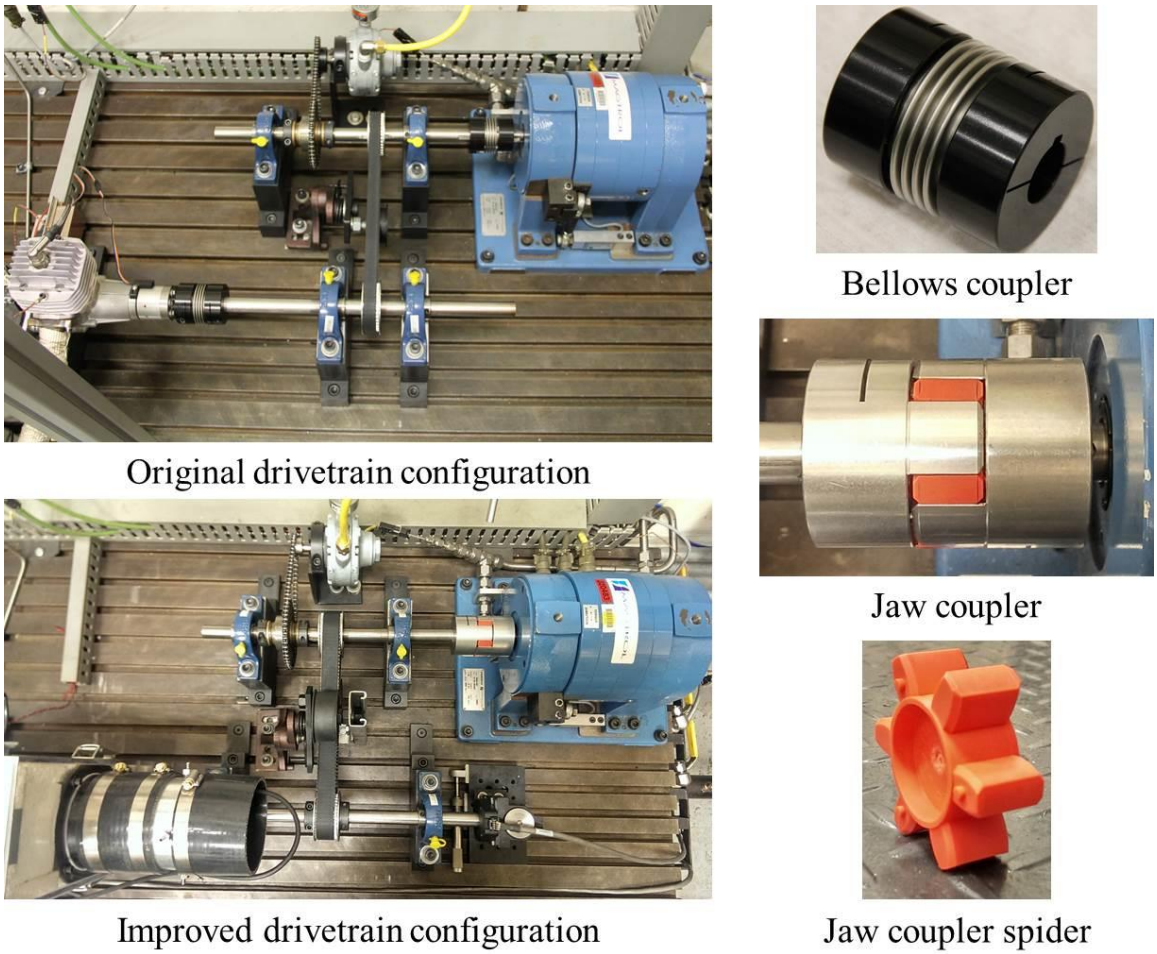

Figure 28: Original vs. improved drivetrain configuration, shaft couplers

A GAST 2A-NCW-7B pneumatic motor was linked to the dynamometer driveshaft with a one-way bearing in order to start the engine and not dissipate power unnecessarily during testing. The pneumatic motor is rated at 0.67 kW and a maximum speed of 3000 rpm. The dual, parallel drive shaft configuration was chosen due to the flexibility in mounting options for additional components such as the optical encoder. Furthermore, alignment was greatly simplified considering the drive shafts only had to align with a component on one end instead of both. Vertical shaft alignment was performed by shimming the drive shaft pillow blocks. Horizontal shaft alignment was

achieved as a result of careful placement of the pillow blocks before being torqued down into place. Shaft alignment for the dynamometer and engine was verified by a combination sliding tight tolerance aluminum sleeves and straight edges to an accuracy of ±0.005". The dynamometer used in this study was a Magtrol 1 WB 65 series eddy current model. Its torque and speed capacity are 10 N-m and 10,000 rpm respectively. Torque and speed measurements are accurate to ±0.5% of full scale. The dynamometer was water cooled to maintain proper functionality over extended periods of loading

3.2.6 Engine Cooling & Thermal Loss

Thermal loss by way of heat rejection to the cooling medium was measured by characterizing the temperature change and mass flow rate of cooling air as it passed over the engine's cylinder head during operation. In order to achieve these results, the engine was tested inside a custom insulated enclosure to isolate the cooling airstream from external air. The enclosure was constructed of ¼" polycarbonate and was insulated internally with ¾" polystyrene foam. The gap between the cylinder head and enclosure walls was approximately 1/8" for the 55 cc and 85 cc engines. The insulation had to be notched for the larger engine to avoid direct contact. For the 28 cc engine, the gap between the cylinder head and enclosure walls was approximately 1" due to the fact that the width was smaller. The cooling airstream velocity was varied to maintain a desired cylinder head temperature. Typically these engines would utilize air flow from an attached propeller for cooling. On the test bench, a Monoxivent D15-3 blower was used to force cooling air across the cylinder head as if the engine were in a pusher prop configuration. The blower was powered by a 1.5 hp 460V Baldor electric motor (Model CM3550). The blower is capable of 965 cfm air flows at 1 inch of static pressure.

Cylinder head temperatures are measured with a J-type ring style thermocouple bolted to the upper cooling fins of the engine's cylinder head. Figure 29 shows the interior of the insulated engine enclosure along with the locations of the cylinder head thermocouples and the pressure measuring spark plug. Cooling air flows from top to bottom in the view shown in Figure 29. During initial enclosure testing, the insulation was not installed. This provided an opportunity to view the inside of the enclosure during operation. The cooling flow was deemed sufficiently turbulent with no stagnation regions based on the movement of the wires inside not unlike flow streamers used in wind tunnel experimentation.

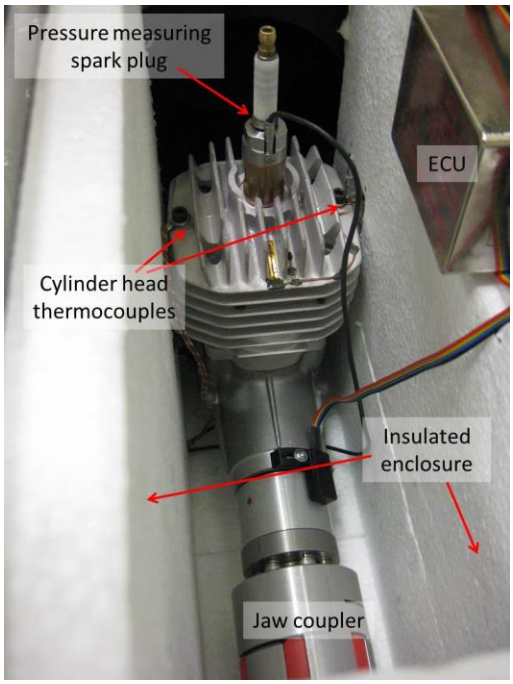

Figure 29: 3W-55i mounted inside insulated enclosure

Cooling air velocity is measured with an Omega Engineering air velocity transmitter with a range capacity of 0 m/s to 50.8 m/s and an accuracy of 2% of full scale. Approximately 10 diameters of duct were added upstream and 5 diameters downstream

from the measurement point for flow development as shown in Figure 30. Mass flow rates are derived similar to the method prescribed for the 85cc engine intake flow.

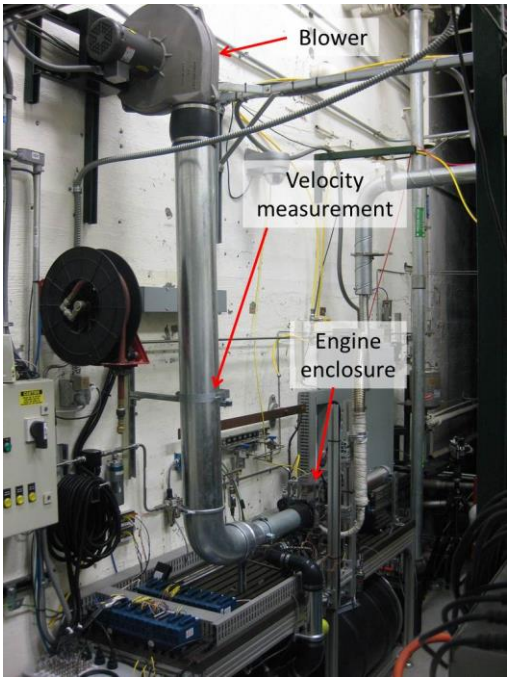

Figure 30: Engine cooling system

Air temperatures are measured at locations upstream and downstream of the engine enclosure with probe style J-type thermocouples. Energy loss due to heat rejection to the cooling airstream can then be calculated based on a constant specific heat for air as shown in Equation 13. Energy loss via radiation was neglected for the course of this study as it was deemed insignificant in comparison to the amounts of energy transfer via other pathways such as convection, exhaust enthalpy flux, and shaft power production among others.

$$\boldsymbol{Q_{cool} = \dot{m}_{cool} c_{p,air} \Delta T} \qquad \textbf{(13)}$$

It is important to note that the engine and enclosure are mounted such that the carburetor, and thus the intake air stream are isolated from the cooling air flow. Exhaust

gases exit the engine through a fiberglass insulated pipe that passes through a sealed port in the side of the enclosure to minimize heat transfer. The left side of Figure 31 shows the engine enclosure during a typical test run. The driveshaft passes through a close-tolerance port in the enclosure with grommets on either side to reduce cooling air leakage as shown on the right of Figure 31. Cooling air inlet temperature is measured upstream of the enclosure with a J-type probe thermocouple. Outlet temperature is measured with a rake of three J-type probe thermocouples.

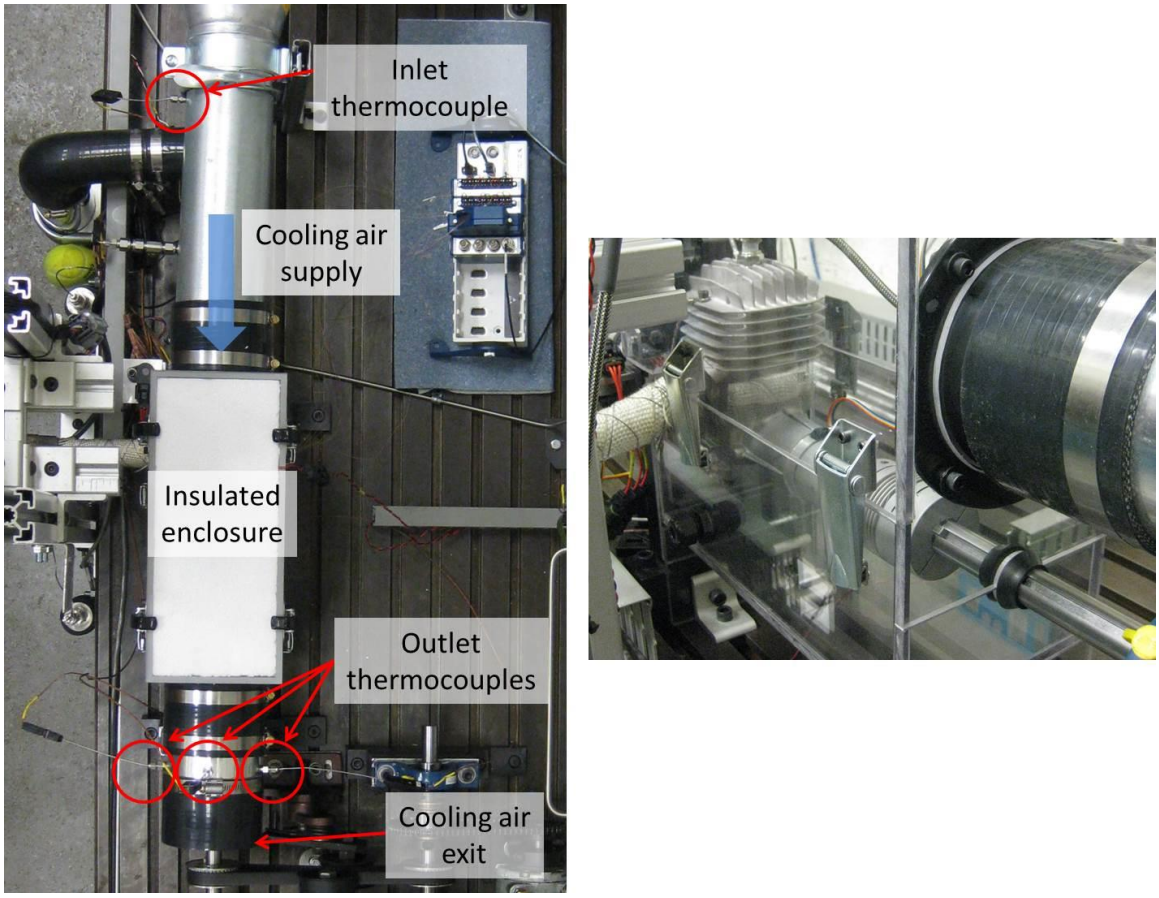

Figure 31: Heat rejection measurement apparatus

3.2.7 Exhaust

The exhaust pipes designed for each engine were modeled qualitatively after those supplied with the engines as they were purchased from the manufacturer. Care was

taken to ensure the exhaust pipe inlet ports closely matched the exhaust ports from the respective engines geometrically. This was done to reduce flow restrictions. The exhaust systems were not tuned for increased scavenging efficiency. Temperature and pressure were measured approximately 10 diameters downstream of the entrance to the exhaust pipe. The exhaust pipes were wrapped with fiberglass insulation to minimize thermal losses prior to measuring exhaust gas temperatures (EGTs). A fabricated exhaust pipe is shown uninstalled and installed on the test bench in Figure 32. The stock exhaust pipe is also depicted for comparison. A Powerdex AFX air/fuel monitor was installed approximately 20 diameters downstream of the exhaust pipe entrance. The air/fuel monitor was a heated wideband lambda sensor used to provide an air/fuel ratio based upon the oxygen concentration in the exhaust stream.

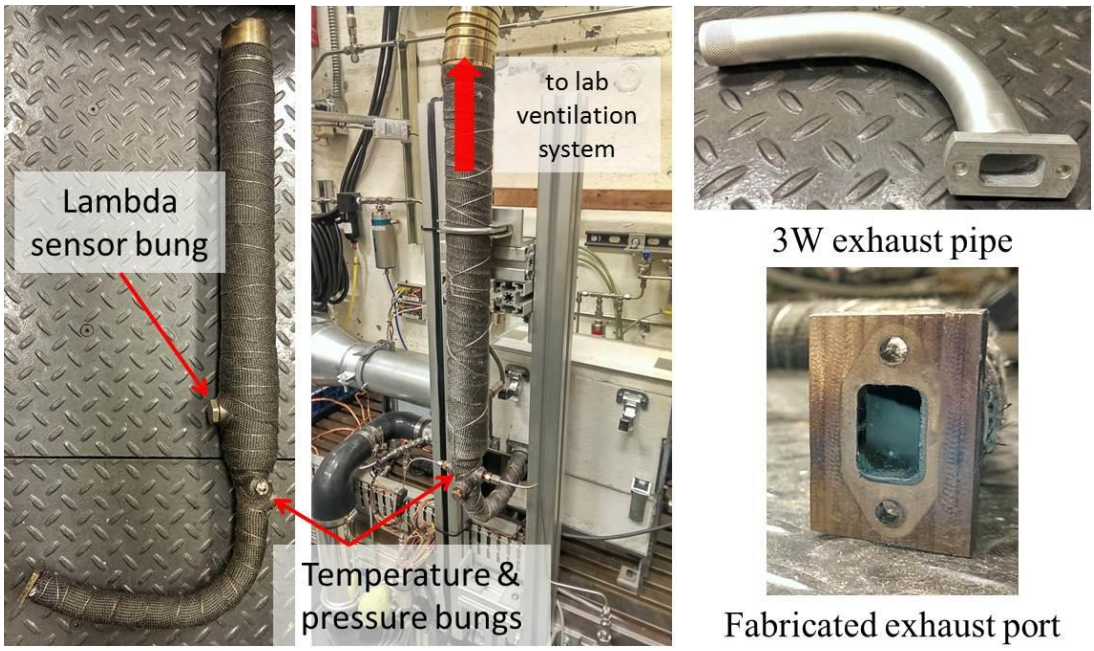

Figure 32: Fabricated exhaust pipe comparison to stock

3.3 Test Methodology

This section discusses how the test engines were broken in and tuned. A description of the methods for determining partial throttle settings is included. Test methods and data reduction procedures follow. Finally, an analysis of measurement and sample uncertainty is provided.

3.3.1 Engine Operation

Before acquiring any performance data, each engine was broken in according to the manufacturer's recommendations. This involved running the engine at moderate, varying speeds and loads (3500 – 4500 rpm, approximately 50% throttle) for at least 2 hours. During break in, two-stroke oil with zinc additives was used in a 32:1 fuel/oil ratio as recommended by the manufacturer. Once break in was completed each engine underwent a tuning process to obtain mixture settings that would allow best possible operation across the breadth of the engine's operating envelope. Tuning began by setting the high and low mixture needles on each carburetor to their respective positions as recommended by the manufacturer test card included with each engine. If necessary, further tuning was performed based on equivalence ratio and indicated mean effective pressure (IMEP) variance data. In other words, the carburetor mixing needles were leaned or richened to produce equivalence ratios as close to unity as possible which usually would lower the coefficient of variance (CoV) on IMEP. Power production and audible feedback also played a large part in engine tuning. The general approach to tuning was that the engine was to run 'decently' at all throttle settings and speeds. This meant the carburetor was set to a point at which no particular operating condition was optimized, but the engine could run reliably at any point. Once that was achieved, the

mixture settings were not changed for the remainder of testing for the particular engine. This approach to tuning was deemed sufficient for the tests considering the ultimate goal was to characterize engine performance at all speeds and over a range of throttle settings. Once break in and tuning were complete, partial throttle settings had to be established. Each engine was operated at a mean piston speed of approximately 7 m/s which equates to roughly 7500 rpm, 6000 rpm, and 5100 rpm for the 28cc engine, the 55cc engine, and the 85cc engine, respectively. The throttle plate was swept from the fully open position to the engine idle position while recording brake power data. Based off the resulting power curve, throttle settings corresponding to maximum power, 75% power, 50% power, and 25% power were chosen. Since the throttle plate was actuated by a servo motor controlled by a LabVIEW graphical user interface (GUI), the corresponding GUI setting was recorded for reference in subsequent tests. In Figure 33 a power curve corresponding to Run 14 in the data was generated for a 3W-55i engine. The subsequent data acquisition runs on this particular engine (Runs 16-25) are plotted against the power curve to display the repeatability of the throttle setting method used for this study.

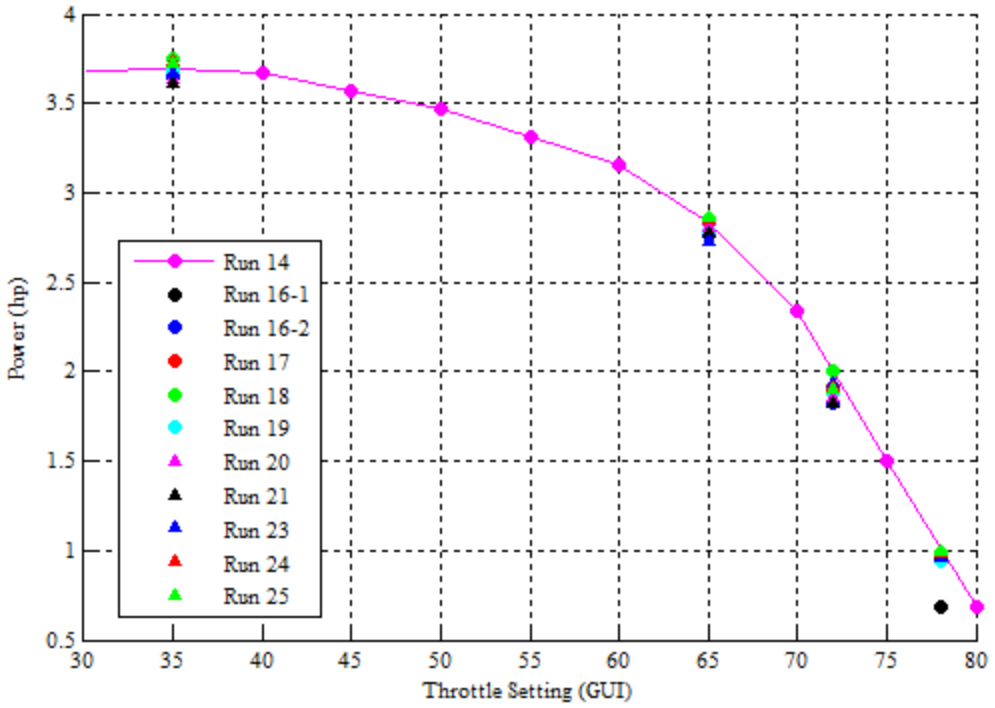

Figure 33: 3W-55i power curve and subsequent test runs

Data acquisition for this study consisted of running the engines from 4000 rpm to 7900 rpm in 500 rpm increments. At each speed, the four aforementioned throttle settings were engaged to obtain 4 operating conditions at each speed. At each operating point, the engine was allowed to stabilize and cooling blower settings were adjusted to maintain cylinder head temperature before test data was recorded. The results of these tests will be discussed in Chapter IV.

3.3.2 Data Acquisition

During engine tests, data was recorded using a National Instruments field point data acquisition (DAQ) system. The DAQ system and the test bench components were controlled through a LabVIEW interface. Data was sampled at approximately 2 Hz. Each operating point was held in order to obtain 10 seconds of data before proceeding to

the next operating point. During data reduction, the ten second samples were averaged down to a single data sample.

3.4 Uncertainty Analysis

The results considered in this study are accompanied by an uncertainty analysis corresponding to measurement uncertainty due to instrumentation accuracies as well as uncertainty due to variability in the measurement over time. For this study, these uncertainties will be referred to instrumentation error and run-to-run error respectively. Run-to-run error was calculated as the standard deviation of a set of multiple runs. Because the performance metrics reported here are calculated from measurements that have associated elemental uncertainties, error has been propagated through the calculations according to the function in equation (14) where R is a function of n independent variables, v. In this case, w with a numeric subscript is the elemental uncertainty and w_R is the resultant uncertainty corresponding to R [35].

$$w_R = \sqrt{\left(\frac{\partial R}{\partial v_1} w_1\right)^2 + \left(\frac{\partial R}{\partial v_2} w_2\right)^2 + \cdots \left(\frac{\partial R}{\partial v_n} w_n\right)^2 \cdots} \qquad (14)$$

Instrumentation error and run-to-run error were combined into a resultant error calculated by the square of the sum of each error squared. Uncertainties reported in this work assume a Gaussian distribution and are reported to a 95% confidence interval.

Table 4 shows the uncertainty due to instrumentation for performance parameters reported in this study. The values are an average of all data points across all engines and test runs.

Table 4: Performance parameter uncertainties due to instrumentation

ϕ	5.8%
P_b	5.9%
$BMEP$	7.9%
$BSFC$	8.6%
η_{fb}	8.0%
$IMEP$	1.5%
P_i	2.4%
$FMEP$	12.5%
Q_{cool} (kW)	17.7%
Q_{cool} (%)	17.7%

Concerning the accuracy of temperature change measurements associated with the engine enclosure (ultimately propagating into Q_{cool}), it was discovered that the quoted accuracy of the thermocouples as per the manufacturer yielded heat rejection measurement uncertainties of 75% or more. According to Holman, however, when measuring a change in temperature instead of an absolute temperature, measurement accuracies often can be much better than advertised [36]. This better accuracy was determined by placing the four thermocouples in a water bath. Temperature signals were reported as the water bath was swept from 5°C to 40°C. The maximum standard deviation of the four signals multiplied by three (for a 99% confidence interval) was then used as the thermocouple accuracy. This allowed the thermocouple accuracy to be narrowed from ±1.1°C to ±0.14°C which improved the heat rejection measurement error from 75% to 18%.

IV. Analysis and Results

A series of small two-stroke IC engines was tested to investigate performance scaling relationships and determine the loss mechanisms that cause significant changes in power scaling trends in the 25 cc to 100 cc displacement size regime. The three engines of the scaling study span the range in which power scaling trends change. This chapter covers the performance results of each engine, followed by a comparison of performance parameters and thermal losses to engine cooling. The results are then used to draw conclusions pertaining to the effects of engine displacement scaling on performance and efficiency.

4.1 Individual Engine Performance

The following subsections (4.1.1-4.1.3) contain the baseline performance data for each of the scaling study engines from a stand-alone perspective. Each engine test consisted of three test runs following the methodology outlined in Table 5. Speeds were varied from 4000 rpm to 7900 rpm in 500 rpm increments (except the last interval). The highest speed was kept at 7900 rpm to eliminate the ECU's built-in speed limiter from negatively impacting performance. Four throttle settings were implemented at each speed to record performance effects as a function of engine load as well as speed. The throttle settings were determined by performing a throttle sweep at an engine speed of 7 m/s mean piston speed for each engine. Throttle settings corresponding to 100%, 75%, 50%, and 25% of maximum brake power were then used in the subsequent data acquisition tests. This method resulted in 36 data points for a complete test run. For repeatability purposes, test runs were performed at least three times with a shutdown

period of approximately 20-30 minutes at a minimum in between to ensure data samples were separate and independent.

Table 5: Scaling study engine test matrix

Point #	Engine Speed (rpm)	Throttle setting	Point #	Engine speed (rpm)	Throttle setting
1	4000	50%	19	6000	50%
2	4000	75%	20	6000	75%
3	4000	100%	21	6500	50%
4	4000	25%	22	6500	75%
5	4500	50%	23	6500	100%
6	4500	75%	24	6500	25%
7	4500	100%	25	7000	50%
8	4500	25%	26	7000	75%
9	5000	50%	27	7000	100%
10	5000	75%	28	7000	25%
11	5000	100%	29	7500	50%
12	5000	25%	30	7500	75%
13	5500	50%	31	7500	100%
14	5500	75%	32	7500	25%
15	5500	100%	33	7900	50%
16	5500	25%	34	7900	75%
17	6000	50%	35	7900	100%
18	6000	75%	36	7900	25%

Test data that follows includes power production from a brake and indicated basis, mean effective pressures, specific fuel consumption, and engine efficiencies. In the plots that follow, colors correspond to a particular test run of an engine or the mean of all test runs for a particular engine. Plot symbols are used to differentiate throttle settings.

4.1.1 28 cc Engine

Performance data for the 28 cc engine reported in this study was an average of three separate and independent test runs. The core measurements upon which all other

performance parameters were based were brake power, IMEP, fuel mass flow rate, and intake air mass flow rate. For this reason, run-to-run variation data is reported for these four parameters only. Figure 34 shows a graphical representation of the resulting brake power at four throttle settings for each individual test run for the 28cc engine. Additionally, the average variation in brake power as well as the remaining core measurement parameters is included numerically in Table 6 for comparison.

Table 6: Average run-to-run variation of primary performance parameters for the 28 cc engine

	25% throttle	**50% throttle**	**75% throttle**	**100% throttle**
P_b	14.2%	6.3%	6.7%	2.6%
IMEP	6.6%	3.4%	4.1%	1.8%
$\dot{m}_f$	11.1%	5.1%	6.3%	3.8%
$\dot{m}_a$	4.3%	1.3%	1.2%	0.6%

The 28cc engine was inoperable at speeds below 5500 rpm at 100% throttle. Typically at throttle position settings at or near fully-open, the engine would be free to increase its crankshaft rotational speed; however, in this study, the engine was loaded by the eddy current dynamometer which held the engine to a constant rotational speed. For cases where the engine speed was held at operation points below 5500 rpm with 100% throttle, the equivalence ratio would become excessively lean and the engine would stall. Therefore, data points #3, #7, and #11 of the test matrix in Table 5 were skipped.

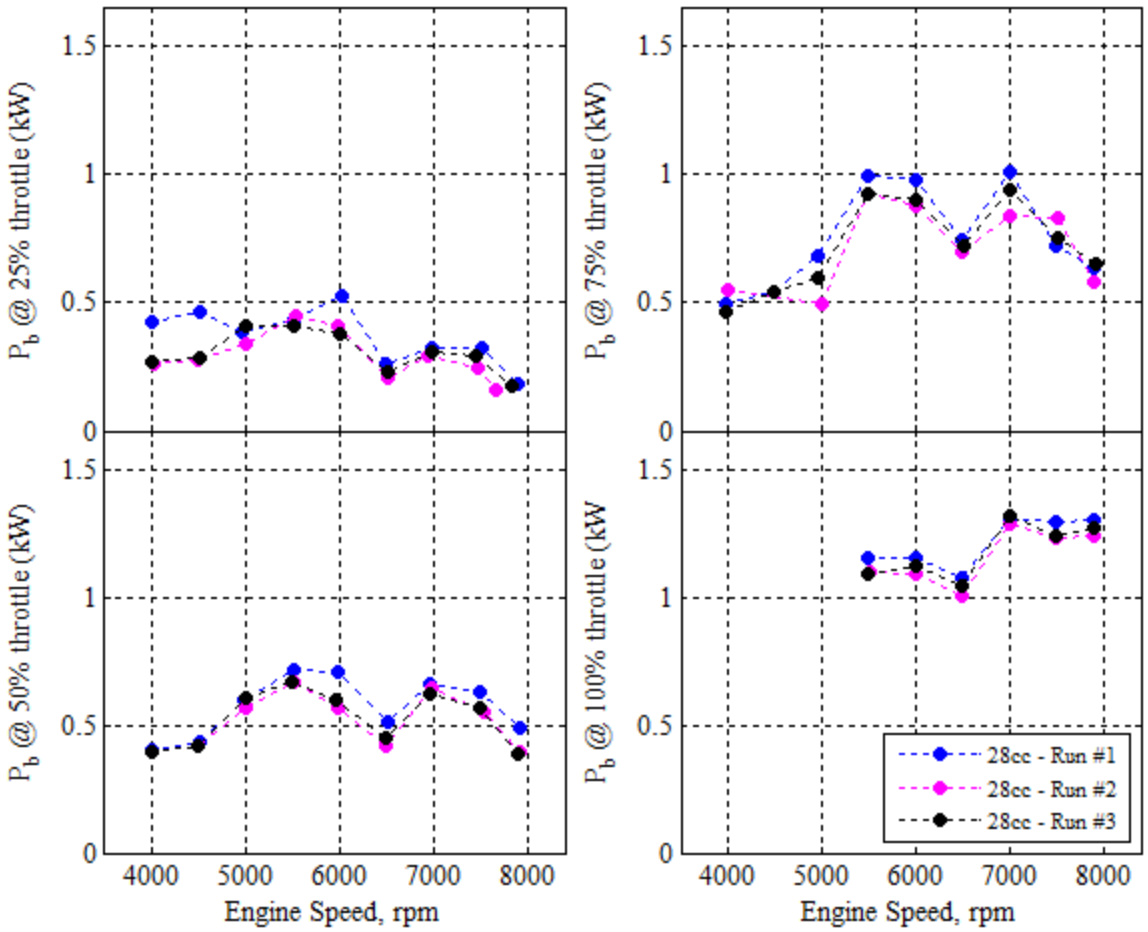

Figure 34: Three test runs of 28 cc engine, brake power at four throttle settings

Figure 35 shows the resulting equivalence ratios for each test run of the 28 cc engine. At 25% throttle, the equivalence ratio spiked during two separate test runs. This was most likely the result of general instability in the 28 cc engine and such a low throttle setting. It should be noted that each data point in a particular run consists of 10 seconds of measurement of raw data at a sampling rate of approximately 2 Hz. Before the data for point is captured, the engine is allowed to stabilize for 30-60 seconds to eliminate transient flow rates, speeds, and temperatures. The data for all throttle settings except for 25% (which is shown to be highly unstable) indicate that equivalence ratio drops at

approximately 6500 to 7000. This behavior is a result of engine speed and how the carburetor mixing needles interact with engine load. At a given throttle setting, as engine speed is increased, air flow rate increases, causing a larger pressure drop across the carburetor venturi which draws more fuel into the intake airstream. At low loads, the low needle supplies the majority of the fuel, but as load is increased, fuel supply by the low mixing falls short of sufficient and the high mixing needle adds additional fuel to attempt to maintain stoichiometric conditions. This transition is intended to happen fluidly, but because of the simple design of the carburetor, this transition causes a drop in equivalence ratio followed by a rise.

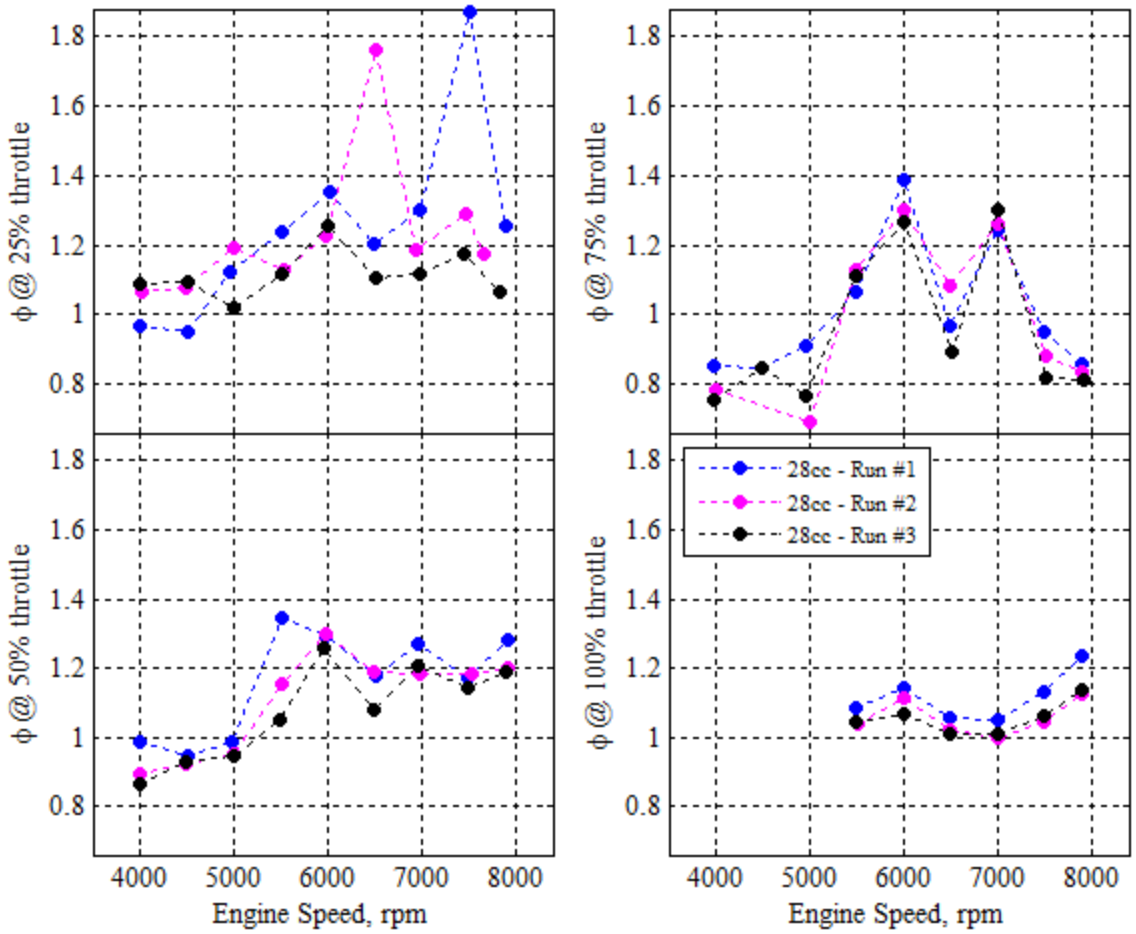

Figure 35: Three test runs of 28 cc engine, equivalence ratio at four throttle settings

At this point it should be re-emphasized that the mixing needles of each engine's carburetor were set to a position to provide best possible equivalence ratios across the entire range of engine speeds and throttle settings. Once the engine tuning was deemed sufficient, the mixing needles were not adjusted for the remainder of engine testing. Overall the 28 cc engine tended to have a larger variation at 75% throttle than 50% throttle. Outside of that, the variation in performance tended to decrease as the throttle plate was opened further. This was most likely due to the fact that intake air flow was steadier when the throttle plate was not acting as an obstruction. Since the engine was

carbureted, fuel flow was directly dependent on air flow. These two parameters ultimately have a large effect on overall engine performance due to the fact that they dictate the equivalence ratio for the fresh charge being delivered to the combustion chamber. Variation values included in Table 6 are one standard deviation of the mean of the corresponding test run data points for a 68% confidence interval. The variations in data across the speed range are then averaged to a single value for each throttle setting.

All data concerning the 28 cc engine henceforth is displayed as a mean of the three associated test runs. Uncertainty due to run-to-run variation and measurement error to a 95% confidence interval is also displayed. Figure 36 shows brake performance data for the 28 cc engine. In the upper left of Figure 36, brake power is plotted as a function of mean piston speed. The 28 cc engine produces a maximum power of 1.3 kW at 7000 rpm. Brake power and BMEP values for 75% throttle are lower at low engine speeds than the corresponding 50% throttle points. This is a result of the same phenomenon that limited the 100% throttle operability, although to a lesser extent in that the engine did not stall, it just produced less power (and a lower BMEP) due to sub-optimal equivalence ratios.

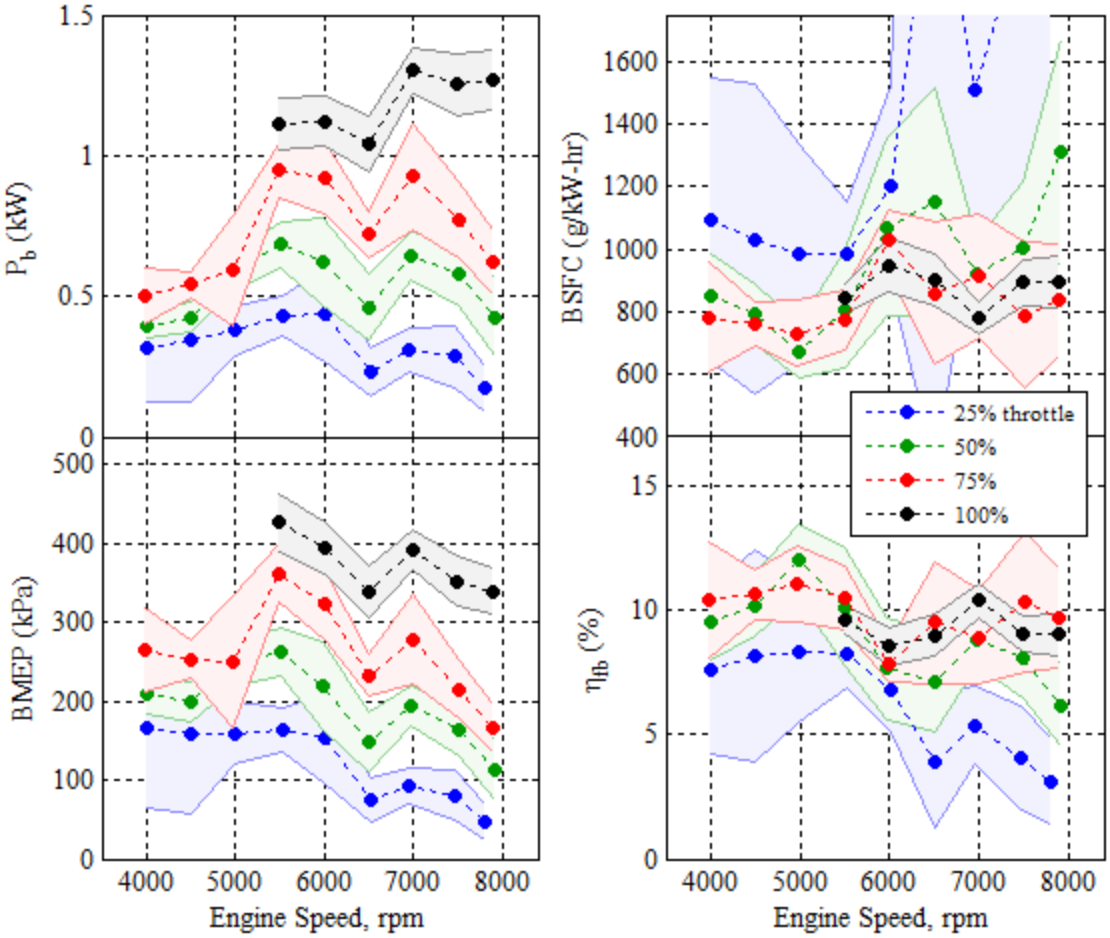

Figure 36: 28 cc engine brake performance

The 28 cc engine produced a maximum BMEP of 426 kPa at 100% throttle and 5500 rpm as shown in the lower left of Figure 36. BMEP is calculated by the function in Equation 2 in Chapter II. The reason maximum BMEP occurs at a mid-range engine speed is because of the trend of fuel conversion efficiency and mechanical efficiency (or friction) with respect to engine speed. As speed increases, an engine's ability to convert available energy to work imparted up on the piston improves because heat transfer out of the cylinder becomes less of a detrimental factor. However, friction between contacting surfaces such as the piston and cylinder walls or the crankshaft and bearings also

increases with increasing engine speed. At a certain point, increasing friction outweighs the benefits of increasing fuel conversion efficiency and BMEP drops off. At low engine speeds friction is reduced, but more heat transfer occurs causing a reduction in fuel conversion efficiency. Decreasing friction is secondary to the losses incurred by lower fuel conversion efficiency, so BMEP decreases. These phenomena combine to result in a peak value for BMEP that typically lies in the middle of an engine's effective speed range [4].

Best BSFC (lowest value) for the 28 cc engine was 674 g/kW-hr at 50% throttle and 5000 rpm as seen in the upper right portion of Figure 36. Minimum BSFC values occur at mid-range speeds for the same reasons as BMEP, but minimum BSFC typically occurs at mid-range throttle settings for the following reasons. Increasing engine load (opening throttle) while holding engine speed constant requires more fuel enrichment to increase torque while the engine becomes more and more air flow limited. This effect increases the rate of fuel consumption. On the other hand, decreasing load (closing throttle) while maintaining constant engine speed introduces more pumping work as a result of the closing throttle plate. The additional pumping work manifests as a friction loss, so power is reduced, causing BSFC to increase [4]. BSFC is calculated using the function in equation (3) from Chapter II. Since specific fuel consumption is a quantity normalized by power produced, BSFC values at 25% throttle and higher engine speeds (>6000 rpm) were excessively high (>2000 g/kW-hr) as result of low power output at approximately 6500 rpm and 7900 rpm. Furthermore, there was a large variation in repeatability from one test run to another proving that these operating points for the 28cc engine were very unstable. Maximum brake fuel conversion efficiency for the 28cc

engine (lower right in Figure 36) was 12% corresponding to the minimum BSFC point at 50% throttle and 5000 rpm.

Figure 37 shows the results of an analysis of indicated pressure measurements for the 28cc engine. Included are indicated power production level, IMEP, FMEP, and mechanical efficiency. The 28 cc engine produced a maximum indicated power of 2.2 kW at 100% throttle 7900 rpm. Peak IMEP was 645 kPa at 100% throttle and 5500 rpm. Friction mean effective pressure (FMEP) is the difference between IMEP and BMEP, and is a measure of the power dissipated by friction losses in an engine and its drivetrain components normalized by engine displacement and speed. FMEP in kPa is calculated by the function in Equation 15 where $(P_i - P_b)$ is the difference between indicated and brake power in kW, n_R is the number of crank revolutions per power stroke, V_d is cylinder swept volume in cubic decimeters, and N is engine rotational speed in revolutions per second. The difference between indicated and brake power is commonly referred to as friction power, P_f.

$$\boldsymbol{FMEP = \frac{(P_i - P_b) n_R}{V_d N}} \qquad \textbf{(15)}$$

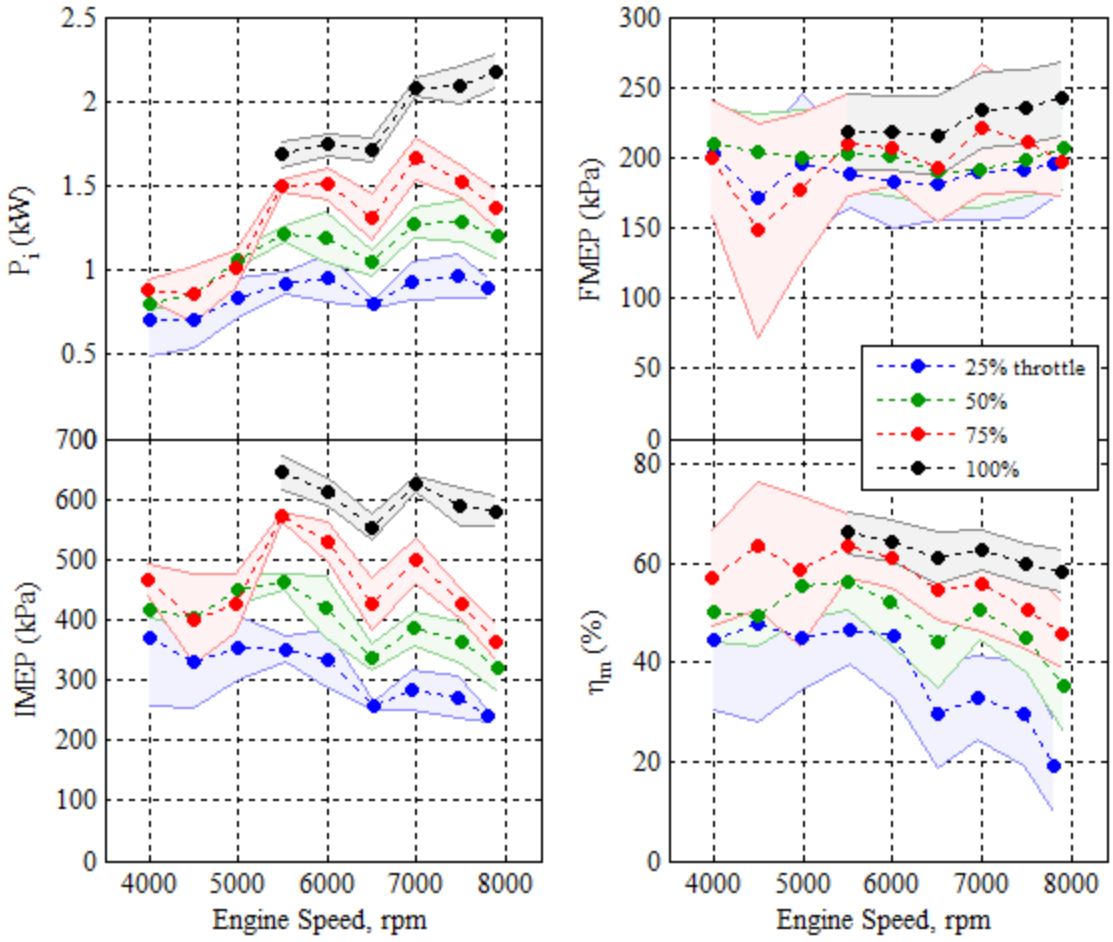

Figure 37: 28 cc engine indicated performance

The minimum FMEP for the 28cc engine was 148 kPa at 75% throttle and 4500 rpm. The minimum FMEP value occurred at a mid-range speed and throttle setting was a result of the balance between fuel conversion efficiency and friction with respect to engine speeds and throttle position much in the same way as the minimum BSFC value. Mechanical efficiency, η_m , is the ratio of brake power to indicated power and is also a measure of the relative amount of friction present in a given engine and drivetrain system. In this case, the 28cc engine produced a maximum mechanical efficiency of 66% at 100% throttle and 5500 rpm as shown in the lower right of Figure 37. The data

indicate that engine speed played a more important role in the balance of fuel conversion efficiency and friction as opposed to throttle position.

4.1.2 55cc Engine

Performance data for the 55 cc engine consisted of three separate test runs in order to evaluate the repeatability of engine performance. Figure 38 shows a graphical representation of the repeatability of brake power measurements from one test run to the next at different throttle settings for the 55 cc engine. Variation in measurements from run to run is included in Table 7 for the four core measurement values for comparison. These values are averaged over the entire speed range for a given throttle setting. The 55 cc engine did not exhibit low speed stalling issues like the 28 cc engine, so full throttle data was taken across the entire range of speeds tested as shown in the lower right of Figure 38.

Table 7: Average run-to-run variation of primary performance parameters for the 55 cc engine

	25% throttle	**50% throttle**	**75% throttle**	**100% throttle**
P_b	5.2%	3.4%	2.4%	1%
IMEP	2.8%	3.3%	2.6%	0.8%
$\dot{m}_f$	2.9%	4.5%	3.7%	2.4%
$\dot{m}_a$	1.4%	1.6%	1.5%	0.7%

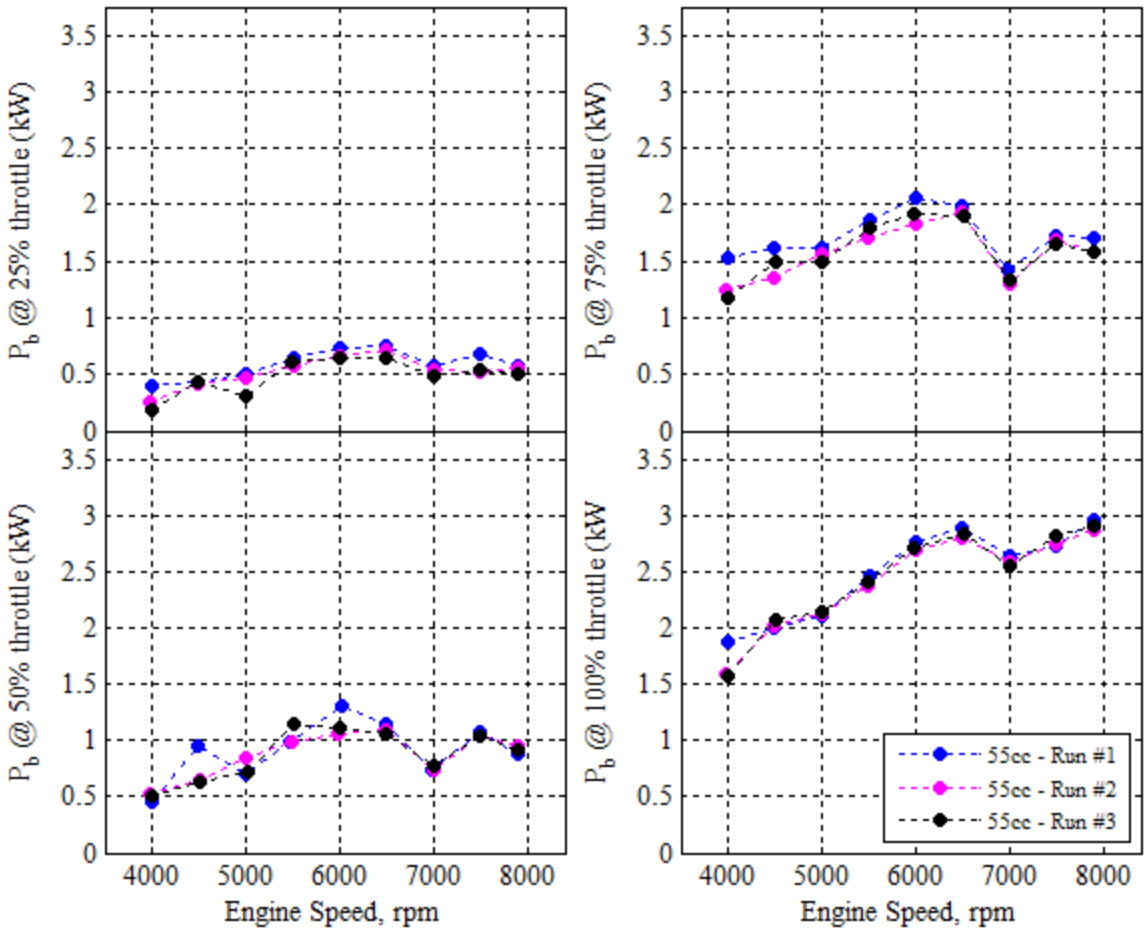

Figure 38: Three test runs of 55 cc engine, brake power at four throttle settings

Figure 39 shows the equivalence ratios for each test run of the 55 cc engine. The air and fuel mass flow rates at 50% throttle were the least stable causing a large variability in equivalence ratios from one run to the next. Despite efforts to maintain external control variables like ambient temperature and cylinder head temperature, variation in equivalence ratio was still large. This was most likely a result of the limitations of the engine's carburetor to meter fuel flow appropriately for the given air flow rates. The first 55 cc test run was performed on one day, while the second and third test runs were both performed on the following day. The extra time surrounding the first

test run could help to explain why equivalence ratios appeared to differ. Generally, the 55 cc engine exhibited the largest amount of performance variation at 50% throttle. The engine was most consistent in terms of performance at 100% throttle. With the throttle plate at or near the fully-open position, steadier air and fuel flow rates promoted a consistent equivalence ratio that tended to improve repeatability.

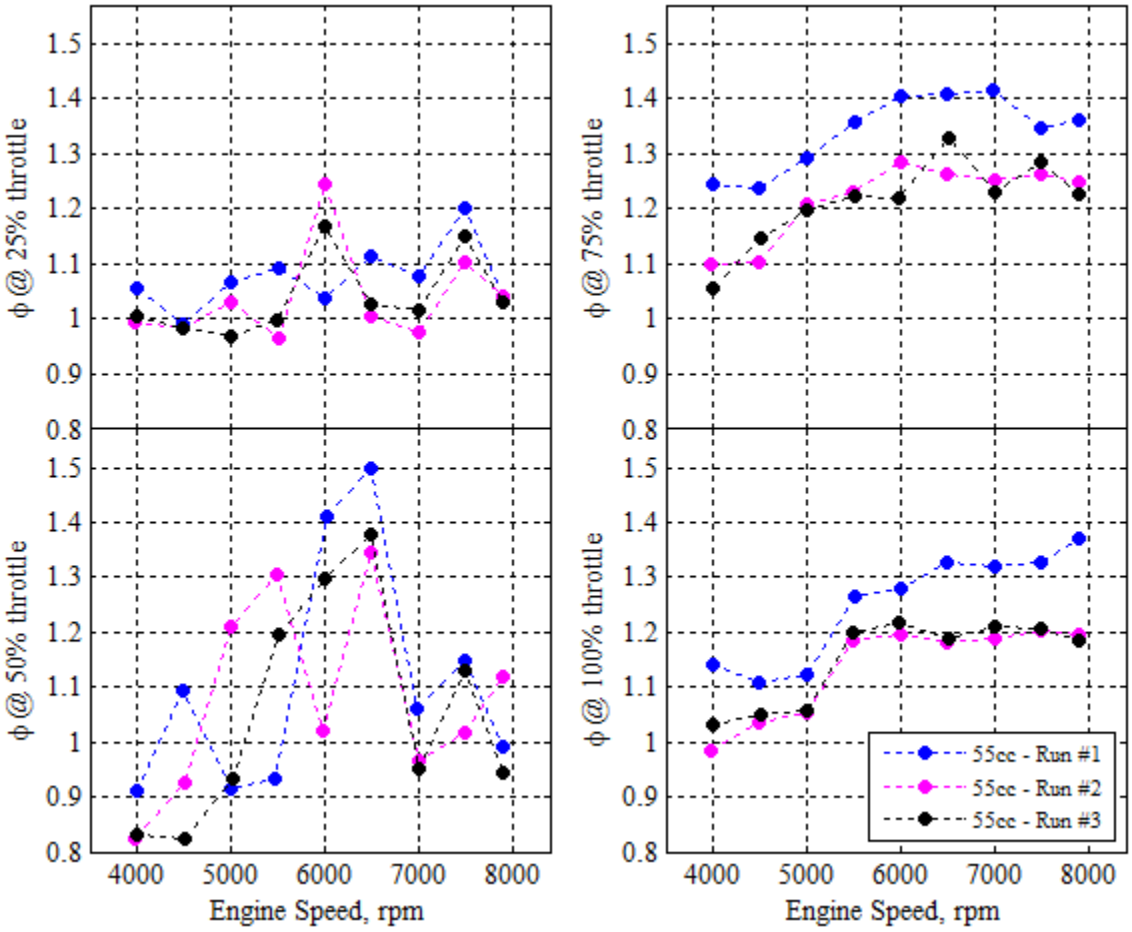

Figure 39: Three test runs of 55 cc engine, equivalence ratio at four throttle settings

The 55 cc data displayed in the remainder of this study will be the mean of the individual test runs completed for this engine's performance testing. Associated uncertainty due to run-to-run variability and measurement error will also be displayed to

a 95% confidence interval. Figure 40 shows the brake performance for the 55 cc engine. Maximum brake power was 2.9 kW at 7900 rpm. Peak BMEP was 489 kPa at 100% throttle and 6000 rpm. A minimum BSFC of 579 g/kW-hr occurred at 100% throttle at 4500 rpm. Although the absolute minimum BSFC point occurred at 100% throttle, the engine tended to exhibit lower BSFC values mid-range throttle settings of 50% and 75% across a range of engine speeds. The same operating point corresponded to a peak brake fuel conversion efficiency of 14%. Brake power and BMEP tended to have a strong correlation with throttle setting while BSFC and fuel conversion efficiency did not. Engine speeds between 5500 and 6500 rpm tended to favor BMEP performance for this engine. Peak power at all throttle settings typically occurred at 6500 rpm. At higher speeds, it seemed that poor tuning caused power levels to drop off.

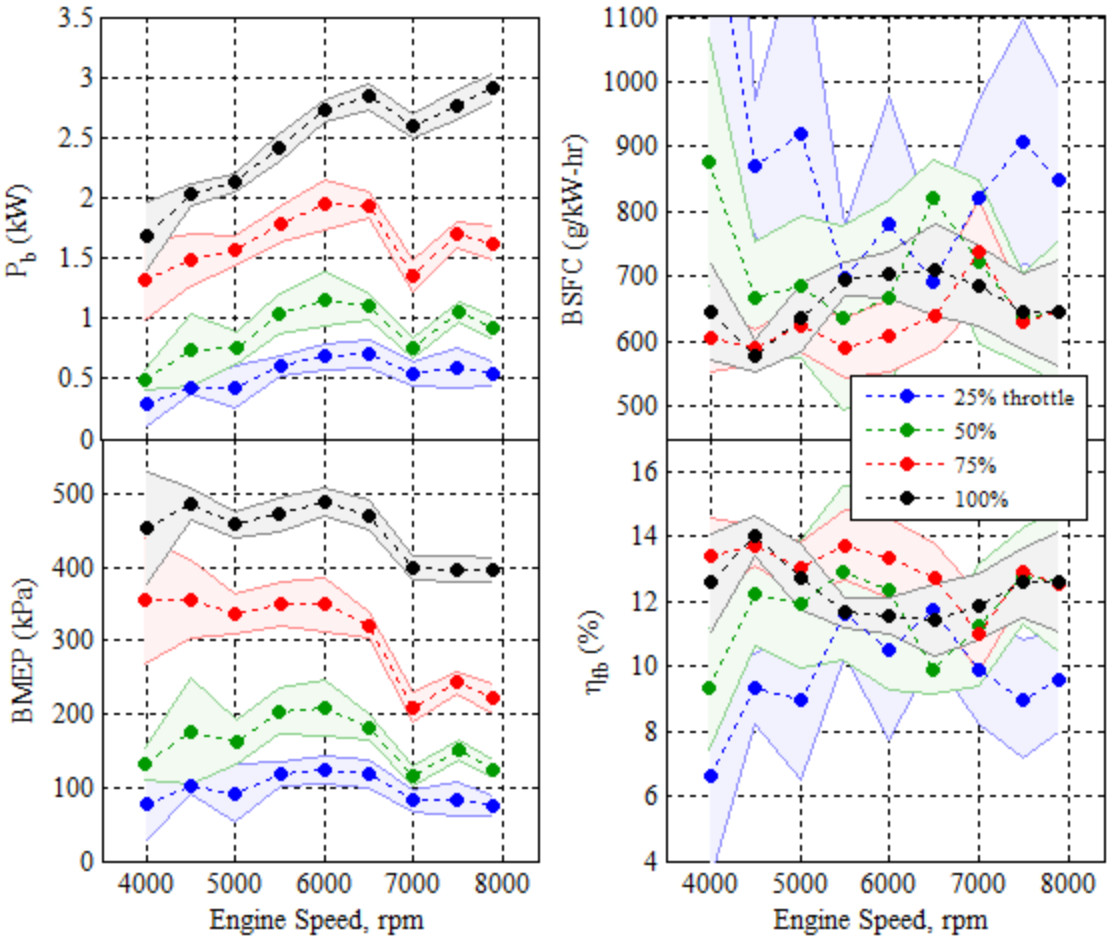

Figure 40: 55 cc engine brake performance

In Figure 41, indicated performance for the 55 cc engine is shown. Indicated power reached maximum of 3.9 kW at 7900 rpm. Maximum IMEP was 630 kPa at 100% throttle and 6000 rpm. It should be noted that the 55cc engine produced an IMEP of 627 kPa at 100% throttle and 4500 rpm as well. Although the data indicate that best FMEP (minimum) for the 55 cc was 74 kPa at 50% throttle and 7500 rpm, there was a large error in the result due to run-to-run variability. Therefore, neglecting that result, a more reasonable minimum FMEP for the 55 cc engine was 93 kPa at 25% throttle and 7000 rpm. Maximum mechanical efficiency for the 55 cc engine was 78% at 100%

throttle and 6500 rpm. The 55 cc engine also produced a mechanical efficiency of 78% at 100% throttle and 6500 rpm. The data indicate that indicated power and IMEP scale with throttle across all speeds. This trend is expected due to the fact that an open throttle plate introduces less pumping losses meaning an engine can produce more power more efficiently. Additionally, the data show that FMEP and mechanical efficiency also scale with throttle position for all speeds. This indicates that BMEP falls off as the throttle plate is opened. If engine speed is held constant while load is increasing (travelling upwards on a vertical line in the upper right plot of Figure 41), then additional fuel enrichment caused by opening the throttle will tend to reduce brake performance. Alternatively, according to the trend of mechanical efficiency, brake power increases faster as a function of throttle position than does indicated power. This is due to the fact that the throttle plate in the open or nearly-open position causes less pumping work, and hence less friction loss. Lower friction drives the engine's mechanical efficiency closer to unity.

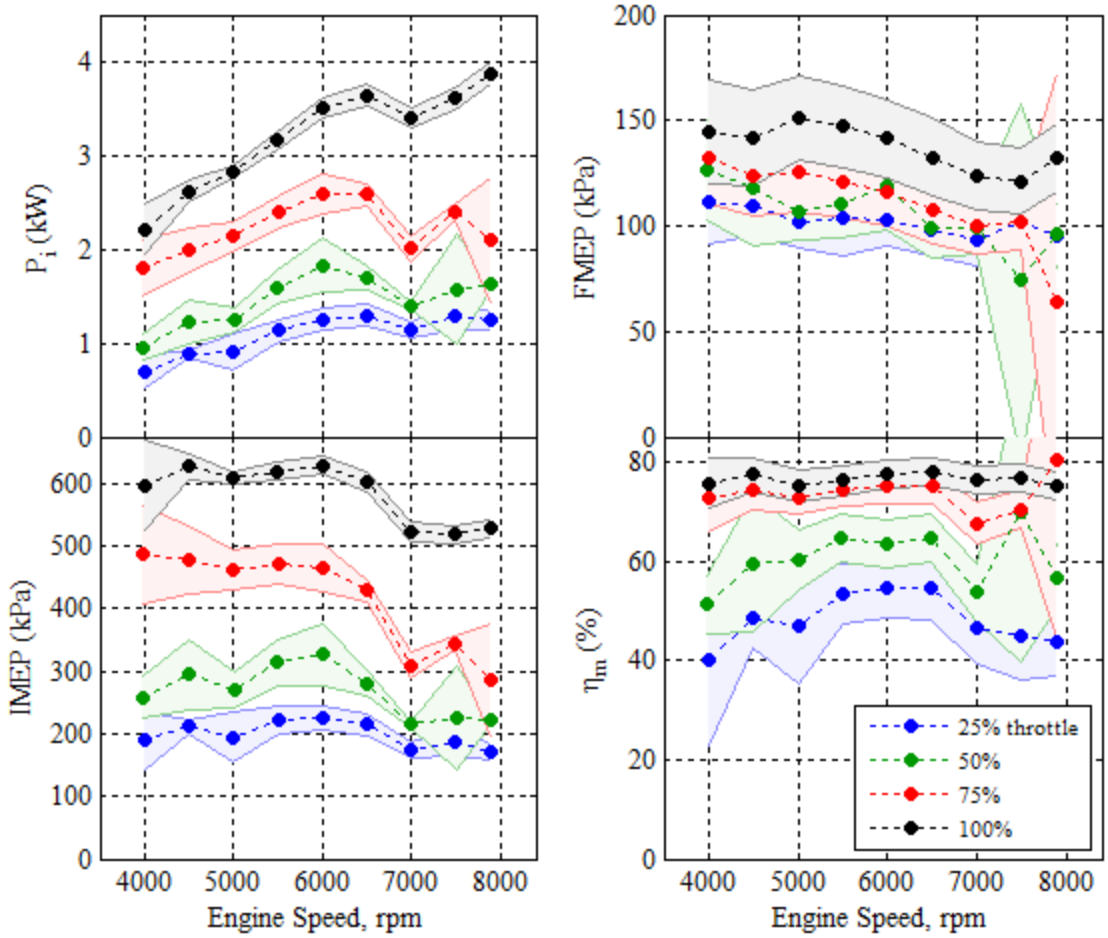

Figure 41: 55 cc engine indicated performance

4.1.3 85 cc Engine

The test data for the 85 cc engine is comprised of three test runs for repeatability analysis. The plots in Figure 42 show the brake power variation from test run to test run for the 85 cc engine. Additionally, brake power variation data as well as variation data for the remaining core measurement parameters at different throttle settings are listed in Table 8. These values are an average of the variation of all data points across the range of engine speeds tested for each throttle setting.

Table 8: Average run-to-run variation of select performance parameters for the 85 cc engine

	25% throttle	**50% throttle**	**75% throttle**	**100% throttle**
P_b	2.7%	1.5%	1%	0.8%
IMEP	1.9%	3.7%	1%	0.8%
$\dot{m}_f$	1.4%	1.5%	1%	0.9%
$\dot{m}_a$	0.9%	1.6%	1.5%	1.6%

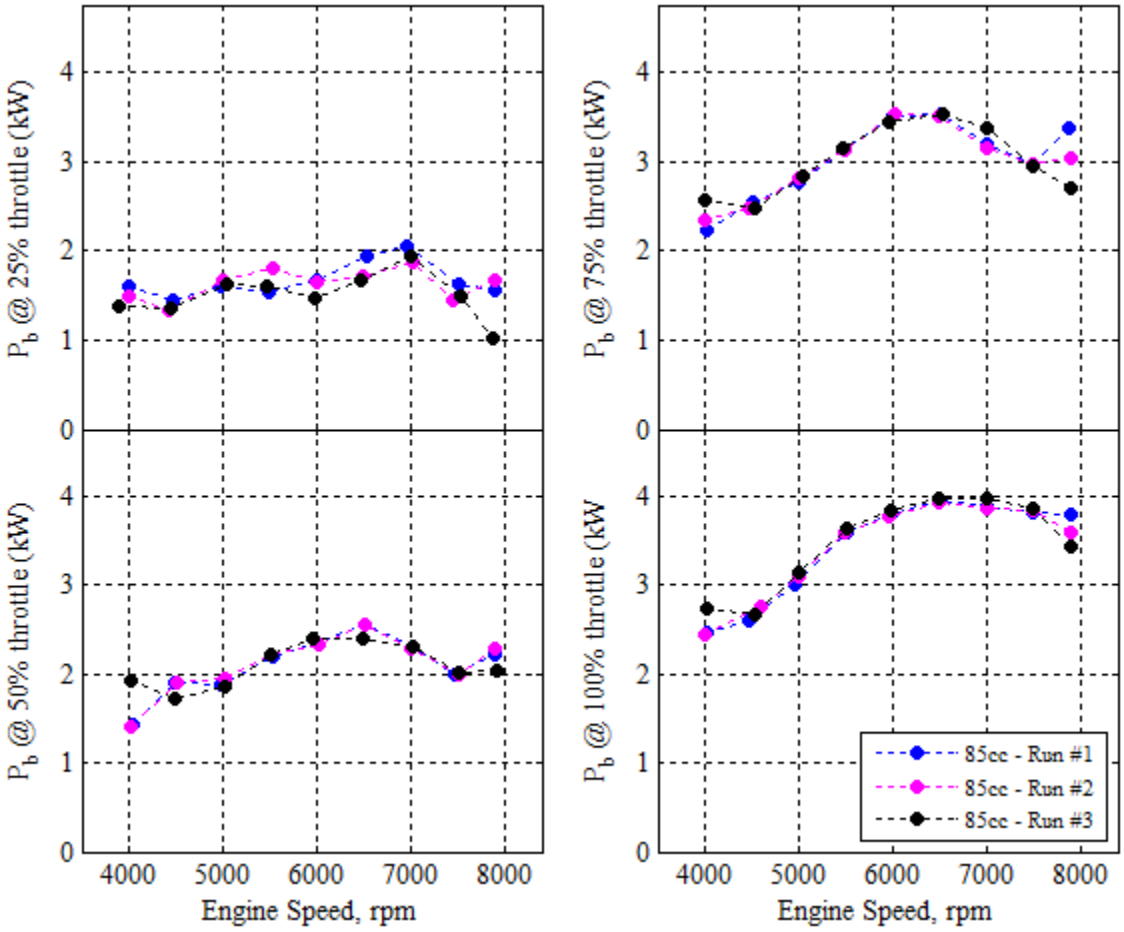

Figure 42: Three test runs of 85 cc engine, brake power at four throttle settings

Figure 43 shows the equivalence ratios for each test run of the 85cc engine. At 25% throttle, the transition to the high mixing needle appeared to occur more gradually based on the absence of a sharp decline followed by a sharp incline in equivalence ratio

as exhibited by the 28 cc engine. The equivalence ratio of the third test run was more fuel-lean across the range of speeds and throttle settings tested. Test runs #1 and #2 were performed on the same day while two weeks passed before data acquisition for test run #3. An examination of ambient pressures during corresponding test runs revealed that runs #1 and #2 were performed on a day when ambient pressure was 14.17 psig, while run #3 was performed on a day when ambient pressure was 14.38 psig. The low pressure corresponding to test runs #1 and #2 effectively lowered the density of the air, which ultimately lowered the mass flow of air being measured. This in turn caused the recorded equivalence ratio to increase.

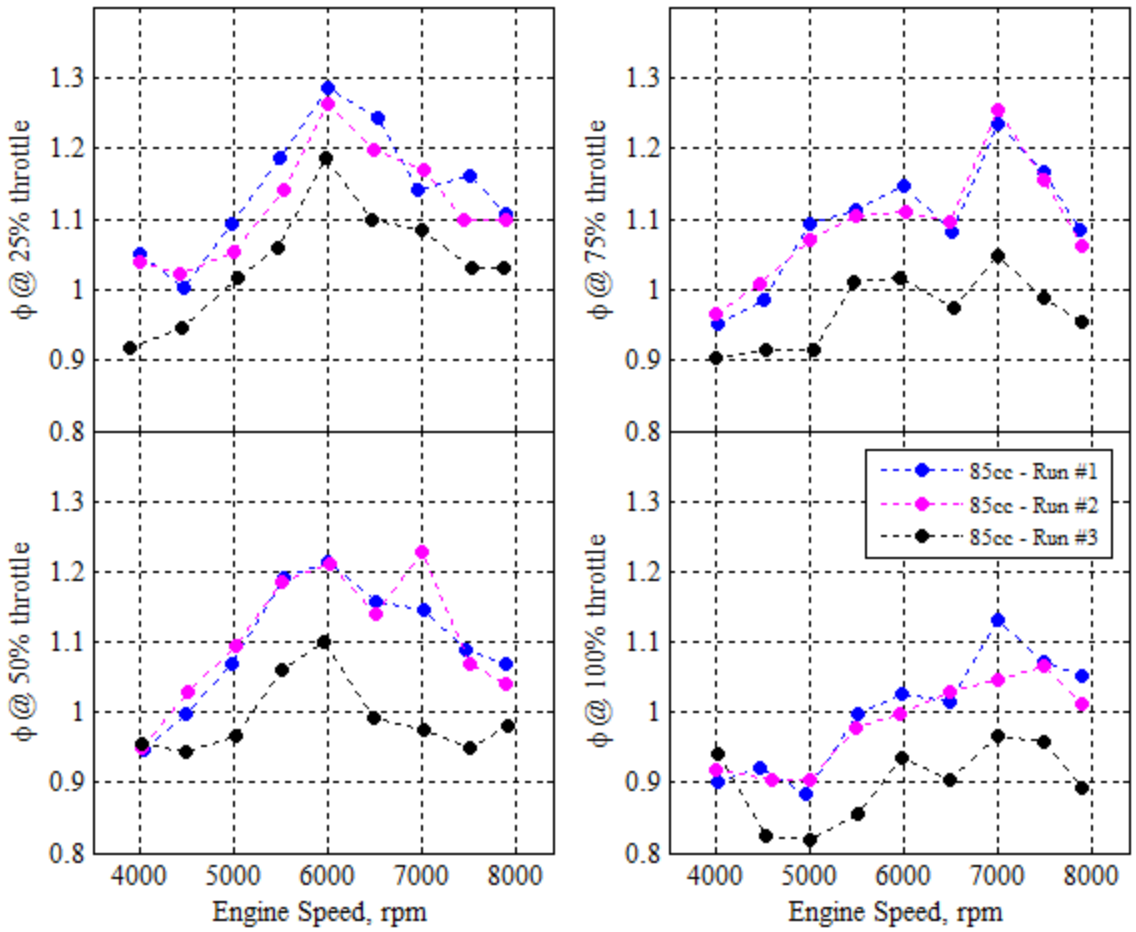

Figure 43: Three test runs of 85 cc engine, equivalence ratio at four throttle settings

For the remainder of this study, 85 cc engine performance data is displayed as a mean of the three test runs with associated uncertainty due to run-to-run variation and measurement error to a 95% confidence interval.

Figure 44 shows the 85 cc engine's brake performance data. As the largest engine in this study, it produced a maximum brake power of 3.9 kW at 6500 rpm. A peak BMEP of 468 kPa was achieved at 100% throttle and 5500 rpm. The 85 cc engine's best BSFC was 448 g/kW-hr at 50% throttle and 6500 rpm. This corresponded to a peak brake fuel conversion efficiency of 18% at the same operating point. The 85 cc engine

exhibited a smoother transition as the carburetor's high mixing needle supplied additional fuel at high engine speeds. For comparison the 28 cc and 55 cc engines exhibited dual peak behavior in terms of brake power as shown in the upper left of Figure 36 and Figure 40 respectively. This is most likely due to poor tuning as the carburetor's high mixing needle added additional fuel in an abrupt manner that diminished performance.

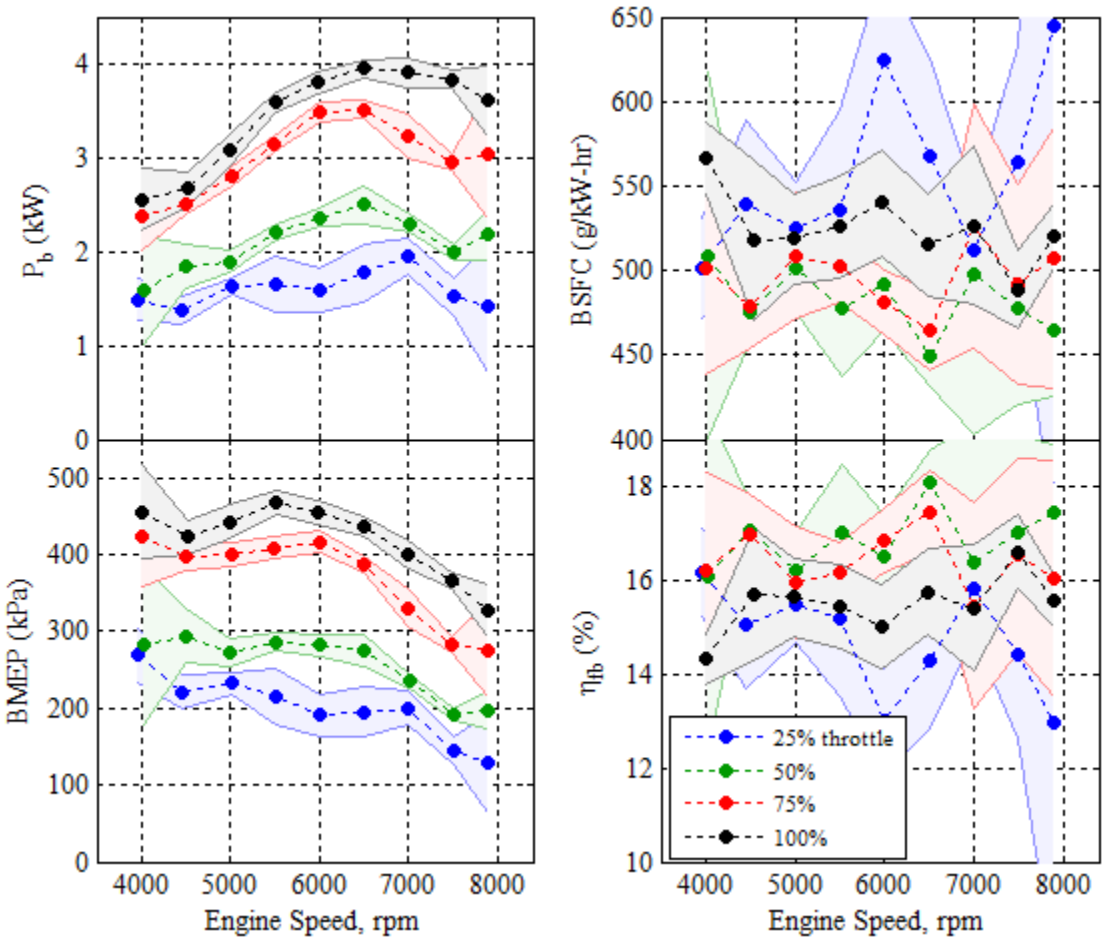

Figure 44: 85 cc engine brake performance

Indicated performance for the 85 cc engine is shown in Figure 45. Maximum indicated power was 5.2 kW at 7900 rpm. Peak IMEP was 584 kPa at 100% throttle and 5500 rpm. The resulting minimum FMEP was 71 kPa at 50% throttle and 7000 rpm.

The maximum mechanical efficiency achieved by the 85cc engine during testing was 81% at 100% throttle and 6500 rpm.

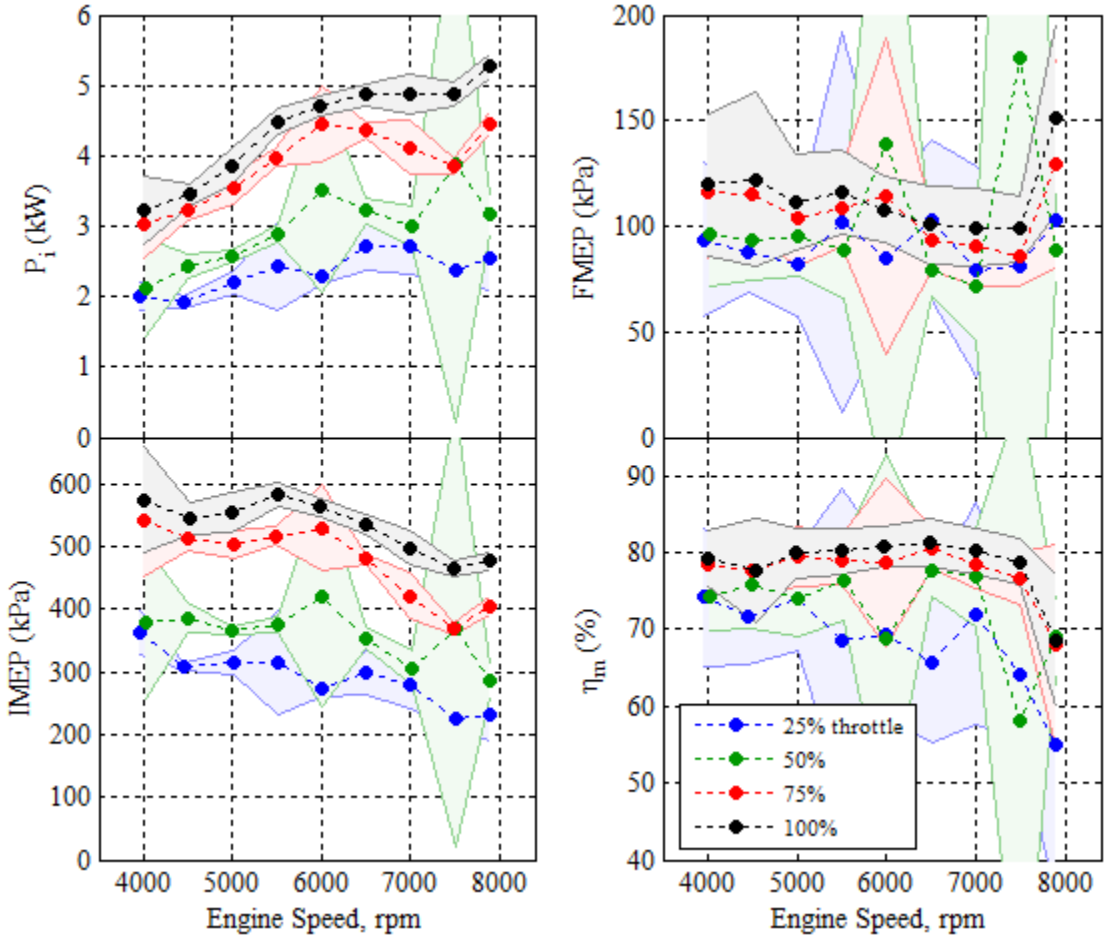

Figure 45: 85 cc engine indicated performance

4.2 Engine Comparisons

The following sections (4.2.1 - 4.2.4) contain comparisons of performance data from each of the three scaling study engines. Discussion includes comparisons of power production, specific fuel consumption, mean effective pressures and friction loss, and thermal loss to the cooling medium. Three energy pathways were quantified in this study. They included power production, friction loss, and heat transfer to the cooling medium. These pathways are reported in terms of percentage of total fuel energy

available. The remaining energy unaccounted for was assumed to be comprised of exhaust enthalpy and other miscellaneous pathways such as radiation and gas kinetic energy. Exhaust enthalpy calculations were based on assumptions from the scientific literature. These assumptions will be discussed further in Section 4.2.4. The engine comparison study concludes with a discussion of the energy pathways and their relative magnitudes for each of the engines.

The data in Table 9 are best case performance parameters for each engine. In most cases these are maximum values except for FMEP and BSFC which are minimums. In this case, all throttle settings and operating speeds are considered for overall best performance values so engine speeds and throttle settings are not necessarily constant.

Table 9: Scaling study engine performance summary

	28 cc	**55 cc**	**85 cc**
P_i (kW)	2.2	3.9	5.2
P_b (kW	1.3	2.9	3.9
IMEP (kPa)	645	630	584
BMEP (kPa)	426	489	468
FMEP (kPa)	148	93	71
BSFC (g/kW-hr)	674	579	448
η_{fb}	12%	14%	18%
η_m	66%	78%	81%

4.2.1 Power & Specific Fuel Consumption

Figure 46 shows the best case brake power and brake specific fuel consumption values for each engine in terms of engine displacement as well as cylinder surface area to swept volume ratio. In the upper left of Figure 46 it can be seen that maximum power scales with engine size as expected. Brake power decreased by 26% from the 85 cc

engine to the 55 cc engine which equated to a power loss per displacement rate of 33 W/cc. The decrease in power from the 55 cc engine to the 28 cc engine was 55%, or a loss rate of 59 W/cc. Considering the fact that these engines span the size regime in which power scaling trends area expected to change, it comes as no surprise that the rate in which power changes with respect to engine displacement differs when stepping down from the middle engine versus stepping up. Brake specific fuel consumption allows an examination of the ability of an engine to convert fuel into usable power. Since it is a normalized value, differences in BSFC can be an indicator of the overall effectiveness of an engine in operation. Lower SFC rates are better, and in the case of this scaling study, the 28 cc engine was out-performed by both of the other engines. A reduction of 3.5 g/kW-hr per cm^3 of displacement was realized when moving from the 28 cc engine to the 55 cc engine. Likewise, the reduction rate from the 55 cc engine to the 85 cc engine was 4.4 g/kW-hr per cm^3. The data for BSFC values can be seen in the lower left and right of Figure 46. It should be noted that the data points in Figure 46 reflect best possible values for brake power and BSFC for all engine speeds and throttles that were tested for each engine. The brake power data points do not necessarily correspond to the same operating conditions at which the BSFC points occurred because maximum power and minimum specific fuel consumption occurred at two separate operating points for every engine.

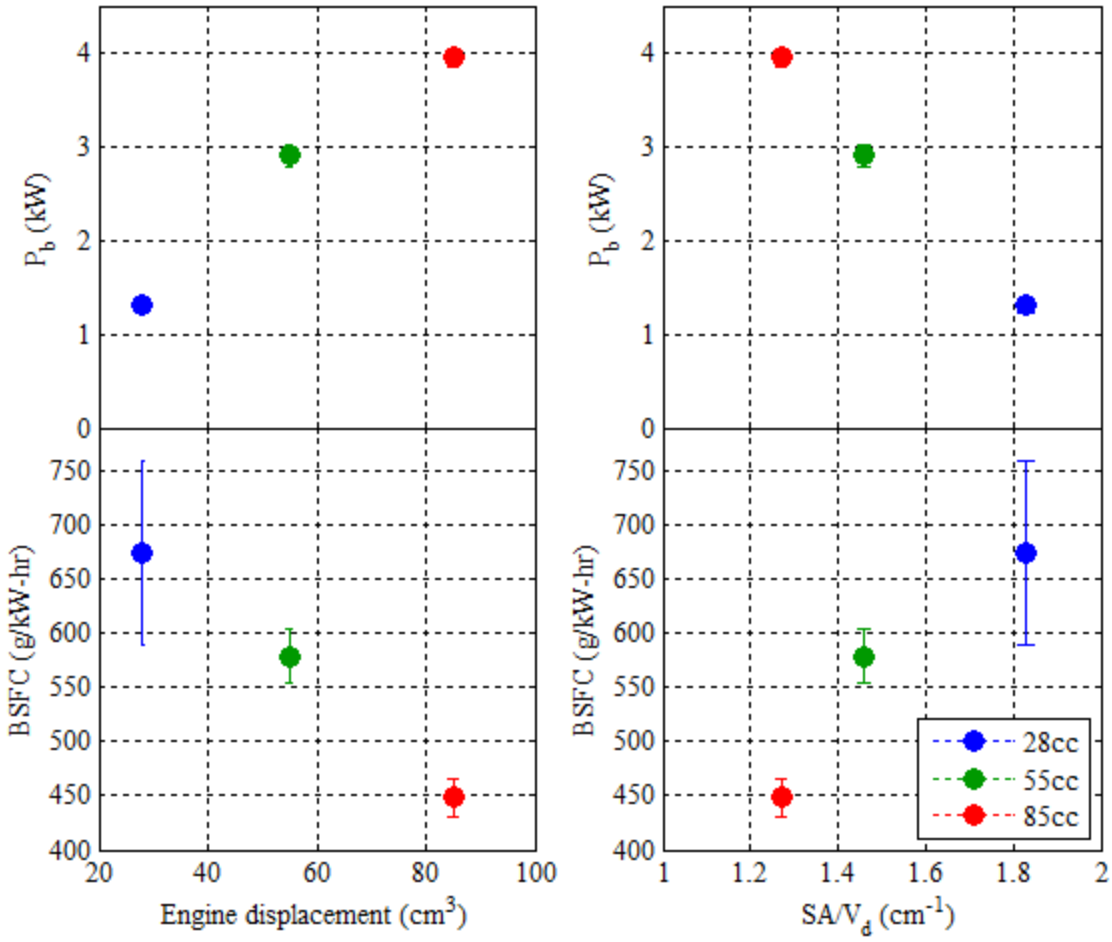

Figure 46: Best brake power and BSFC for three engines

4.2.2 Mean Effective Pressure

Figure 47 shows the indicated, brake, and friction mean effective pressures at 100% throttle and 6000 rpm in this scaling study as a function of cylinder surface area to swept volume ratio. Due to the effect of increasing cylinder surface area to swept volume ratio, it was expected that the IMEP values would decrease with decreasing engine size. However, the 85cc engine produced a lower IMEP value than both of the smaller engines. This was most likely due to the fact that the equivalence ratio for the 85 cc engine at 1.0 was lower than that of the other two, 1.2 for 55 cc and 1.1 for 28 cc. Another possibility is that the largest engine is experiencing more short-circuiting or lower combustion

efficiency. This is unlikely however, as brake fuel conversion efficiency increases with increasing engine size as will be discussed in Section 4.2.4.

The lower left of Figure 47 shows the corresponding BMEP values for each engine. The 7% increase in BMEP from the 85cc engine to the 55 cc engine is most likely a result of the same phenomenon causing lower IMEP values in the 85 cc engine. Since BMEP takes into account the friction losses that an engine experiences, it stands to reason that the second combustion sealing piston ring in the 85 cc engine could have caused enough additional friction loss to reduce maximum BMEP below that of the 55 cc engine. In other words, the cost in terms of friction of having an extra piston ring could have outweighed the benefit of the 85 cc engine's extra displacement volume and then some. BMEP decreased 19% from the 55 cc engine to the 28 cc engine. This was expected due to the increasing cylinder surface area to swept volume ratio of the smallest engine. Upon examination of the corresponding FMEP for each engine as shown in the upper right of Figure 47 though, the 85 cc engine's normalized friction losses were less than the other engines. FMEP values shown are 108 kPa for the 85 cc engine, 141 kPa for the 55cc engine, and 218 kPa for the 28 cc engine. There was a 31% increase in FMEP from the 85 cc engine to the 55 cc engine. This change indicates that the second piston ring of the 85 cc engine may not have been the sole culprit of its lower maximum BMEP. The corresponding increase in FMEP from the 55 cc to the 28 cc engine was 55%. Considering both engines had the same number of piston rings (one in this case) and the mean piston speed of the 28 cc engine was lower (meaning friction should have been lower) and the associated FMEP of the 28 cc engine was still the highest, friction losses are clearly a dominating factor in the performance of the smallest engine.

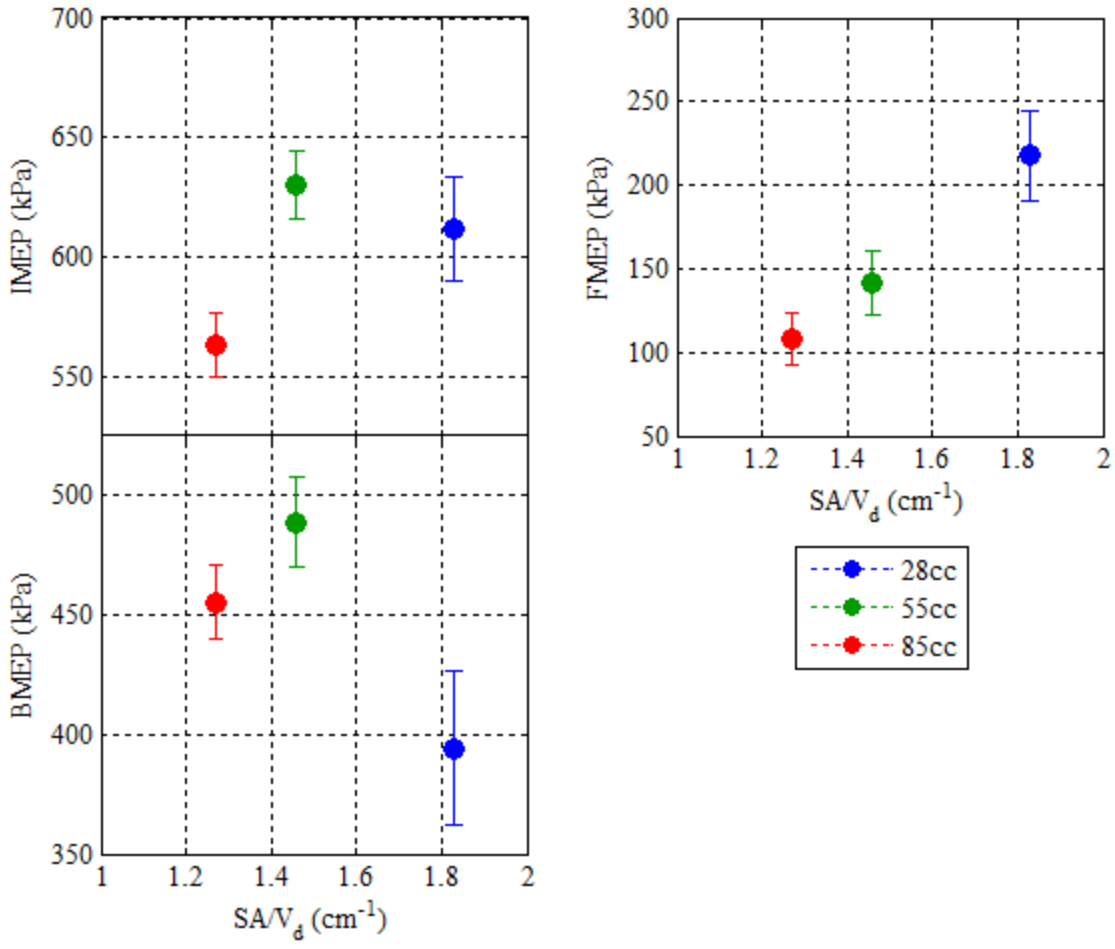

Figure 47: Mean effective pressures at 100% throttle, 6000 rpm for each engine

An examination of FMEP across all speeds and for all throttle settings would show that the 28 cc engine experienced more friction loss relative to its size than either of the other scaling study engines by a considerable margin. Since each engine was tested over the same range of speeds using the same drivetrain configuration, drivetrain friction losses remain a constant across all engines. Therefore, internal friction losses within the 28 cc engine itself are causing the detrimental effect on performance. This stands to reason as the cylinder surface area to swept volume ratio of the 28 cc engine is highest, so

this surface area based loss phenomenon is a driving factor in poor relative performance as compared to the 55 cc and 85 cc engines.

4.2.3 Thermal Loss

Figure 48 shows the results of the heat rejection measurement method involving the insulated engine enclosure apparatus. Data are displayed for all engine speeds at four throttle settings as tested for each engine. At this point it should be restated that the cylinder head temperature of each engine was maintained at 285°F ±5°F for every operating point to maintain consistency. There is a definitive trend in heat rejection with respect to engine displacement. As the engines got larger, they ingested more fuel per cycle, and hence more energy. It stands to reason that the amount of energy exiting the IC engine control volume as heat transfer to the cooling medium increased as well. The data reflect that heat rejection increased with engine speed also. The number of combustion events on a per time basis is directly tied to engine speed, so as engine speed increased heat was generated at a faster rate for all engines. Because engine temperature was held constant for the experiment, cooling air mass flow had to be increased at higher engine speeds, thus resulting in larger amounts of heat transfer.

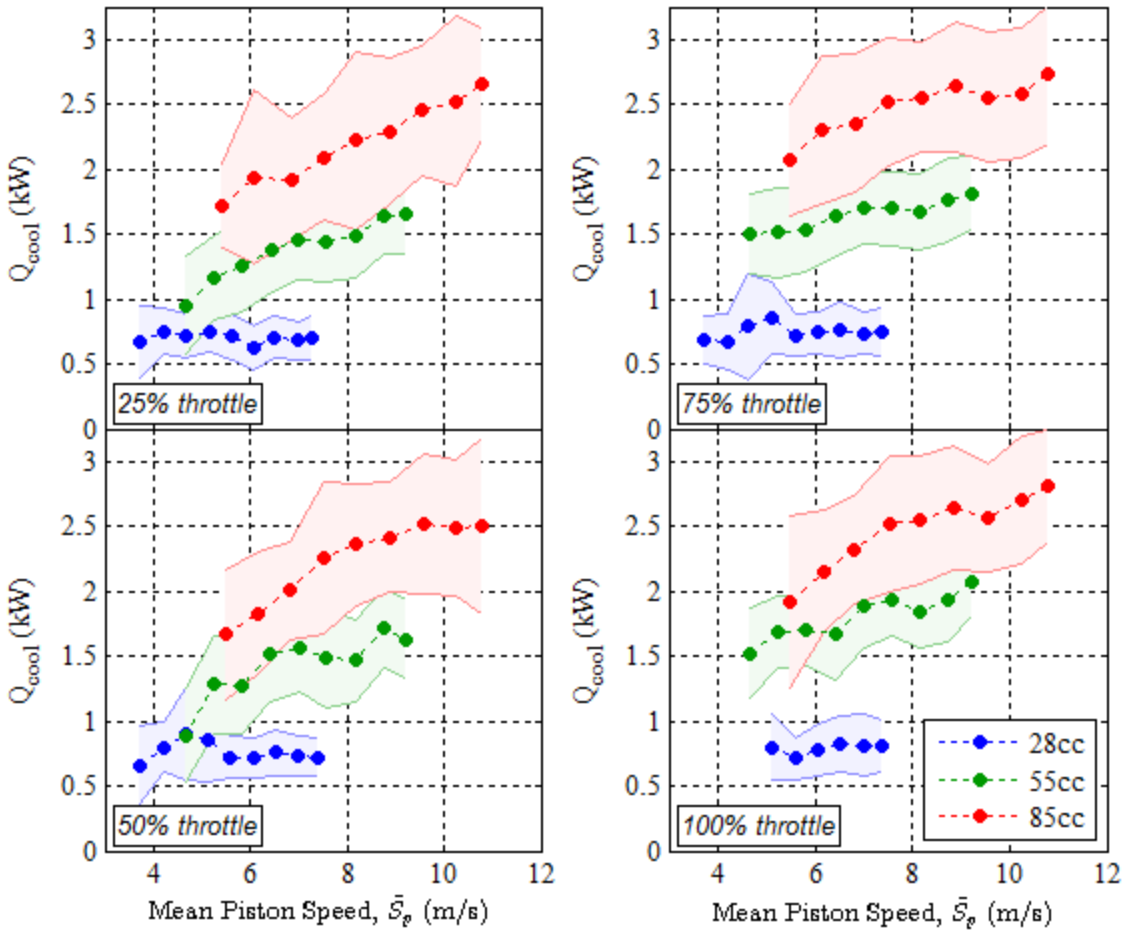

Figure 48: Heat rejection comparisons at four throttle settings

Although the data in Figure 48 show that the smaller an engine is the less energy it loses to cooling, it does not indicate the influence of heat rejection on engine performance as a loss mechanism. In other words, the 28 cc engine lost less heat to cooling, but it also produced less power. A better way to examine the scaling effects on heat rejection is to normalize Q_{cool} by the total amount of energy entering the system as fuel enthalpy. This energy is characterized by the mass flow rate of fuel, $\dot{m}_f$ multiplied by the fuel's heating value, Q_{HV}. These normalized heat rejection values are discussed in the following section (4.2.4) on characterization of energy flows.

4.2.4 Energy Pathway Characterization

The data in Figure 49 and Figure 51 represent energy flow values as functions of throttle position at constant mean piston speeds. These energy flows are normalized by total available fuel energy on a per cycle basis. Three energy pathways were measured in this study; power production via brake fuel conversion efficiency, normalized friction power, and normalized heat transfer to engine cooling. In Figure 49, a mean piston speed of 5.5 m/s was chosen because it was the lowest mean piston speed at which all engines were tested. In other words, the limiting factor for this case was the 85 cc engine at 4000 rpm. It should be noted that although the normalization parameter accounts for 100% of the incoming energy, the three plots of measured energy pathways do not account for all of the outgoing energy. The remainder of outgoing energy unaccounted for is primarily associated with the exhaust stream including sensible enthalpy change and unburned fuel due to short-circuiting and combustion inefficiency. Because exhaust enthalpy measurements were not taken in this study, the associated energy flow pathways are not reported. Estimations of exhaust enthalpy will be discussed for the 100% throttle case immediately following this discussion. The data in the upper-left of Figure 49 indicate that brake fuel conversion efficiency tended to increase as the throttle was opened.

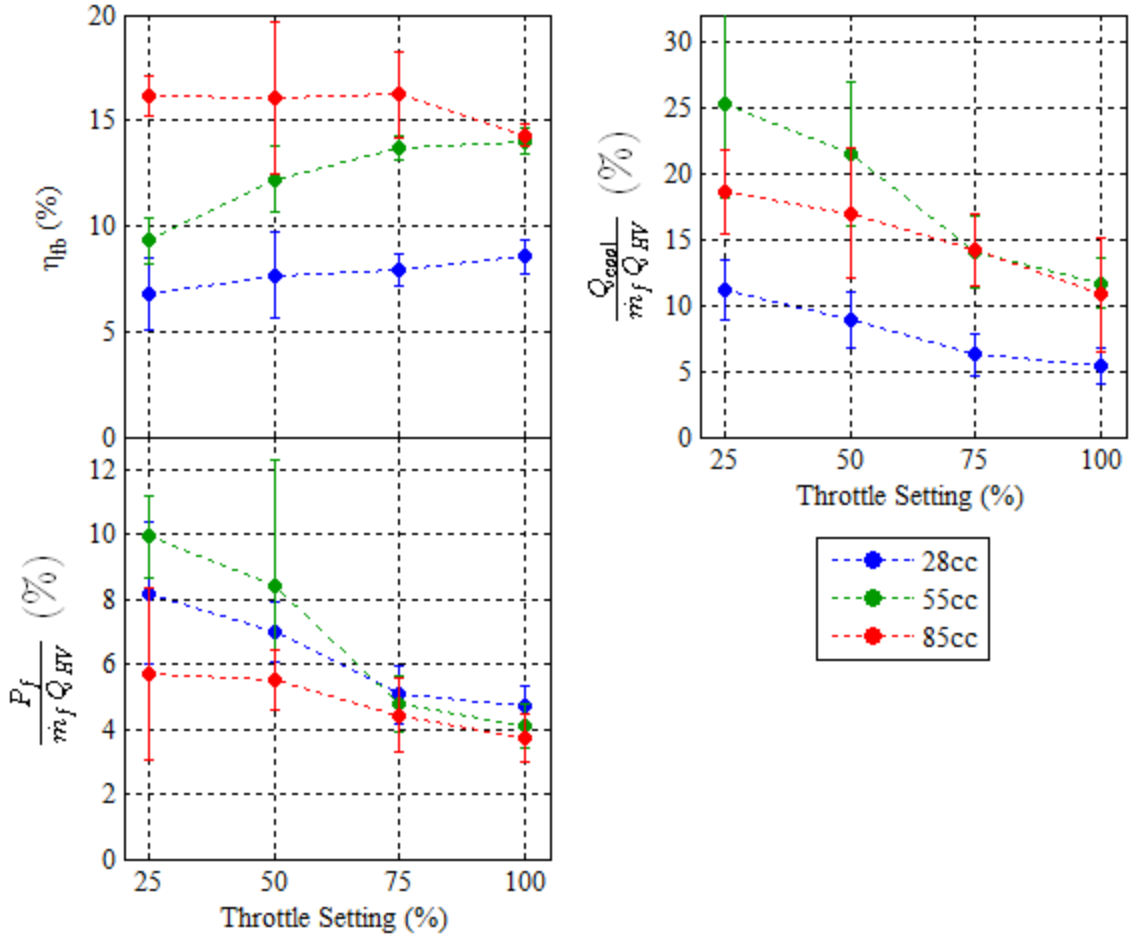

Figure 49: Energy pathways at 5.5 m/s mean piston speed

An examination of the friction and cooling pathways shows that these losses tended to decrease with opening throttle. In the case of friction, as the throttle plate opens, the amount of pumping work the engine must overcome decreases, thus decreasing friction loss. For engine cooling, as the throttle plate opens, the mass flow through the engine increases, reducing the amount of heat transfer from the combusting gases to the cylinder walls and eventually to the cooling medium. It stands to reason that if the friction and cooling energy loss pathways decrease with opening throttle, then the ability of the engine to convert available energy to shaft power should increase. At 5.5

m/s mean piston speed, brake fuel conversion efficiency decreases with engine size as expected. It can be seen that friction losses tend to increase with decreasing engine size, while normalized engine cooling losses decrease with decreasing engine size. At throttle settings lower than 75%, the friction losses of the 28 cc engine are lower than the 55 cc engine. This is most likely due to the throttling effects on friction. Figure 50 shows the measured energy pathways for each engine at a constant mean piston speed of 6.5 m/s. Overall trends with respect to throttle setting are similar to those corresponding to the 5.5 m/s data.

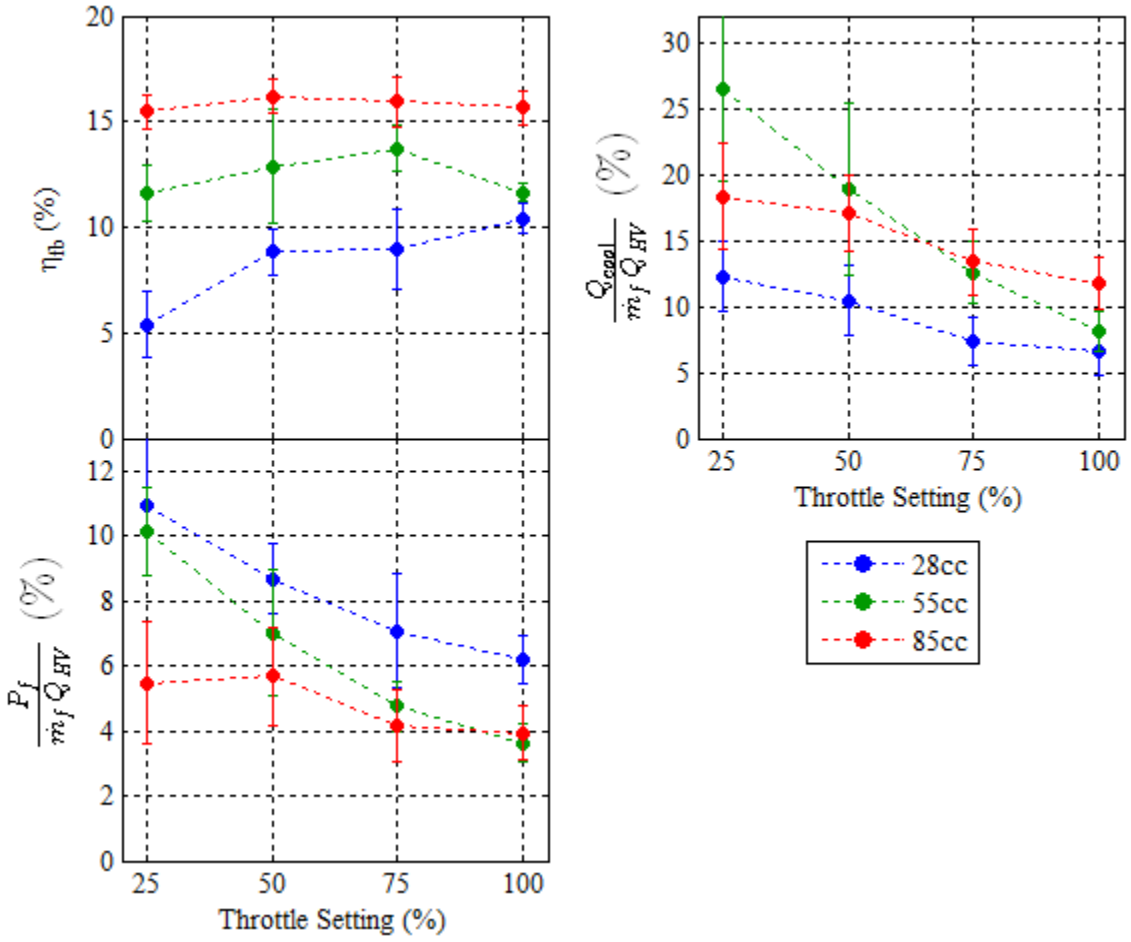

Figure 50: Energy pathways at 6.5 m/s mean piston speed

Figure 51 shows measured energy pathways for each engine as a function of throttle setting for a constant mean piston speed of 7.5 m/s. This speed was chosen similarly to the speed in Figure 49 except that it was the highest mean piston speed at which all engines were tested. The limiting factor in this case was the maximum tested speed of the 28 cc engine at 7900 rpm. Like the data at the lower mean piston speeds, brake fuel conversion efficiency tended to increase with opening throttle, and friction and cooling tended to decrease with opening throttle.

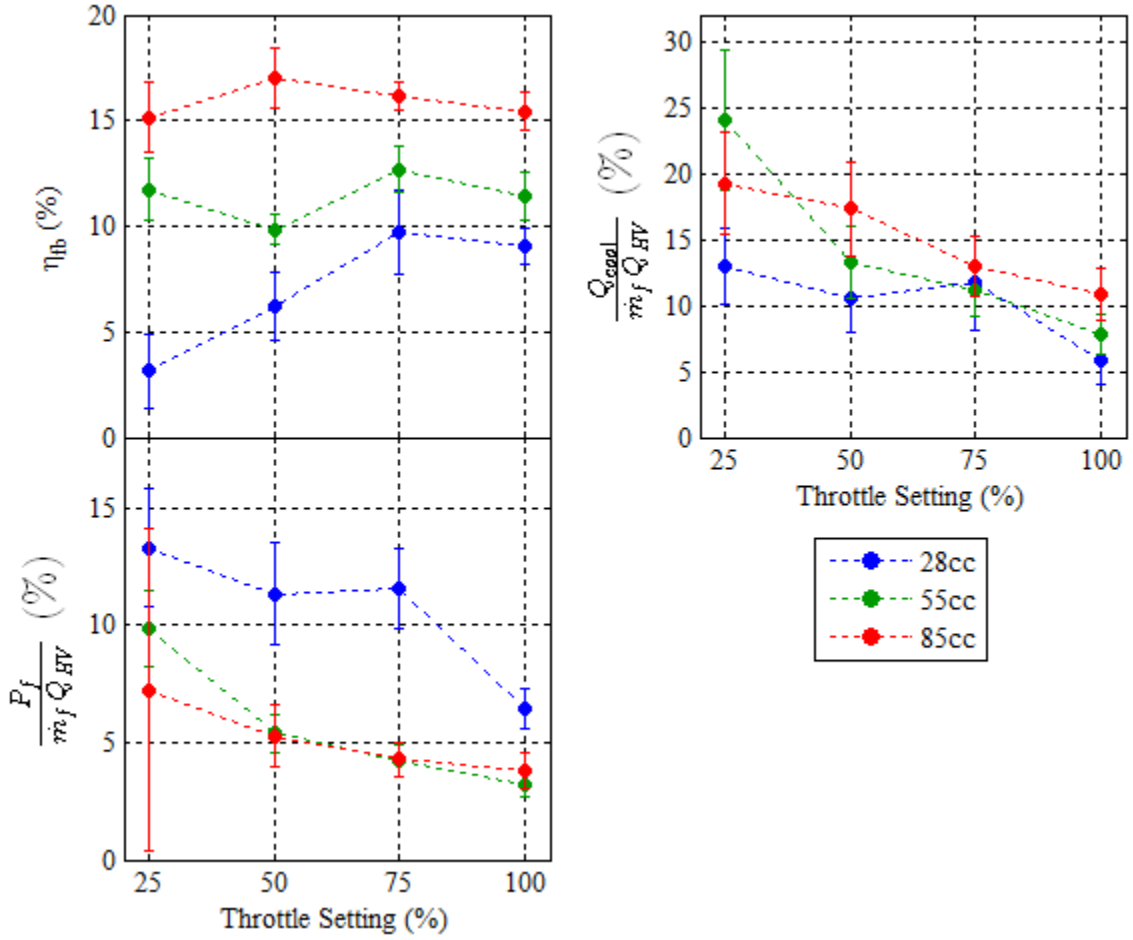

Figure 51: Energy pathways at 7.5 m/s mean piston speed

The plots in Figure 52 show the portions of total available fuel energy exiting the IC engine control volume in terms of power production, friction loss, and heat rejection for each engine. The data points within correspond to operating conditions for each engine that produced maximum brake fuel conversion efficiency over the entire range of engine speeds and throttle settings tested. To re-iterate, maximum brake fuel conversion efficiency was 12%, 14%, and 18% for the 28 cc, 55 cc, and 85 cc engines respectively as shown in the upper left of Figure 52. The operating conditions at which these maxima were produced follows in Table 10.

Table 10: Engine operating conditions for maximum brake fuel conversion efficiency

	28 cc	**55 cc**	**85 cc**
Throttle	50%	100%	50%
Speed (rpm)	5000	4500	6500
Speed ($\bar{S}_p$, m/s)	4.67	5.25	8.88

Brake fuel conversion efficiency decreased by 4% from the 85 cc engine to the 55 cc engine. Likewise, a decrease of 2% occurred from the 55cc to the 28 cc engine. This trend supports the hypothesis that decreasing engine size tends to reduce engine efficiency. To determine the cause, a characterization of friction loss and heat rejection loss is included for comparison. To maintain consistency with the brake fuel conversion efficiency data reported in the upper left, friction power was calculated and normalized by total available energy entering the IC engine system. Friction power is defined as the difference between indicated power and brake power for a given engine operating condition. It represents the amount of power dissipated by frictional losses within the

engine (piston to cylinder contact, bearings, pumping losses) as well as friction associated with any drivetrain components attached to the engine.

Normalized friction power losses for the engines in order of increasing displacement volume are 10%, 4%, and 5% as shown in the lower left of Figure 52. The data indicate that friction losses increased from the 55 cc engine to the 85cc engine. Again this loss is mostly likely caused by the additional friction of the second piston ring in the larger engine. Additionally, the data point corresponding to the 85 cc engine was obtained at 50% throttle and a mean piston speed of 8.88 m/s. The 55 cc point was at 100% throttle and only 5.25 m/s mean piston speed. The open throttle plate and lower relative speed of the 55 cc point serve to reduce pumping losses and piston to cylinder friction which manifest as normalized friction losses; another reason why the normalized friction of the 55 cc engine was lower than that of the 85 cc engine.

Normalized friction loss increased 6% by stepping down from the 55 cc engine to the 28 cc engine despite a decrease in mean piston speed. Although the 28 cc data point occurred at a more throttled condition (increasing pumping work, and hence friction loss), the normalized friction loss was still 5% higher in the 28cc engine as compared to the 85 cc engine in which relative throttle positions were the same. The additional loss associated with the smallest engine can be accounted for by the additional surface-to-surface friction as a result of increasing cylinder surface area to swept volume ratio. Based on the hypothesis of cylinder surface area to swept volume ratio effects on performance, the normalized heat rejection of the 85 cc engine should have been the lowest of the three engines. However, it exhibited a 6% increase as compared to the 55 cc engine.

According to the data in Figure 48, there is an apparent correlation between heat rejection and throttle setting in that heat rejection tends to increase as the throttle plate is opened. However, when normalized by total available fuel energy, engine cooling energy loss decreases as the throttle plate is opened as shown in the upper right of Figure 49, Figure 50, and Figure 51. Since the 55 cc engine's normalized heat rejection value below occurred at a throttle setting of 100% while the 85 cc engine's corresponding throttle setting was only 50%, the additional amount of available fuel energy is most likely the cause for an increase in heat rejection as displacement increases from 55 cc to 85 cc. At the point of maximum brake fuel conversion efficiency, it appears that the normalized heat rejection value for the 28 cc engine is approximately 6% higher as compared to the 55 cc engine. This would support the hypothesis of increased thermal losses with increasing cylinder surface area to swept volume ratio; however, the associated uncertainty in the 28 cc data point in particular prohibits any valid conclusions from being made.

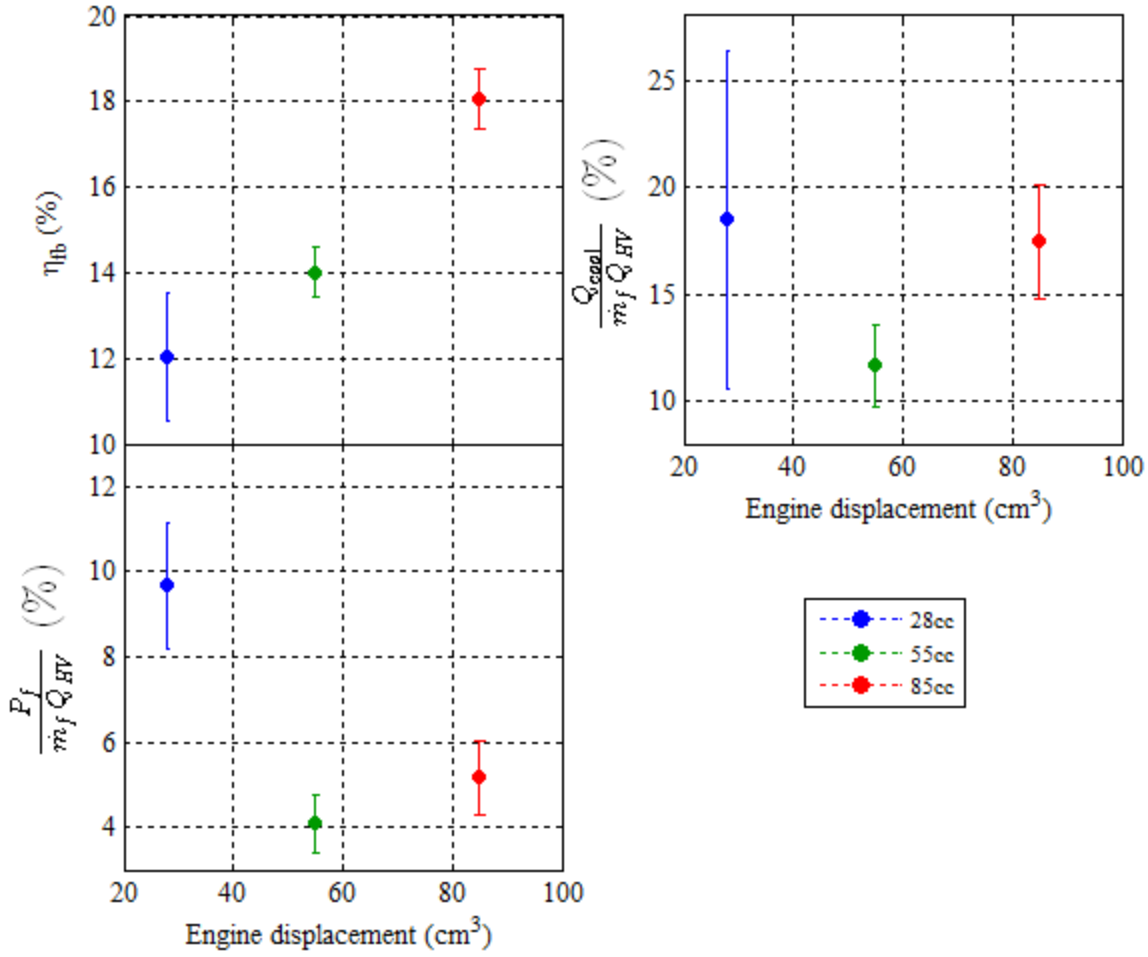

Figure 52: Energy pathway percentages at point of max. brake fuel conversion efficiency

As mentioned previously, only three energy pathways were measured and reported above. A large amount of outgoing energy yet to be accounted for was contained in the exhaust streams of each engine. An analysis of exhaust gas composition was not performed in this work, so the precise amount of unburned fuel and combustion products in the exhaust stream remains an unknown. However, based on some assumptions from literature and measured exhaust gas temperature, an estimate of the energy contained in the exhaust stream can be made. The assumptions used to make exhaust energy estimates are listed here. First, these engines are assumed to short-circuit

20% of the mass fuel delivered every cycle as suggested by Heywood and Sher [7]. Second, the best possible combustion efficiency for these engines cannot exceed 95% [4]. With these points in mind, 25% of the total available fuel energy is lost upfront. Additionally, in the case of equivalence ratios greater than unity, a corresponding amount of unburned fuel is assumed to be in the exhaust since it cannot react due to a lack of sufficient oxygen. Concerning the fuel and air that does react, the combustion reaction is assumed to go to completion resulting in only carbon dioxide, water, and nitrogen. Finally, in the calculation of sensible enthalpy of combustion products, a constant specific heat based on the average of the measured manifold air temperature and measured exhaust gas temperature is assumed for each constituent.

Figure 53 shows the relative magnitude of outgoing energy for each engine at 100% throttle at a constant mean piston speed of 5.5 m/s. The measured values represented as the power, friction, and cooling blocks correspond to the 100% throttle data points in Figure 49. The exhaust chemical enthalpy block (orange) and exhaust sensible enthalpy block (maroon) based on the assumptions laid out previously. According to the calculations, exhaust chemical enthalpy accounts for 35%, 31%, and 25% of the outgoing energy for the 28 cc, 55 cc, and 85 cc engines, respectively. Likewise, exhaust sensible enthalpy calculations account for 14%, 20%, and 19% of the outgoing energy for the engines in order of increasing size. There is a certain amount of energy not accounted for in each engine's case that is comprised of miscellaneous energy pathways such as gas kinetic energy and radiation. Additionally, the 20% and 5% fuel loss assumptions are just that. It is entirely possible that these engines short-circuit more than 20% fuel and/or have lower combustion efficiencies than the assumed 95% baseline.

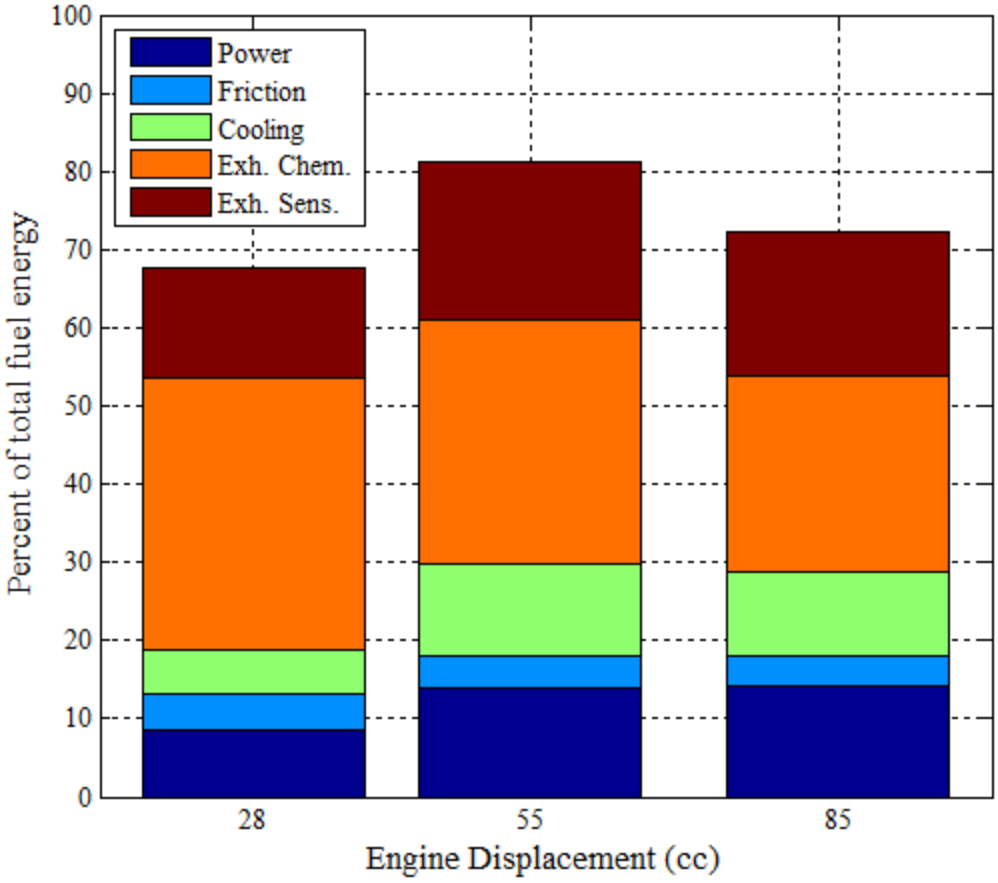

Figure 53: Energy Pathways at 100% throttle, 5.5 m/s mean piston speed

Figure 54 shows the outgoing energy pathways normalized by total available fuel energy of each engine at 100% throttle and a constant mean piston speed of 6.5 m/s. Exhaust chemical enthalpy calculations accounted for 27%, 43%, and 25% of the total available energy for the 28 cc, 55 cc, and 85 cc engines, respectively. Similarly, exhaust sensible enthalpy calculations accounted for 17%, 17%, and 20% of total available fuel energy for the engines in order of increasing size.

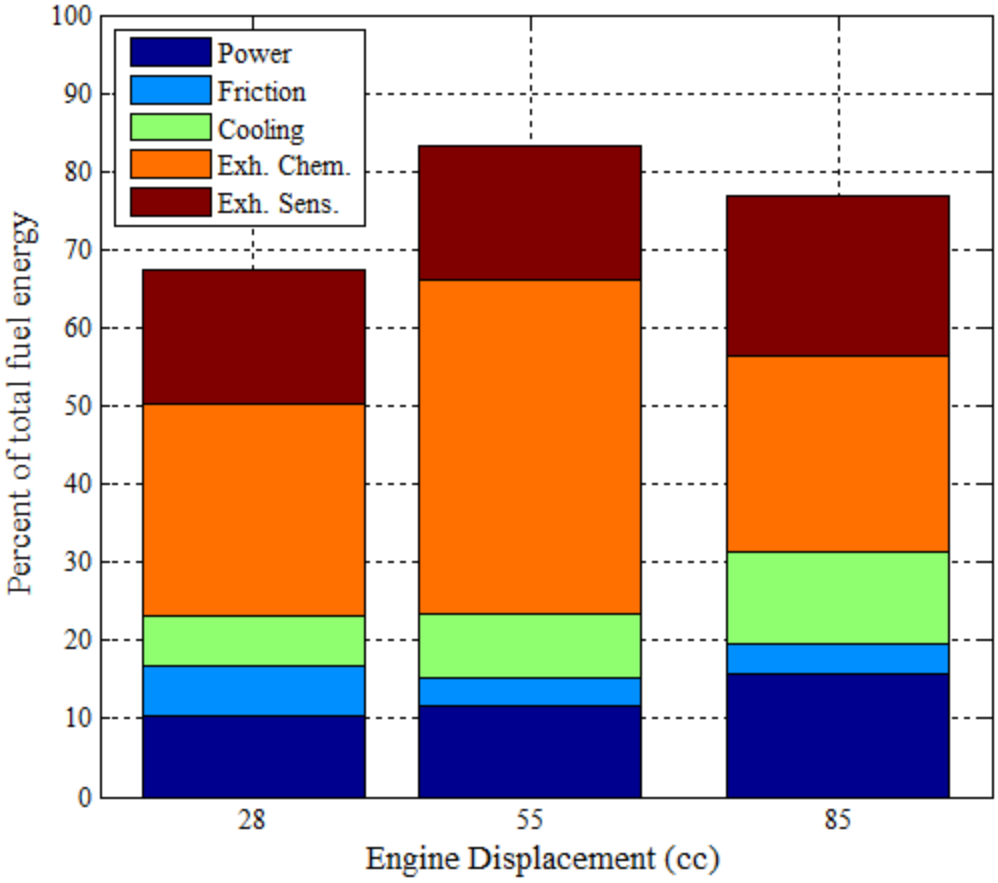

Figure 54: Energy Pathways at 100% throttle, 6.5 m/s mean piston speed

Figure 55 shows the outgoing energy pathways for each engine at 100% throttle and a constant mean piston speed of 7.5 m/s. Exhaust chemical enthalpy calculations accounted for 39%, 44%, and 25% of total energy for the engines in order of increasing displacement. Exhaust sensible enthalpy calculations accounted for 15%, 16%, and 20% of total energy for the 28 cc, 55 cc, and 85 cc engines, respectively.

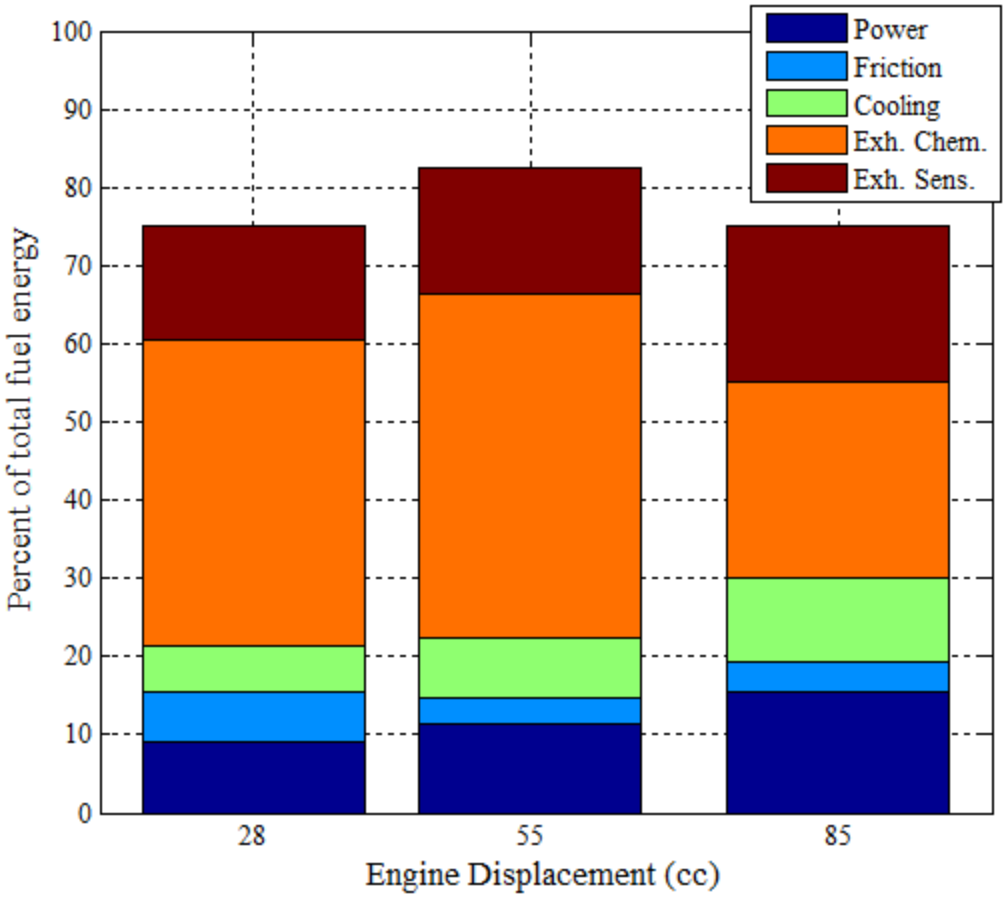

Figure 55: Energy Pathways at 100% throttle, 7.5 m/s mean piston speed

There is strong evidence to suggest that an engine's ability to convert available energy to shaft work (power out) decreases with decreasing engine size. Likewise, friction losses tend to increase relative to available energy as engine size is decreased. The data in this study indicate that thermal loss via heat transfer to the cooling medium does not increase with decreasing engine size as expected. Ultimately, it seems that the largest portion of energy exiting the IC engine thermodynamic system is associated with the energy state and composition of the exhaust gas.

4.3 Measured Scaling Behavior

As a result of this scaling study, power outputs were measured as a function of cylinder surface area to swept volume ratio for series of small IC engines in a size regime where power scaling trends are expected to change. Those results are included in Figure 56 along with the results of the UMD scaling study [30] and previous AFIT IC engine tests [31] [32]. A curve fit of this collection of trusted results generated a scaling model for measured power outputs as opposed to manufacturer rated power outputs. The modified scaling model based on measured results is shown as a red dashed line in Figure 56. The original curve based on manufacturer rated performance as suggested from Figure 15 is included for comparison. The function of the modified scaling model is shown in Equation 16 where surface area, SA, is reported in square centimeters, swept volume, V_d, is reported in cubic centimeters, and expected power output, $P_{meas.}$, is reported in kW.

$$\boldsymbol{P_{meas.} = 10\left(\frac{SA}{V_d}\right)^{-3}} \quad \textbf{(16)}$$

The difference in scaling model equations from Equation 10 which was for manufacturer rated power outputs to Equation 16 for measured power outputs is expected. As mentioned previously, the accuracy of performance data from the manufacturer in this size regime is often inaccurate. What the new scaling model represents is an offset from the original curve as each maintains the same exponent. This accounts for the overestimation of the produced power by manufacturers.

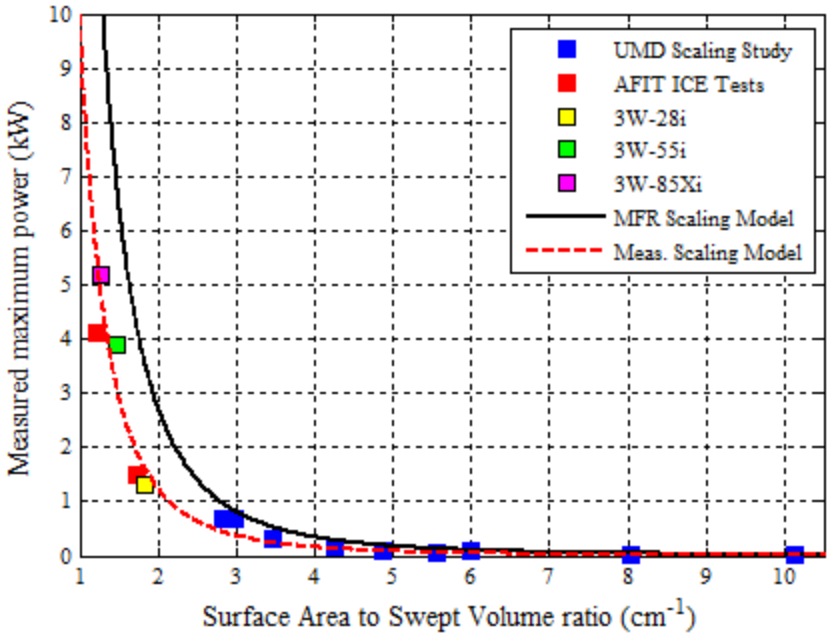

Figure 56: Measured power scaling model [30] [31] [32]

Using a similar technique to arrive at a scaling model for maximum power output as a function of cylinder surface area to swept volume ratio in Equation 16, scaling relationships to describe trends in brake fuel conversion efficiency, normalized friction power, and normalized heat rejection to cooling can be formulated. An examination of the resulting measured energy pathways for each engine at 100% throttle and 7.5 m/s mean piston speed as shown in Figure 51 and Figure 55 yielded new scaling models. The following functions for brake fuel conversion efficiency, friction power normalized by total available fuel energy, and heat transfer to engine cooling normalized by total available fuel energy were generated as functions of cylinder surface area to swept volume ratio:

$$\eta_{fb}(\%) = 21\left(\frac{SA}{V_d}\right)^{-1.5} \quad (17)$$

$$\frac{P_f}{\dot{m}_f Q_{HV}}(\%) = \mathbf{1.4}\left(\frac{SA}{V_d}\right)^{\mathbf{2.5}} \quad \textbf{(18)}$$

$$\frac{Q_{cool}}{\dot{m}_f Q_{HV}}(\%) = \mathbf{18}\left(\frac{SA}{V_d}\right)^{\mathbf{-2}} \quad \textbf{(19)}$$

It should be noted that a power function form was assumed for the scaling relationships presented. Furthermore, equivalence ratio was not necessarily consistent from one test engine to another. This factor is known to have a significant impact on performance and engine cooling characteristics. However, even though varying equivalence ratios can have a large impact on engine performance, the impact should be consistent from an indicated and brake performance basis. Since friction losses are a result of the difference in indicated and brake performance, then the amount of friction experienced by each engine should not be dependent on equivalence ratio. It follows that the suggested scaling relationship for normalized friction power in Equation 18 is a valid representation of how friction losses scale with engine size.

Using the test results at 100% throttle and a constant mean piston speed of 7.5 m/s as well as a constant rotational speed of 6000 rpm, scaling laws were generated for brake fuel conversion efficiency as a function of swept volume, and normalized friction power and heat rejection to cooling both as functions of cylinder surface area. A discussion of the scaling laws and how they compare to experimental results graphically follows.

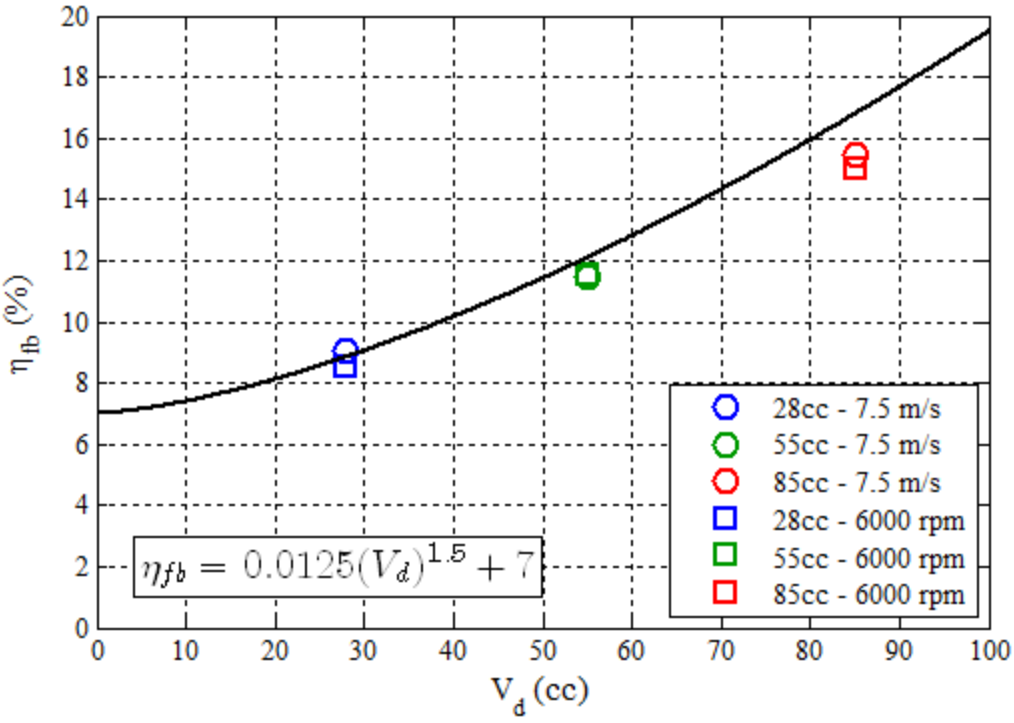

Figure 57: Brake fuel conversion efficiency scaling law

Figure 57 shows the generated scaling law for brake fuel conversion efficiency as a function of swept volume for engines in the 25 cc to 100 cc size regime. The function of the scaling law tends to be higher than the actual results corresponding to the 85 cc engine. This was done intentionally due to the fact that the 85 cc engine had a lean equivalence ratio during testing. It is expected that with more precise control of equivalence ratio, the 85 cc engine will produce more power and hence, a higher brake fuel conversion efficiency.

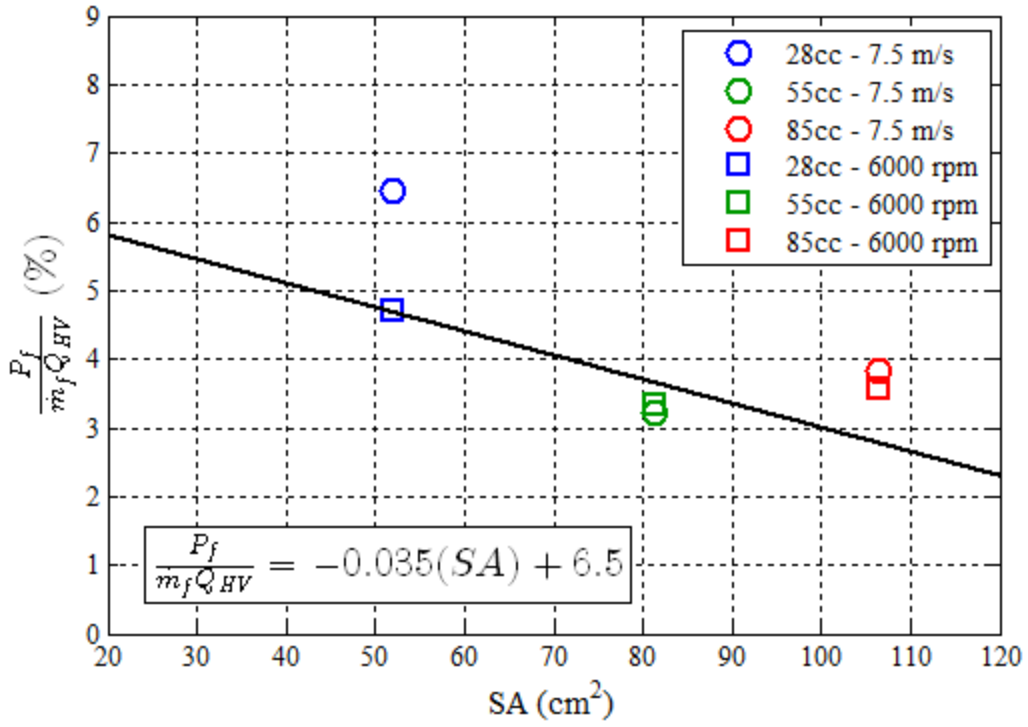

Figure 58: Normalized friction power scaling law

Figure 58 shows the generated scaling law for normalized friction power as a function of cylinder surface area. The scaling law is based on experimental results from this study for each engine at a constant mean piston speed of 7.5 m/s as well as a constant rotational speed of 6000 rpm. The data points corresponding to the 28 cc engine suggest that friction increases at a faster rate when constant mean piston speed is considered. This makes sense because the rotational speed corresponding to 7.5 m/s for the 28 cc engine was 7900 rpm, the fastest speed tested in this scaling study. It is assumed that additional friction exhibited by the mean piston speed data point is a result of additional loading due to drivetrain friction. Since the drivetrain friction was not characterized in this study, the scaling law emphasizes the points corresponding to 6000 rpm which suggest a linear trend that decreases as surface area increases. This stands to reason

because the scaling law describes friction as a fraction of total available energy per cycle. As engines decrease in size, total available energy decreases at a faster rate than friction, so the relative loss due to friction actually increases as engines get smaller, thus suggesting lower efficiencies in smaller engines as a result of more prevalent losses like friction.

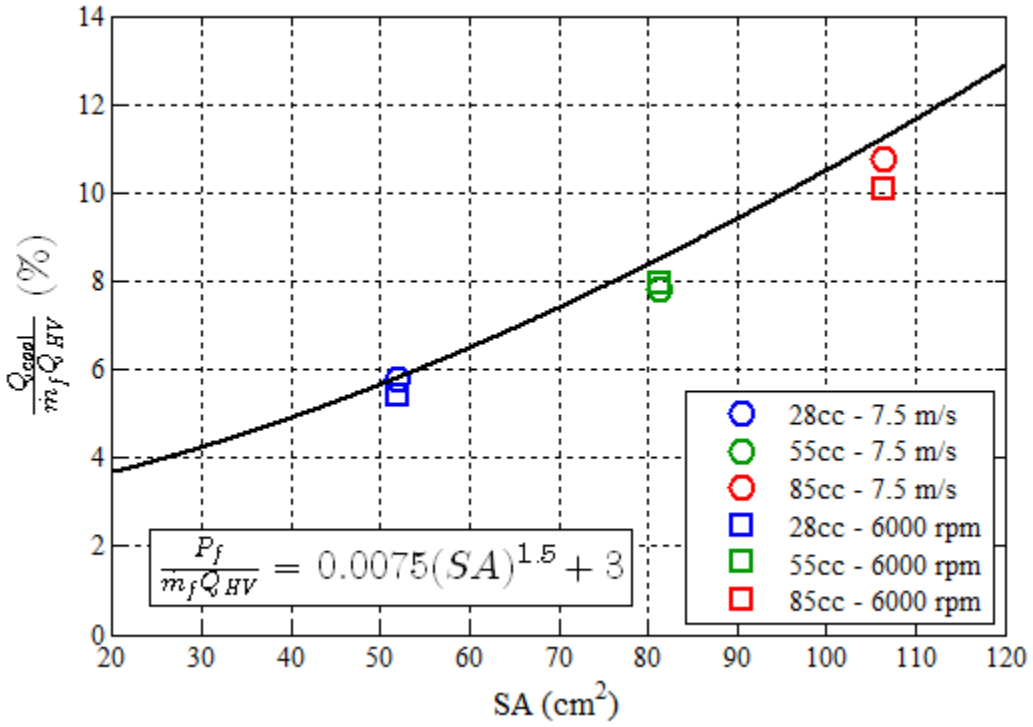

Figure 59: Normalized cooling heat transfer scaling law

Figure 59 shows the generated scaling for normalized heat rejection due to engine cooling as a function of cylinder surface area. The scaling law is based on heat rejection measurements taken for each engine at 100% throttle and a constant mean piston speed of 7.5 m/s as well as a constant rotational speed of 6000 rpm. The data indicate that engine cooling heat transfer does not change significantly whether constant mean piston or constant rotational speed is considered, so a single scaling law was generated for both

data sets. According to the data upon which this scaling law is based, engine cooling heat transfer should decrease as engines get smaller. However, as mentioned previously, the equivalence ratios during each engine test were not necessarily the same. Since equivalence ratio can have a large effect the amount of heat transfer to the cylinder walls of an engine and ultimately to the engine's cooling medium, these results are expected to change as equivalence ratio control is refined.

V. Conclusions and Recommendations

This chapter includes a review of the objectives for this research as well as discussion of how each one was met. A summary of the conclusions drawn from experimental data follows. The chapter concludes with the author's recommendations for future work to improve the results and expand upon the conclusions obtained from this work.

5.1 Research Objectives

Throughout this process, this study remained focused on achieving three primary research objectives as outlined in Chapter I. The research objectives are included here:

1. Develop a test facility capable of testing small IC engines in the 1-10 kW power range and gathering relevant data to characterize performance and efficiency.
2. Test a series of engines spanning the power scaling transition regime of approximately 1.5 cm^{-1} (in terms of cylinder surface area to swept volume ratio) to establish accurate performance baselines.
3. Analyze and create scaling relationships for performance and efficiency among the scaling study engines.

In order to develop a test facility adequate for running small IC engines in the 1-10 kW power range, the research team had to select a series of appropriately sized engines. The research team chose three engines manufactured for remote control aircraft propulsion ranging from 28cc to 85cc in displacement. Based on expected performance levels, the team designed and constructed systems appropriate for air and fuel supply, engine cooling, and power transmission. To promote consistency in results, the

configuration of the test facility remained constant, except when the engines were experiencing external performance-altering influences. Case in point, the air intake measurement setup had to be adjusted for the largest engine as mentioned previously in Chapter III. With these goals accomplished, engine testing began with an initial troubleshooting period to ensure the engines were operating properly and quality data was recorded. Once it was determined that engine operation and data recording abilities were accurate enough to discern differences and trends among the performance of each test engine, scaling study research began.

Since each engine shared key design features such as compression ratio and scavenging method, potential differences in performance were reduced. The cylinder surface area to swept volume ratios of the scaling study engines were 1.81 cm^{-1}, 1.46 cm^{-1}, and 1.28 cm^{-1} for the 28 cc, 55 cc, and 85 cc engines, respectively. Since it was determined that a significant change in power scaling trends occurred in the vicinity of 1.5 cm^{-1}, these engines were ideal for a scaling study of this size regime. Furthermore, the technical literature lacked sufficient technical performance data on IC engines in the 25 cc to 100 cc range to the best of the author's knowledge, so filling this research gap would provide a significant contribution to the understanding of scaling effects on performance and loss mechanisms for IC engines of this size.

Sufficient data was collected to analyze and establish trends in performance for the scaling study engines. This work focused on establishing a performance baseline for the three engines. Data were gathered on brake performance, indicated performance, air and fuel flow characteristics, and heat transfer to engine cooling. The results allowed an accurate characterization of actual brake power production as compared to manufacturer

rated power production. Aspects such as fuel conversion efficiency, specific fuel consumption, and friction loss were determined for each engine as functions of engine displacement as well as cylinder surface area to swept volume ratio.

5.2 Research Conclusions

A summary of the best case performance values for each of the three scaling study engines can be found in Table 9 in Chapter IV. In terms of loss mechanisms measured in this study, friction was found to be a dominating factor in the diminishing performance and efficiency of the smallest engine due to the increasing cylinder surface area to swept volume ratio. In terms of FMEP at 100% throttle, the 28 cc engine exhibited values 66% and 108% higher values on average than the 55 cc and 85 cc engines respectively. An examination of friction mean effective pressure at 100% throttle and 6000 rpm revealed that friction increased at a rate of approximately 1.9 kPa for every cubic centimeter of displacement reduction. Since rotational speed was constant, drivetrain friction was the same for each engine; therefore, the resulting friction losses were caused by components within the engines themselves. The primary difference among the three engines was cylinder surface area relative to swept volume, so the additional friction loss as the engines were reduced in size was a result of more surface friction with cylinder walls. Although the data indicate that heat rejection to the cooling medium increased as engine displacement increased, the equivalence ratio varied from engine to engine for these tests. It is known that equivalence ratio can have a large effect on heat transfer rates in an IC engine. With fuel-rich conditions, more heat from combustion can be absorbed by the excess, unburned fuel. This energy then passes out the exhaust port and does not transfer to the cylinder walls and eventually to the cooling medium. In this study, the 85 cc

engine typically operated at a lower equivalence ratio in comparison to the other two engines. This caused higher combustion temperatures which resulted in more heat transfer to the cooling medium relative to total available energy. In order to draw conclusive results about heat rejection effects among the engines, equivalence ratio should be held constant for each engine at a given operation condition. The limitations of the tuning strategy for this study prohibited such testing. The experimental results of this study were used in conjunction with the previous AFIT IC engine tests of Crosbie [31] and Wilson [32] along with the scaling study results of micro IC engines from Menon at the University of Maryland [30] to develop a scaling model of maximum measured IC engine power output as a function of cylinder surface area to swept volume ratio. The resulting function in Equation (16) was found to differ from a similar scaling model equation based on manufacturer rated power outputs of a collection of IC engines due to the fact that manufacturer performance claims for engines in this size class (25 cc to 100 cc) are frequently inaccurate. Specifically, at 1.5 cm^{-1}, the measured scaling model gives a power level 55% lower than the same point of the model based on manufacturer claimed performance.

5.3 Recommendations for Future Work

Over the course of this work four primary aspects of the experiment were identified to benefit from improvement. These were air/fuel mixture control, engine load measurement, exhaust gas composition, and drivetrain friction characterization. During engine testing, equivalence ratio proved to have a large variation from test run to test run. This was most likely a result of the limitation on control of equivalence ratio inherent in the simplistic design of each carburetor. Equivalence ratio has a large influence on

engine performance including power production, efficiency, and fuel consumption rate. The basic carburetors installed on these engines simply cannot control equivalence ratio sufficiently over a range of engine speeds and loads to investigate the true performance potential of these engines. Electronic fuel injection, although more complex, has been proven universally to control equivalence ratios more precisely so an engine can realize better performance and efficiency levels without excess waste of fuel. Ideally, direct injection would benefit the performance of these engines the most; however, to the author's knowledge, no appropriately sized injectors are currently commercially available for use in these engines. Implementation of port fuel injection would be a good next step to further the research of scaling effects on engines of this size.

The method used to establish throttle settings in this study was limited to the repeatability of the servo motors used to actuate the throttle plates. In research performed on the 34 cc Fuji engine by both Wilson [32] and Groenewegen [18], it has been shown that these types of servos exhibit a hysteresis that can affect the position of the throttle plate from one operating point to the next. Ultimately, the engine loads reported in this study contained some inherent variability that was not controlled. An accepted method of measuring engine load in the scientific literature for related engine testing is to install a pressure transducer downstream of the throttle plate in the engine's intake manifold. This pressure transducer, commonly known as a manifold absolute pressure (MAP) sensor, can relay pressure signals that correlate to engine load. With the use of a MAP sensor, knowledge of the precise position of the throttle plate would be irrelevant. A desired engine load could be set by establishing a particular MAP via throttle actuation. The

throttle would simply open or close then to maintain the desired manifold pressure over various operating conditions.

The results of this study indicated that the largest outgoing energy pathway for each of the three scaling study engines was the exhaust stream. This energy is comprised of sensible enthalpy change plus unburned hydrocarbons due to short-circuiting and combustion inefficiency. In order to quantify the amount of energy contained in this pathway, exhaust gas emissions measurements would need to be performed. In this way, a more thorough description of the incoming and outgoing energy pathways of the engines could be expressed.

The configuration of the drivetrain for the test bench provides for excellent accessibility in terms of adding instrumentation and changing engines while keeping all rotating components within alignment tolerances. However, the use of several pillow block bearings, an external pneumatic starter motor, multiple shaft couples and most notably, a cogged belt drive did provide a significant amount of extra friction loading that was not measured independently during the experiment. Overall friction losses were characterized as a result of indicated and brake performance analysis, but drivetrain friction specifically could not be distinguished. Decoupling the engines and spinning the drivetrain with an instrumented power source could serve to quantify the friction of the drivetrain as a function of rotational speed. These results would allow for an accurate analysis of internal engine friction and how it scales with engine size.

Bibliography

[1] United States Air Force, "United States Air Force RPA Vector: Vision and Enabling Concepts 2013-2038," Headquarters, USAF, 2014.

[2] J. K. Ausserer, "Integration, Testing, and Validation of a Small Hybrid-Electric Remotely-Piloted Aircraft," Master's Thesis, Air Force Institute of Technology, 2012.

[3] E. Sher and I. Sher, "Theoretical limits of scaling-down internal combustion engines," *Chemical Engineering Science*, vol. 66, no. 3, pp. 260-267, 2011.

[4] J. B. Heywood, "Internal Combustion Engine Fundamentals," New York, McGraw-Hill, 1988.

[5] Bosch, Automotive Handbook, 8th ed., Plochingen, Germany: Robert Bosch GmbH, 2011.

[6] M. J. Moran, H. N. Shapiro, B. R. Munson and D. P. DeWitt, Introduction to Thermal Systems Engineering: Thernodynamics, Fluid Mechanics, and Heat Transfer, Hoboken, New Jersey: John Wiley & Sons, Inc., 2003.

[7] J. B. Heywood and E. Sher, The Two-Stroke Cycle Engine, New York: Taylor & Francis Group, 1999.

[8] S. R. Turns, An Introduction to Combustion: Concepts and Applications, New York: McGraw-Hill, 2012.

[9] C. Arcoumanis and C. S. Bae, "Correlation Between Spark Ignition Characteristics and Flame Development in a Constant-Volume Combustion Chamber," *SAE Technical Paper Series*, 1992.

[10] C. R. Ferguson and A. T. Kirkpatrick, Internal Combustion Engines Applied Thermosciences, 2nd Edition ed., New York: John Wiley & Sons, Inc., 2001.

[11] D. T. Falkowski, D. L. Abata and P. Cho, "The Performance of a Spark-Ignited Stratified-Charge Two Strok Engine Operating on a Kerosene Based Aviation

Fuel," Society of Automotive Engineers, 1997.

[12] A. Kinnen, W. Layher and H. Daschner, "Electronically Controlled Batteryless Injection System for Small Two-Stroke SI Engines," SAE International, 2012.

[13] M. W. Stockel, M. T. Stockel and C. Johanson, Auto Fundamentals, Tinley Park, Illinois: The Goodheart-Willcox Company, Inc., 2005.

[14] M. R. Mataczynski, "Design and Simulation of Pressure Wave Supercharger for Small Two-Stroke Engine," Air Force Institute of Technology, Wright-Patterson Air Force Base, Ohio, 2014.

[15] W. P. Attard, E. Toulson, H. Watson and F. Hamori, "Abnormal Combustion including Mega Knock in a 60% Downsized Highly Turbocharged PFI Engine," SAE International, 2010.

[16] N. Mavinahally, J. Veerathappa, S. Rajgiri and V. Mavinahalli, "Multi-Layer Stratified (MuLS) Two-Stroke Engine," SAE International, 2012.

[17] S. Menon, N. Moulton and C. Cadou, "Development of a Dynamometer for Measuring Small Internal-Combustion Engine Performance," *Journal of Propulsion and Power*, vol. 23, no. 1, pp. 194-202, 2007.

[18] J.-R. J. Groenewegen, "The Performance and Emissions Characteristics of Heavy Fuels in a Small, Spark Ignition Engine," Master's Thesis, University of Dayton, 2011.

[19] "3W Engines & Airplanes," 3W Modellmotoren GmbH, [Online]. Available: www.3w-modelmotoren.com. [Accessed 19 April 2014].

[20] "Centurion Aircraft Engines," [Online]. Available: www.centurion.aero. [Accessed 19 April 2014].

[21] "DeltaHawk Diesel Engines," Flightfunds, Inc., 31 January 2014. [Online]. Available: www.deltahawkengines.com. [Accessed 19 April 2014].

[22] "Desert Aircraft," 2008. [Online]. Available: www.desertaircraft.com. [Accessed 19 April 2014].

[23] "Compact Radial Engines," [Online]. Available: www.compactradialengines.com. [Accessed 19 April 2014].

[24] "Freedom Motors," 2010. [Online]. Available: www.freedom-motors.com. [Accessed 19 April 2014].

[25] "Kodiak Research Ltd," 2014. [Online]. Available: www.kodiakbs.com. [Accessed 19 April 2014].

[26] "O.S. Engine," Hobbico, Inc., 2014. [Online]. Available: www.osengines.com. [Accessed 19 April 2014].

[27] "Recreational Power Engineering," [Online]. Available: www.recpower.com. [Accessed 19 April 2014].

[28] "Super Tigre," Hobbico, Inc., 2014. [Online]. Available: www.supertigre.com. [Accessed 19 April 2014].

[29] "Zenoah," 2012. [Online]. Available: www.zenoah.co.jp. [Accessed 19 April 2014].

[30] S. Menon, "The Scaling of Performance and Losses in Miniature Internal Combustion Engines," Doctoral Dissertation, University of Maryland, 2010.

[31] S. C. Crosbie, "Increasing Reliability of a Small 2-stroke Internal Combustion Engine for Dynamically Changing Altitudes," Master's Thesis, Air Force Institute of Technology, 2012.

[32] C. W. Wilson, "Performance of a Small Internal Combustion Engine using n-Heptane and Iso-Octane," 2010.

[33] J. A. Rittenhouse, "Thermal Loss Determination for a Small Internal Combustion Engine," Master's Thesis, Air Force Institute of Technology, 2014.

[34] "ServoCity," Robotzone, LLC, 2014. [Online]. Available: www.servocity.com. [Accessed 11 May 2014].

[35] S. J. Kline and F. A. McClintock, "Describing Uncertainties in Single-Sample

Experiments," *Mechanical Engineering,* pp. 3-8, 1953.

[36] J. P. Holman, Experimental Methods for Engineers, New York: McGraw-Hill Book Company, 1984.

REPORT DOCUMENTATION PAGE

Form Approved
OMB No. 074-0188

PLEASE DO NOT RETURN YOUR FORM TO THE ABOVE ADDRESS.

1. REPORT DATE *(DD-MM-YYYY)*	2. REPORT TYPE	3. DATES COVERED *(From – To)*
20-06-2014	Master's Thesis	October 2013 – June 2014

TITLE AND SUBTITLE

Measuring Scaling Effects in Small Two-Stroke Internal Combustion Engines

5a. CONTRACT NUMBER

5b. GRANT NUMBER

5c. PROGRAM ELEMENT NUMBER

6. AUTHOR(S)

Rowton, Alex K., Captain, USAF

5d. PROJECT NUMBER

5e. TASK NUMBER

5f. WORK UNIT NUMBER

7. PERFORMING ORGANIZATION NAMES(S) AND ADDRESS(S)

Air Force Institute of Technology
Graduate School of Engineering and Management (AFIT/ENY)
2950 Hobson Way, Building 640
WPAFB OH 45433-8865

8. PERFORMING ORGANIZATION REPORT NUMBER

AFIT-ENY-T-14-J-36

9. SPONSORING/MONITORING AGENCY NAME(S) AND ADDRESS(ES)

Intentionally left blank

10. SPONSOR/MONITOR'S ACRONYM(S)

11. SPONSOR/MONITOR'S REPORT NUMBER(S)

12. DISTRIBUTION/AVAILABILITY STATEMENT

DISTRUBTION STATEMENT A. APPROVED FOR PUBLIC RELEASE; DISTRIBUTION UNLIMITED.

13. SUPPLEMENTARY NOTES

This material is declared a work of the U.S. Government and is not subject to copyright protection in the United States.

14. ABSTRACT

As internal combustion (IC) engines decrease in displacement, their cylinder surface area to swept volume ratio increases. Examining power output of IC engines with respect to cylinder surface area to swept volume ratio shows that there is a dramatic change in power scaling trends at approximately 1.5 cm^{-1}. At this size, thermal quenching and friction losses are expected to dominate , so power production and efficiency characteristics suffer. Furthermore, small IC engines (<100cc displacement) have limited technical performance data compared to IC engines in larger size classes. Therefore, it is critical to establish accurate performance figures for a family of geometrically similar engines in the size class of approximately 1.5 cm^{-1} in order to better predict the phenomena that contribute to lower efficiencies in small ICEs. A series of three two stroke, single cylinder, spark ignited, air cooled, and carbureted IC engines were tested in this study. They had a displacement of 28cc, 55cc and 85cc corresponding to cylinder surface area to swept volume ratios of 1.81 cm^{-1}, 1.46 cm^{-1}, and 1.28 cm^{-1} respectively. The engines share design features like compression ratio, gas exchange port design, and scavenging method.

15. SUBJECT TERMS

small IC engine, two-stroke, scaling study, efficiency, indicated performance, friction losses

16. SECURITY CLASSIFICATION OF:			17. LIMITATION OF ABSTRACT	18. NUMBER OF PAGES	19a. NAME OF RESPONSIBLE PERSON
a. REPORT	b. ABSTRACT	c. THIS PAGE			Marc Polanka, AFIT/ENY
U	U	U	UU	151	19b. TELEPHONE NUMBER *(Include area code)* (937) 785-3636, ext 4714 *(marc.polanka@afit.edu)*

Standard Form 298 (Rev. 8-98)
Prescribed by ANSI Std. Z39-18